NANOPARTICLE MEDIATED RELEASE FROM POLYMERSOMES USING ULTRAFAST IRRADIATION

By

ABBY ROBINSON

A thesis submitted to the

Graduate School-Camden

Rutgers, The State University of New Jersey

In partial fulfillment of the requirements

For the degree of Master of Science

Graduate Program in Chemistry

Written under the direction of

Dr. Hao Zhu

And approved by

_____

Dr. Hao Zhu

_____

Dr. Julianne Griepenburg

_____

Dr. Sean M. O'Malley

_____

Dr. Jinglin Fu

Camden, New Jersey

May 2019

THESIS ABSTRACT

Nanoparticle Mediated Release from Polymersomes using Ultrafast Irradiation

By ABBY ROBINSON

Thesis Director:
Dr. Hao Zhu

The self-assembly of amphiphilic diblock copolymers into polymeric vesicles, commonly known as polymersomes, has attracted significant research interest due the broad applicability in various fields ranging from drug delivery to nanoreactors. Polymersomes are fully synthetic robust vesicles comprised of a hydrophilic core and bilayer, hydrophobic membrane; this provides the ability for stable, dual-encapsulation of a variety of molecules within the two regions. While most diblock copolymers yield vesicles that are inherently insensitive to stimuli, efforts have been made to design polymersomes that rupture in response to temperature, pH, and light such that encapsulated cargo can be released on demand. Light is a particularly attractive trigger for initiating cargo release as it can be controlled in a high spatiotemporal fashion and can be minimally damaging and deeply penetrating in biological systems. In this work, methods have been developed for triggered encapsulant release using ultrafast, single-pulse irradiation with visible and near infrared light to provide a non-invasive method of achieving spatial and temporal control. Gold nanoparticles (AuNPs) have been incorporated into the vesicle membrane as photosensitizers to allow for wavelength specific vesicle rupture congruent with the localized surface plasmon resonance (LSPR) of the particle. Thus,

the encapsulation of gold nanorods provides the ability to shift the polymersome response wavelength to the near-infrared. Initial studies were performed on micron-scale polymersomes to facilitate release studies at the single vesicle level. Additonally, scale down to the nano-regime was optimized for future applications in biomedical systems where diameters range from 80-200 nm deemed optimal for in-vivo drug delivery.

Acknowledgments

I would like to express my greatest appreciation to all of the people in my life who helped make this thesis possible. To my advisors Dr. Griepenburg and Dr. O'Malley; learning from the two of you will always remain my most valued experience. Dr. Griepenburg, thank you for seeing the potential in me when I was unable to see it for myself. Without the both of you, I know I would not be where I am today. Thank you both for extensively training, teaching, and trusting me with all aspects of this amazing project.

Thank you to the Chemistry Department and to my graduate thesis director, Dr. Zhu. Thank you to my thesis committee members, Dr. Fu and Dr. O'Malley. To my lab members, Cory, Gina, and Tyler, thank you all for all of your help, support, and the memories along the way. Thank you, Sean, Mohamed, Manpreet, Diaab, Anna, and Kristi for all of your help and hard work as well. Thank you, Mrs. Craig, for being the most supportive and caring mentor.

Mom and Dad, thank you both for working to make college a possibility for me. I love you both and I hope I have, and continue to make you proud. To the rest of my family and friends, thank you for all of the endless support. Eric, thank you for continuously having my back and always supporting my dream to be a part time scientist and a part time Joanna Gaines. I am thankful to have you by my side as I move on to the exciting next chapter in my life.

Thank you, Rutgers-Camden for an amazing experience. I have received an amazing education, have learned valuable life lessons, and have made lifelong friendships here.

Table of Contents

THESIS ABSTRACT ..... **ii**

Acknowledgments ..... **iv**

Table of Contents ..... **v**

Table of Illustrations ..... **vii**

Chapter 1 : Introduction **1**

Targeted drug delivery *1*

Carrier vesicles *2*

Stimuli responsive polymersomes *6*

Light as a stimulus *12*

Light delivery methods *16*

Metal nanoparticles as photosensitizers *20*

Conclusion *25*

Chapter 2 : Micron-scale system **26**

Introduction *26*

Methods and Materials *32*

Results and Discussion *38*

Conclusion *41*

Chapter 3 : Nano-scale system **42**

Introduction *42*

Materials and Methods *44*

Results and Discussion *50*

Conclusion *66*

Chapter 4 : System optimization **68**

Introduction *68*

Materials and Methods *69*

Results and Discussion *70*

Conclusion *75*

Chapter 5 : Concluding remarks **77**

Conclusion *77*
Future directions *80*
Appendix **81**
Table of Abbreviations *81*
Data tables *82*
References **115**

Table of Illustrations

Figure 1-1: Schematic representation of a liposome 3

Figure 1-2: Polymersome self-assembly and structure 5

Figure 1-3 pH responsive polymersomes 7

Figure 1-4: Redox potential triggered release from polymersomes 8

Figure 1-5: Temperature sensitive polymersomes 9

Figure 1-6 Ultrasound and pH dually responsive polymersomes 11

Figure 1-7: UV-sensitive polymersomes 13

Figure 1-8: Bright field images of UV responsive polymersomes 14

Figure 1-9:Light responsive PZn_2 polymersomes 15

Figure 1-10: Schematic representation of the optical gain stage of a conventional laser system [36] 17

Figure 1-11: Localized surface plasmon resonance (LSPR) of metal nanoparticles .. 20

Figure 1-12: LSPR shift for AuNPs [46] 21

Figure 1-13: Extinction spectra for AuNRs 22

Figure 1-14: Window for in-vivo imaging. 22

Figure 1-15: Thermo- and photo-responsive polymersomes 24

Figure 2-1: Schematic representation of a plasmonic polymersome 26

Figure 2-2: Fluorescence microscopy images of micron-scale polymersomes [52] 27

Figure 2-3: Complete rupture of an AuNP loaded polymersome [52] 28

Figure 2-4: Polymersomes without AuNPs as a control [52] 29

Figure 2-5: Time series of cargo release from a polymersome containing AuNPs in the membrane [52] 29

Figure 2-6: Cargo release from plasmonic polymersomes as a function of pulse energy [52] 31

Figure 2-7: Gel-assisted rehydration method for polymersome preparation 33

Figure 2-8: Top-down schematic for removal of non-encapsulated FITC-dextran 34

Figure 2-9: Ultrafast (fs) laser-microscope setup 35

Figure 2-10: Pulse spot size determination 36

Figure 2-11: FITC-dextran diffusion from polymersomes with two different AuNP concentrations 38

Figure 2-12: Polymersome poration leading to structural instability 39

Figure 2-13: Polymersome cargo diffusion as a function of time with varying AuNP concentration 40

Figure 3-1: Graphical representation of the nano-scale plasmonic polymersomes .. 43

Figure 3-2: Direct solvent injection for nano-scale polymersome preparation..... 44

Figure 3-3: Beam profile for nano-scale polymersome irradiation..... 47

Figure 3-4: Irradiation setup for nano-scale polymersome irradiation 48

Figure 3-5: Nano-scale polymersome size as a function of AuNP concentration..... 50

Figure 3-6: Representative cryo-TEM image of polymersomes prepared without AuNPs 51

Figure 3-7: Representative cryo-TEM images of AuNP (0.05% (w/v)) loaded polymersomes 52

Figure 3-8: Cryo-TEM polymersome size analysis 52

Figure 3-9: Representative views of a cryo-TEM tomogram of one AuNP loaded polymersome 53

Figure 3-10: 2D Hexagonal array of AuNPs within polymersomes..... 54

Figure 3-11: Spacing of AuNPs in 2D hexagonal array 54

Figure 3-12: Fate of AuNPs following vesicle irradiation 56

Figure 3-13: Comparative population overlays for irradiated vs non-irradiated samples 57

Figure 3-14: Nano-scale polymersome size as a function of time at various pulse energies 59

Figure 3-15: Time required to rupture polymersomes at varying pulse energies 60

Figure 3-16: Time required for polymersome rupture with varying AuNP concentrations 61

Figure 3-17: Rupture threshold detection for nano-scale polymersomes with varying AuNP concentrations 61

Figure 3-18: Size time series following rupture 62

Figure 3-19: DLS results for Triton X resistant polymersomes 64

Figure 3-20: DLS results for Tween 20 resistant polymersomes 64

Figure 3-21: Surfactant resistant polymersomes 65

Figure 3-22: Nile red control experiment 66

Figure 4-1: Setup for visualizing real-time gel-assisted rehydration 69

Figure 4-2: Polymersome formation time series 70

Figure 4-3: Polymersome size optimization – without AuNPs 71

Figure 4-4: Polymersome size optimization – w/ AuNPs 72

Figure 4-5: Vesicle size and PDI as a function of diblock copolymer concentration . 73

Figure 4-6: Size effects upon AuNP encapsulation 74

Figure 4-7: Table displaying the percent change in polymersome size after 10 days 75

Figure 5-1: Plasmonic polymersomes spanning the visible and NIR wavelengths 80

Chapter 1 : Introduction

Targeted drug delivery

Over the past several decades, the development of controlled drug delivery technologies has significantly advanced towards the ultimate goal of increasing drug efficacy and specificity while mitigating harsh side effects.[1] Nanoparticle based systems for drug delivery, such as metallic NPs, polymer carriers, and carbon nanostructures, are attractive for a variety of reasons and have the potential to advance the field of nanomedicine. Nanoparticle based carriers have unique chemical and physical properties that can be tailored towards the design of an ideal drug carrier system; this includes optimal size for bloodstream circulation, enhanced penetration depth in tumor tissue, cell uptake specificity, controlled payload release, and circumvention of tumor drug resistance.[2] Systemic drug delivery, while historically proven effective in the treatment of disease, has many suboptimal limitations. Cancer, for example, being one of the most deadly diseases with over 100 specific types and high associated mortality rates[3], is extremely challenging to treat. Treatments including chemotherapy, radio therapy, tumor surgery, and hormonal therapy are accompanied by harsh and long-term side effects, and in some cases, are not always effective.[4] Conventional chemotherapy treatment involves the delivery of a therapeutic agent which non-specifically circulates throughout the body, affecting both target cells as well as healthy, off-target cells. [5] This non-specific delivery results in undesirable side effects including fatigue, hair loss, nausea, loss of appetite, to name only a few. Often, high mortality rates of cancer patients can be attributed to the adverse side effects of the treatment in addition to the primary disease. Conventional

chemotherapy often requires high drug dosages to achieve efficacy due to the poor bioavailability of the drugs at tumor sites; these dosage requirements lead to even greater toxicity to healthy cells. Thus, a long-term goal in the field of drug delivery is to develop methods which reduce adverse systemic side effects while increasing localized bioavailability and overall efficacy of the treatment.

The use of nanocarriers as drug delivery systems has the potential to circumvent the problems associated with conventional anticancer therapies by enhancing bioavailability and efficiency of anticancer drugs.[6] There are various types of nanocarriers designed to transport a drug to a specific target site including, but not limited to, liposomes, polymeric micelles, polymeric nanoparticles, polymersomes, carbon nanotubes, and viral nanoparticles.[7]

Carrier vesicles

Of particular interest are vesicle-based nanocarrier delivery systems, namely liposomes and polymersomes. These vesicles have a structure in close resemblance to cellular membranes, consisting of a hydrophilic lumen and bilayer membrane. While typically robust, these vesicles can be designed to release their cargo in response to various stimuli. A vast amount of research has been directed towards their design and implementation as drug delivery systems in clinical practice and in various stages of clinical research.[8] However, there is still much room for improvement in the ability to deliver cargo with precise spatiotemporal control.

Liposomes are naturally occurring phospholipid vesicles containing one or more lipid bilayer membrane and an aqueous core [Figure 1-1]. These two distinct compartments allow for encapsulation of both lipophilic and hydrophilic compounds which provide the ability for a wide range of drug molecules to be encapsulated within the vesicle. Their biocompatibility, ability to self-assemble, and capacity to dual-encapsulate a wide variety of drug payloads make liposomes advantageous as a drug delivery system. Liposomes are self-assembled from phospholipids with molecular weights between 100-1000 g/mol, yielding a bilayer membrane thickness ranging from 3-5 nm. [9] Vesicle formation is thought to be a two-step process, where the amphiphile first forms a bilayer sheet structure which then closes to form a spherical vesicle.[10]

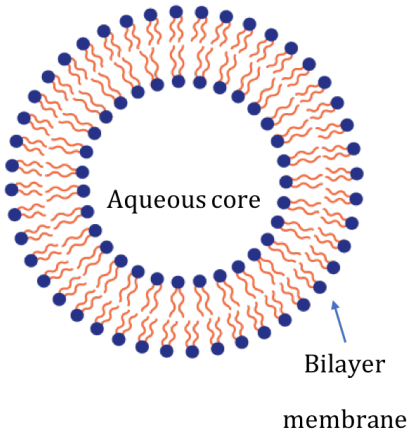

Figure 1-1: Schematic representation of a liposome

There are a variety of examples of liposomes designed for drug delivery applications. In fact, the first FDA-approved nano-drug, "Doxil" is a liposomal system encapsulating Doxorubicin HCl, a chemotherapeutic, which is effective against many different types of cancer. [11] The liposomal system in which Doxil is based off of is functionalized with polyethylene glycol (PEGlyated), which has been shown to increase blood circulation and decrease clearance rates by the renal system. Doxil is passively targeted to tumors due to the enhanced permeability and retention (EPR) effect, which leads to tumor penetration. While many preclinical and clinical studies

with liposomal drug delivery systems have had favorable results, there are a variety of challenges and problems associated with their use. One of the major challenges is the ability to deliver the encapsulated drug in high concentrations from the vesicle, as many systems release drugs slowly.[12] Additionally, liposomes often lack stability and tunability, making it very challenging to precisely control cargo delivery.[13] In response to the need for a fully synthetic and tunable carrier vesicle, polymersomes were designed over a decade ago. Polymersomes overcome some of the structural challenges associated with liposomes as a drug delivery system.

Amphiphilic diblock copolymers are attractive for a variety of applications due to their unique properties and their ability to self-assemble into numerous types of structures, including spherical micelles, cylindrical micelles, bilayer films, and polymersomes. At solution concentrations above the critical micelle concentration (CMC), amphiphiles self-assemble to form aggregates. The self-assembly is driven by the attractive force between the hydrophobic blocks and the repulsive force between the hydrophobic and hydrophilic blocks.[14] The structure of the polymer assembly is based on the packing parameter, *p,* of the diblock copolymer. The unitless packing parameter, where v is the volume of the hydrophobic block (~ molecular weight of that segment), a_e is the equilibrium area per molecule at the aggregate surface, and l_0 is the length of the hydrophobic block, is defined as:

$$p = \frac{v}{a_e l_0} \tag{1}$$

Self-assembly will result in a spherical micelle when $p \leq \frac{1}{3}$, a cylindrical micelle when $p \leq \frac{1}{2}$, a bilayer vesicle when $p<1$, and a planar bilayer when $p\sim1$.[15] Upon amphiphilic

diblock copolymer self-assembly into polymersomes, two distinct regions exist: a hydrophilic core and a hydrophobic membrane as shown in Figure 1-2. This provides the ability for encapsulation of a wide variety of molecules in either one or both of the vesicle compartments. Polymersome membrane thickness can be controlled by varying the molecular weight of the diblock copolymer, making these carriers more tunable as compared to their natural analogues. Typical liposome membrane thickness is on the order of 3-5 nm, whereas polymersome membrane thickness is significantly greater, ranging from 10-50nm.[9] The ability to control membrane thickness allows for greater chemical versatility when designing the carrier system. Additionally, the fully synthetic nature of polymersomes greatly increases their stability in comparison to liposomes. Polymersome diameter can be controlled by the method of preparation and can yield vesicles with sizes ranging from the nanometer scale to the micron scale. While the formation of polymersomes and encapsulation within them has been extensively researched, a remaining challenge involves triggering release from the polymersomes.

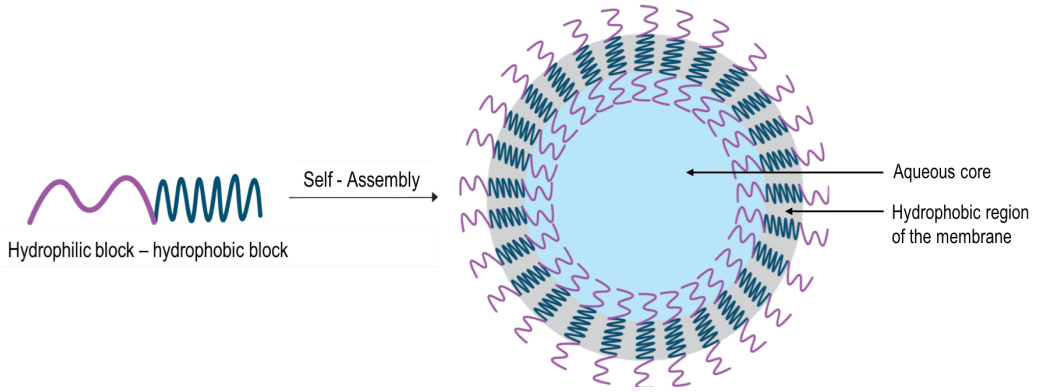

Figure 1-2: Polymersome self-assembly and structure

Stimuli responsive polymersomes

While much research has been directed towards the goal of efficient self-assembly and encapsulation within polymersomes, an equally important challenge is the ability to release the cargo encapsulated within them. These vesicles, known as stimuli-responsive polymersomes, are designed to initiate encapsulant release in response to a specific trigger. These triggers which initiate release are classified as either internal biological stimuli or external physical stimuli. Examples of internal biological stimuli include pH changes and redox potential, while examples of external physical stimuli include temperature, light, ultrasound, and application of a magnetic field. [16] While many examples exist of successfully triggering encapsulant release in response to stimuli, there is still much room for improvement in regards to precise spatiotemporal control as well as biological compatibility.

Physiological pH gradients within the body make pH responsive polymersomes ideal candidates for drug delivery carriers. The extracellular pH of a tumor and inflammatory tissues ranges from approximately 7.0-7.2 whereas normal tissues and blood have a pH ranging from 7.2-7.6. [17] Endosomes and lysosomes have even lower pH values at 5.0-5.5 and 4.5-5.0, respectively.[16] Ahmed et. al. synthesized one of the first pH-responsive polymersome systems to demonstrate effective shrinkage of tumor cells upon polymersome uptake and drug release.[18] Polymersomes are prepared from polyethylene glycol (PEG) – polylactic acid (PLA) and PEG- polycaprolactone (PCL) which are copolymers with hydrolysis -susceptible hydrophobic moieties. These polymersomes are loaded with hydrophobic drug paclitaxel (TAX) in the membrane and hydrophilic drug doxorubicin(DOX) in the

aqueous core [Figure 1-3A]. This dual-encapsulated drug cocktail was chosen in response to clinical studies showing that a mixture of both TAX and DOX leads to better tumor regression than either drug alone. [19] Upon exposure to conditions which mimic endosomal temperature and pH (37°C, 5.5), poration of the polymersomes and drug release is observed [Figure 1-3A]. Upon tumor uptake, a decrease in relative tumor size is observed over the course of 5 days [Figure 1-3C]. [18]

Figure 1-3 pH responsive polymersomes

(A) TAX and DOX loaded PEG-PLA polymersomes. (B) Percentage of pH responsive PEG-PLA polymersomes porated under different pH and temperature conditions. (C) Relative tumor size after DOX and TAX loaded polymersome uptake and release. Inset shows control studies. Reprinted with permission from reference [18]. Copyright 2006 American Chemical Society.

While pH responsive polymersomes have shown sufficient drug release and reduction in tumor size, there are limitations in the biological efficacy of these systems. One major challenge is the non-specific uptake and release from these delivery systems cannot mitigate the harsh side effects associated with chemotherapy

agents. Another major challenge associated with pH sensitive polymersomes is the lack of temporal control. The timescale for which the pH responsive carrier systems release drugs is difficult to control, as they are relying on the internal biological environment. Obtaining spatial and temporal release is of key importance in the development of drug delivery systems.

Redox potentials have also been demonstrated to initiate cargo release based on the difference between intracellular and extracellular environments. This is controlled by the concentration of glutathione, free cysteine, and free homocysteine, with glutathione (GSH, L-y-glutamyl-L-cysteinylglycine, a tripeptide) being the most prevalent reduced thiol source with concentrations greatly varying greatly between intracellular and extracellular environments. [21] Glutathione is especially elevated in breast, ovarian, head, neck, and lung tumor tissue compared to healthy, disease free tissues; thus, redox potential is an attractive trigger for targeted drug therapy. [22,21] One such example of a redox responsive polymersome system, demonstrated by Nahire et. al., uses the inherent thiol-based reducing agent concentration differential to trigger release in cancer cells. [20] Vesicles were

Figure 1-4: Redox potential triggered release from polymersomes

Encapsulant release from polymersomes upon varying concentrations of reducing agents, glutathione (green), dithiothreitol (purple), and cysteine (pink).

Reprinted from reference [20] with permission from Elsevier.

prepared from polymers polyethylene glycol and polylactic acid (PLA) linked with a disulfide bond (PEG-S-S-PLA). Upon exposure to various concentrations of several reducing agents (glutathione, dithiothreitol, and cysteine), degradation of the disulfide bond occurs, compromising the polymersome structure and subsequently releasing encapsulated cargo [Figure 1-4].[20] While this system is functionalized to target specific cells, achieving precise control over the delivery can be challenging as this system relies on internal reducing agent concentration gradients. This also can employ non-specific release within the body which leads to the side effects which targeted delivery seeks to circumvent.

Thermoresponsive polymersomes represent an example of an external stimuli responsive carrier system. Liu et. al. report the first example of a triblock copolymer polymersome system which allows for control over membrane permeability. [23] Polymersomes are self-assembled using poly(N-vinylcaprolactam) (PVCL) as the hydrophilic temperature sensitive blocks, and polydimethylsiloxane (PDMS) as the hydrophobic block. This polymersome

Figure 1-5: Temperature sensitive polymersomes

(a) % DOX release from polymersomes with varying PVCL block lengths at corresponding sensitive temperatures.
(b) Schematic illustrating temperature induced polymersome permeability.

Reprinted from reference [23]. Copyright 2015 American Chemical Society

system is considered a bolaamphiphile, which is defined as an amphiphilic molecule that has hydrophilic blocks at both ends of a sufficiently long hydrophobic chain. [23] PVCL undergoes a coil-to-globule phase transition from 36 to 50 °C depending on molar mass and concentration, and thus, temperature sensitivity can thus be conveniently controlled based on molecular weight. $PVCL_n$ – $PDMS_{65}$– $PVCL_n$ polymersomes were synthesized with n = 10, 15, 19, 20, 19, and 50 and loaded with DOX HCl in the aqueous core. The different PVCL block lengths chosen are responsive at physiological temperatures ranging from 37-42°C. Upon exposure to temperatures specific to the phase transition of the PVCL block(n), membrane permeability is induced [Figure 1-5b]. Figure 1-5a shows the percentage of Doxorubicin released as a function of time for each of the different polymersomes. For polymersomes at 25°C, the temperature at which the PVCL chain remains in its expanded coil phase shows very little DOX release. However, increasing the temperature to 42°C, where the PVCL chain is in its collapsed globule phase, polymersome permeability is induced and DOX is subsequently released. While temperature sensitive polymersomes have been shown to effectively release cargo, these systems still do not overcome current challenges with targeted drug delivery systems, specifically the lack of spatiotemporal control. The timescale required for thermo-sensitive release is on the scale of hours, which is not ideal for biological treatment.[23] Additionally, temperature sensitive drug release has limitations in terms of achieving spatial control. [24]

Ultrasonic triggering has also been successfully utilized to initiate cargo release from polymersomes. Ultrasound consists of pressure waves at frequencies greater than 20,000 Hz. Ultrasonic waves are absorbed relatively little by water, flesh,

and other tissues, making it an attractive trigger for drug delivery with the ability to achieve non-invasive, spatial control as a local stimulus.[25] One of the few examples to date involving ultrasound responsive polymersomes is reported by Chen and Du. [26] Polymersomes are prepared with PEO-b-P(2-(diethylamino)ethyl methacrylate(DEA)-*stat*-(2-(tetrahydrofuranloxy)ethyl methacrylate(TMA), rendering them dually responsive to ultrasound and pH. Ultrasound radiation of ultrasound responsive polymersomes is shown to disrupt polymersome self-assembly, releasing core encapsulants before reassembling into smaller vesicles. Figures 1-6b and 1-6c display a significant decrease in size as a result of ultrasonic exposure, measured using dynamic light scattering (DLS). As a control, solely pH responsive polymersomes, prepared with PEO_{43}-b-$PDEA_{41}$ and thus unresponsive to ultrasound radiation, and are subjected to the same conditions and show no significant change in size [Figure 1-6a]. This polymersome system effectively demonstrates response and cargo release upon ultrasound radiation.

Figure 1-6 Ultrasound and pH dually responsive polymersomes

DLS measurements of (A) pH responsive polymersomes, (B) ultrasound responsive polymersomes, and (C) dually responsive (pH and ultrasound) polymersomes subjected to ultrasound radiation at 180W and 40kHz. Reprinted with permission from reference [26]

There are, however, many challenges and problems associated with using ultrasound as a stimulus for drug delivery. One main limitation is that ultrasound is strongly attenuated by bone. Ultrasound radiation is also heavily scattered by blood at clinical diagnostic frequencies. These two factors limit the use of ultrasound radiation as a polymersome trigger for clinical drug delivery.[27]

While the aforementioned examples of internal and external triggers successfully demonstrate cargo release from polymersomes, these stimuli have various challenges and/or dangers associated with their use in vivo. System development has shifted away using internal physiological triggers due to the high probability of non-specific release, as it is well-known that achieving high precision is pertinent to mitigate the harsh side effects that exist in normal medicine. It is also of equal importance to achieve temporal control in targeted therapy, where the payload is delivered on-demand. Many of the current polymersome systems which are responsive to external stimuli release their encapsulants over the course of many minutes or even hours. This would not be ideal for treatment in dynamic biological systems, as the carriers may circulate away from the target site before effective local drug concentrations could be administered. Current research has now shifted towards utilizing light to trigger polymersome release as it has the potential to overcome many of the problems and challenges associated with existing stimuli responsive systems. [16]

Light as a stimulus

Light is a particularly attractive trigger for targeted drug delivery as it has the capability of achieving high spatiotemporal control.[28] At specific wavelengths, deep

tissue penetration can be achieved with minimal cellular damage. [29] Light responsive systems often do not require any additional internal reagents or triggers, giving them strong potential for on-demand drug delivery and clinical application. Light responsive polymersomes have attracted significant interest in recent years, resulting in a variety of systems which have been developed to disrupt vesicle structure and release encapsulated cargo in response to ultraviolet (UV) light and continuous wave(CW) irradiation. This has been achieved in a variety of ways, namely due to the incorporation of a photoresponsive polymer block, a photosensitive moiety, or the introduction of a photosensitizer.

One notable example of a UV-responsive polymersome system, shown by Mabrouk et. al., synthesize UV-responsive polymersomes through the use of the UV-sensitive liquid crystalline(LC) polymer, polyethylene glycol-*b*-poly(4-butyloxy-2'-(4-methacryloxy)butloxy)-4'-(4-butyloxybenzoyloxy)azobenze)(PEG-*b*-PMAazo444) where the incorporated azobenzene group undergoes a *trans*-to-*cis* conformational change upon UV exposure. This isomerization induces a nematic to isotropic transition in the LC polymer resulting in a conformational change of the chain from a rod to a coil [30] [Figure 1-7].

Figure 1-7: UV-sensitive polymersomes

Schematic illustration of polymersome membrane conformation. In the absence of UV light, the copolymer has a rod-like conformation. Upon exposure to UV light, the polymer undergoes a conformational change to the coil phase, resulting in an instantaneous destabilization, and burst of the vesicle. Reprinted from reference [30] Copyright 2009 National Academy of Sciences.

This conformational change causes a rapid destabilization of the vesicle structure, thus releasing any encapsulants. Upon UV exposure, polymersome membrane destabilization and vesicle bursting occurs instantaneously. Figure 1-8 displays bright field images of polymersomes before and following UV illumination. Vesicle structure begins to be affected 50 ms after UV exposure, and after 280 ms, the polymersome has burst.

While this immediate bursting and release of encapsulants would prove very effective as a drug delivery system in terms of temporal control, UV light is not ideal for use in vivo due to the limited tissue penetration and associated phototoxicity. [31] [32]

Figure 1-8: Bright field images of UV responsive polymersomes

Images pre and post UV illumination. Visible structural changes are observed 50ms post UV exposure. Polymersome structure is fully compromised 280 ms after UV illumination. Scale bar represents 5μm. Reprinted from reference [33] Copyright 2009 National Academy of Sciences.

Shifting away from the use of UV light as a stimulus, there are some notable examples of light-responsive polymersome systems which utilizes visible light to initiate release. The Dmochowski group reports a photoactive polymersome system which is formed by dually encapsulating a protein, horse spleen apoferritin (HSAF) in the aqueous core and a meso-to-meso ethyne-bridged bis[(porphinato)zinc] (PZn_2) chromophore in the hydrophobic membrane of micron-scale polyethylene oxide$_{30}$(PEO)-polybutadiene$_{46}$ (PBD) vesicles.[34] PZn_2 chromophores absorb across the near-UV and visible spectrum with a strong near-IR absorbance feature. As most of the absorbed energy absorbed by PZn_2 is dissipated as heat, local disruptions to the self-assembly can result.[34] Thus, the incorporation of PZn_2 into the polymersome hydrophobic membrane induces sensitivity to light of near-UV to near-IR wavelengths. Figure 1-9 displays confocal micrographs of polymersomes loaded with (A) PZn_2 and BODIPY-FL-labeled HSAF and (B) PZn_2 and unlabeled HSAF. As shown in

Figure 1-9:Light responsive PZn_2 polymersomes

(A) Confocal microscopy images of a polymersome loaded with PZn_2 (purple) and fluorescently labeled HSAF(green) in the hydrophobic membrane. Polymersome is imaged with 488 and 543 nm lasers simultaneously over a period of approximately 5 minutes.
(B) Confocal microscopy images of a polymersome loaded with PZn_2 (purple) and unlabeled HSAF in the membrane. Vesicle is imaged with three lasers simultaneously (488, 543, 633 nm). Reprinted from reference [34]. Copyright 2009 American Chemical Society.

Figure 1-9A, a single polymersome was simultaneously irradiated with 488 and 532nm lasers for approximately 5 minutes. The vesicle in Figure 1-9B was simultaneously irradiated with 3 lasers (488, 543, and 633nm) for ~5 minutes. Both sequences show polymersome structural changes with increased exposure time. Additionally, Griepenburg et. al. reports a similar system where PZn_2 is used as a photosensitizer for nano-scale polymersomes, which are shown to be responsive to visible light.[35]

The use of visible and NIR wavelengths circumvent the problems associated with UV light in terms of phototoxicity and also increase the potential for tissue penetration depth. However, the long irradiation times which are required to stimulate polymersome rupture can induce local heating effects which would prove problematic in a biological system. Additionally, circulation of the carrier away from the target could occur within this timeframe, limiting spatiotemporal control. These long irradiation times are typically associated with the use of continuous wave irradiation, and thus it is important to move away from this for systems requiring precision delivery.

Light delivery methods

Light is commonly delivered by a laser as they are the brightest, most coherent, and monochromatic source of light. Depending on the type of laser, light emission can be either continuous or pulsed irradiation. There are key differences between these two operational modes, which typically results in one mode being more suitable for a particular application than the other. Both modes have found use in multiple applications in various biomedical areas such as surgery, drug

delivery, cosmetic treatment, and dental procedures.

To provide some background, "laser" is an acronym for the phrase "Light Amplification by Stimulated Emission of Radiation".[37] Light emission is spatially coherent in nature, allowing for the output to be in the form of a highly collimated beam of light. The emission is also typically quasi-monochromatic (i.e. the beam has a central wavelength and a narrow spectral width).

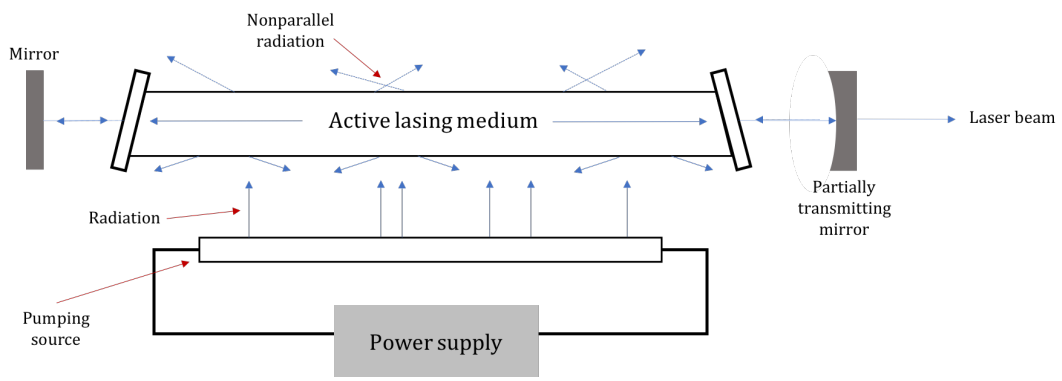

Figure 1-10: Schematic representation of the optical gain stage of a conventional laser system [36]

Note, in this case the rod ends are cut at the Brewster's angle to minimize reflection of p-polarized light.

Figure 1-10 shows a schematic representation of a conventional laser cavity. The active lasing (gain) medium can be a variety of different materials, in differing physical states, and is used to categorize the types of lasers. Examples include: gas, vapor, liquid, solid-state, and semiconductor lasers. Solid-state lasers, which are the most common type found in the sciences, consists of a crystal rod, such as ruby or neodymium:yttrium aluminum garnet (Nd:YAG). This crystal is optically excited by a pump source which itself can be another laser (often a semiconductor laser).[36] Figure 1-10 also serves to illustrate the fact that lasers function as a light oscillator, where

the produced radiation is passed back and forth through the gain medium by way of the end mirrors, where one is a 100% reflector while the other is only a partial reflector. Each passage through the gain medium generates additional photons which leads to large amplification. The mechanism of laser amplification is the contribution of the actions: pumping(absorption), spontaneous emission, and stimulated emission.[36] In the case of solid-state lasers, pumping is the absorption of light, produced by the pump source, within the gain medium (i.e. the crystal) and subsequent electronic excitation to a higher energy state, possibily emitting a photon, or the transition back to the ground state can be initiated by an incident photon which is called stimulated emission. Stimulated emission results in the release of two photons with identical properties, i.e. same energy (wavelength), phase, and direction.[38] Absorption competes with stimulated emission, so in order for the process to result in light amplification, there must exist population inversion, i.e. more electrons in the excited state than the ground state.[38] Due to this inversion, stimulated emission predominates absorption, causing a net gain in emitted photons, and thus the emission of a bright beam of light. Naturally, the output wavelength is determined by the energy difference between the excited state being pumped and the ground state of the crystalline medium. [36]

As stated previously, lasers can be operated in one of two exclusive modes: continuous wave (CW) or pulsed. CW lasers generate a single, uninterrupted beam of light which has a constant, stable output, as a function of time. The aforementioned examples of light responsive polymersomes, utilized CW irradiation to trigger polymersome release. CW irradiation is often chosen due to the broad availability of

such lasers in research labs. While it is shown to be effective in some polymersome systems, future clinical efficacy and safety can be impacted due to long laser irradiation times. [39]

Pulsed lasers, as the name suggests, emit light in the form of optical pulses by introducing additional optical components in the laser cavity. As the beam now has a temporal profile, both pulse duration and repetition rates are important parameters. As compared to CW lasers, pulsed lasers can achieve much higher peak power. Pulsed lasers are typically classified by their pulse duration, specifically nanosecond (10^{-9} s), picosecond (10^{-12} s), and femtosecond (10^{-15} s). Initially upon their discovery, laser pulses were approximately 10 ms long with a peak power of kilowatts. The *Q-switching* technique reduced the pulse duration from milliseconds to nanoseconds achieving peak powers of megawatts. The *modelocking* technique reduced the pulse duration from nanoseconds to picoseconds and increased the peak power up to gigawatts. Finally, femtosecond pulses were produced using *colliding-pulse modelocking.* [40]

Femtosecond pulses, which are considered ultrafast, have contributed to the advancement of various fields due to their ability to achieve nonlinear interactions.[41] Examples include: (1) two-photon excitation microscopy, where the fluorescent dye is excited by a wavelength greater than the emission wavelength through the nonlinear process of multiphoton absorption. Such absorption is extremely dependent on the photon intensity at the excitation spot and as such, emission is highly localized. This results in two photon excitation microscopy having high image resolution comparable to, and in some instances superseding, confocal microscopy.

[42, 43] (2) *fs* laser-assisted corneal flap surgery utilizes a strongly focused ultrafast *fs* beam to induce multiphoton absorption in the transparent corneal tissue of the eye which induces breakdown within a narrow plane within the eye. Benefits include more consistent flap thickness and morphology with improved patient recovery time.[44]

Metal nanoparticles as photosensitizers

Metal nanoparticles (NPs) have attrached tremendous research interest in recent years due to the unique properties they exhibit in comparison to the bulk metal. In particular, noble metal nanoparticles, such as AuNPs, have been of primary focus of interest due to their ability to exhibit a localized surface plasmon resonance (LSPR). Excitation of the LSPR is characterized by the presence of a pronounced absorption band in the visible/NIR range of the electromagnetic spectrum. This is brought about when the oscillating electric field of incident light induces a collective oscillation of the free, conduction band electrons in the metal nanoparticle [Figure 1-11].[45]

In the presence of an external electric field, the electron cloud of the metal will be displaced giving rise to charge separation and the

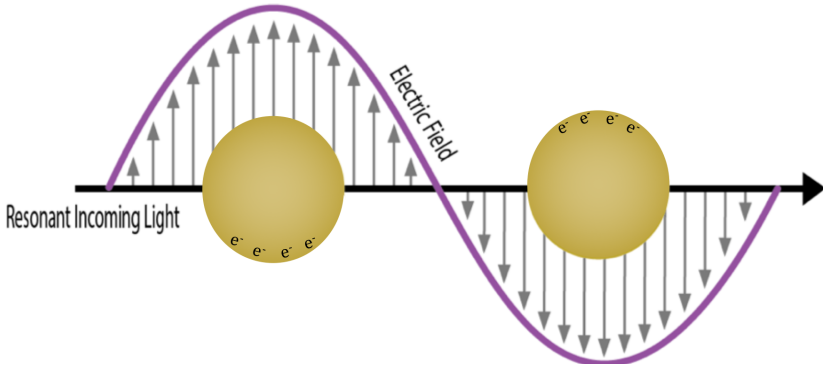

Figure 1-11: Localized surface plasmon resonance (LSPR) of metal nanoparticles

formation of a dipole aligned with the electric field. When the external field is removed, a Coulombic restoring force is responsible for pulling the electrons back to equilibrium in an oscillatory nature. Quantization of this motion gives rise to a plasmon that can be resonantly excited by an incident electromagnetic wave of a frequency (wavelength) matching the plasmonic mode. Such extinction generates a strong field enhancement in the vicinity of the particle and is accompanied by strong absorption of light at the resonance frequency. The position of the LSPR can be tuned throughout the visible – NIR spectral region by altering the nanoparticle composition, size, and shape. Figure 1-12 displays the characteristic red shift of the LSPR band for spherical AuNPs with increasing size. Larger nanoparticles have a smaller restoring force, thus resulting in in oscillations of lower frequency, hence the LSPR occurs at longer wavelengths.

Another method of tuning the LSPR is through altering the nanoparticle composition. For example, a 20 nm gold nanoparticle has a LSPR ~520 nm, however, 20 nm silver NP has an absorption maximum at ~ 420 nm. Additionally, gold nanoparticles with a rod like morphology, known as gold nanorods (AuNR), have two absorption bands due to their asymmetrical shape. The lower wavelength peak is associated with extinctions along the short-axis while the higher band is from oscillations along the long-axis. The LSPR mode can exist out into

Figure 1-12: LSPR shift for AuNPs [46]

Figure 1-13: Extinction spectra for AuNRs

(a) extinction spectra for AuNRs with increasing aspect ratios (left to right). (b-f) corresponding TEM images. Reprinted from reference [47]. Copyright 2016 Faraday Discussions of the Chemical Society.

the NIR region of the spectrum. Figure 1-13 shows the extinction spectra for various aspect ratio AuNRs. Nanoparticles with the ability to strongly absorb in the NIR are of great interest in drug delivery applications, because the biological window falls within this region [Figure 1-14]. This biological region represents a range of wavelengths that are minimally scattered and/or absorbed by blood, skin, and fat, therefore, allowing for deeper tissue penetration. [29]

Figure 1-14: Window for in-vivo imaging.

Light absorption and scattering in skin, fat, and oxygenated and deoxygenated whole blood. Adapted from reference [29]Copyright 2009 Nat Nanotechnol.

Nanoparticles are a great candidate for photosensitizing polymersomes due to not only their tunable LSPR, but also for the photothermal and/or photomechanical response they display upon excitation. Light interaction with a nanoparticle can occur through either absorption or scattering, and these processes are greatly enhanced for wavelengths at or near the LSPR. The degree to which absorption dominates scattering is, in general, size dependent. Mie scattering predicts that scattering/absorption cross-sectional ratio is ~0.65 for 80 nm AuNPs and decreases rapidly to ~0.05 for 40 nm particles. Below 30 nm, absorption completely dominates the extinction coefficient for AuNPs.[48] This works in the favor for the use of AuNPs as photosensitizers in polymersomes, as absorption is the preferred interaction and smaller particles are more easily encapsulated within the bilayer membrane.[49]

Once a particle is excited, the subsequent relaxation pathway will determine the fate of the particle and the response produced in its surroundings. These processes are governed by the pulse fluence and duration. For the case of low fluence and long pulse durations (>ns), the particle will heat to a temperature below its melting point, resulting in minimal change to its shape and moderate heating of its surroundings, with the possible formation of a vapor layer. For low to medium fluences and short pulse durations (ns – 10's ps), the particles will experience a rapid temperature increase that can include a phase change in the particle, from solid to liquid and/or vapor, and a similar response in its surroundings as thermal transport from the metal to the liquid surroundings can trigger a shockwave and expansion of a large vapor bubble. In the case of ultrafast pulses (*fs*), strong repulsive forces brought about by ionization can fragment the particle before that lattice has time to

melt, thereby delocalizing the thermalization process and the formation of a vapor in favor of more energetic process, such as breakdown, which results in a strong photomechanical response. [50]

Amstad et. al. report thermo- and photo-responsive polymersomes through the incorporation of AuNPs. [51] Polymersomes are prepared by incorporating 9 nm hydrophobic functionalized AuNPs into the bilayer membrane formed from polyethylene glycol-*b*-polylactic acid (PEG-*b*-PLA) with varying weight percent of a temperature responsive diblock copolymer, poly(N-isopropylacrylamide)-*b*-poly(D,L-lactide-co-glycolide) (PNIPAM-*b*-PLGA).[51] Polymersomes with and without AuNPs were irradiated with CW laser at 488,532, and 633nm [Figure 1-15]. Over the course of 50 minutes, the percent of intact polymersomes was tracked with confocal

Figure 1-15: Thermo- and photo-responsive polymersomes

a) schemactic representation of the 2 types of polymersomes prepared with(green) and without(red) AuNPs in the hydrophobic membrane.

b) percent of intact polymersomes upon continuous laser irradiation with 488, 532, and 633 nm.

c) Representative confocal micrographs of polymersomes with (green) and without (red) AuNPs initially and following laser irradiation a 488, 532, and 633 nm. Reprinted with permission from reference [51]. Copyright 2012 John Wiley and Sons.

microscopy [Figure 1-15c], and it was shown that 0% of the polymersomes with AuNPs in the membrane remained intact after 25 minutes of irradiation.

For polymersomes lacking AuNPs in the membrane, 80% of the vesicles remain intact following 60 minutes of laser irradiation [Figure 1-15b]. While this confirms that the polymersomes are in fact photosensitized by the incorporated AuNPs, the long irradiation times and requirements of the thermo-responsive PNIPAM-b-PLGA block limits the versatility of this system.

Conclusion

Stimuli-responsive polymersomes are promising tools for drug delivery, given their tunablity, stability, and dual-compartment encapsulation capabilities. To maximize this potential, light can be used as a stimulus to achieve precise spatiotemporal control over encapsulant release. Prior examples, as discussed, have limitations primarily due to wavelength selection and long irradiation times. The work presented in this thesis provides a solution to these limitations through the use of ultrafast laser irradiation and the incorporation of nanoparticles as photosensitizers. The system presented herein is the first example to date utilizing such methods and is a promising tool for future use in delivery applications.

Chapter 2 : Micron-scale system

Introduction

The work presented herein describes the design of "plasmonic polymersomes", a carrier system responsive to single pulse, *fs* irradiation via the incorporation of AuNPs into the hydrophobic region of the vesicle membrane. Figure 2-1 displays a schematic representation of our plasmonic polymersome system where a single *fs* pulse with a wavelength on resonance with the LSPR of the nanoparticle induces cargo release from the polymersome. The encapsulation of hydrophobic, spherical AuNPs into the membrane renders this system responsive to 532 nm, however, this release wavelength can be tuned into the NIR region of the spectrum with the incorporation of gold nanorods (AuNRs).

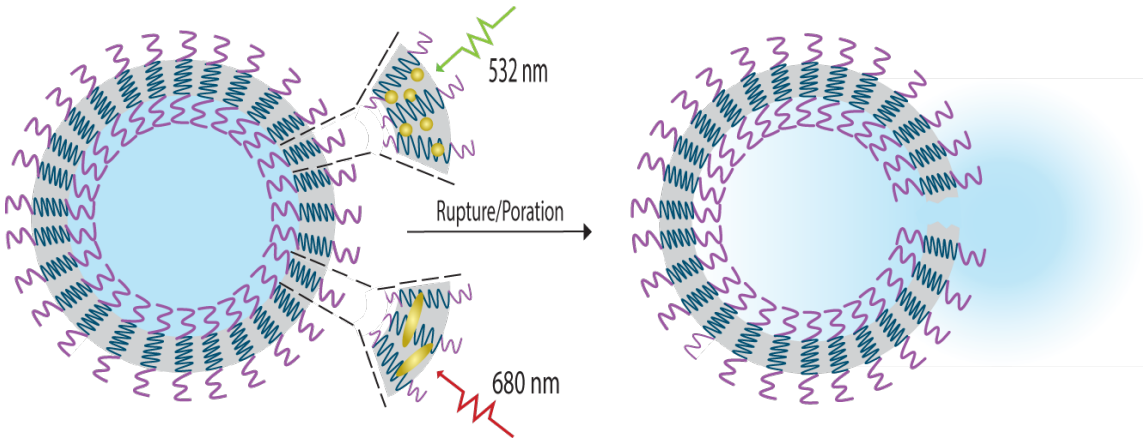

Figure 2-1: Schematic representation of a plasmonic polymersome

This chapter will discuss the plasmonic polymersome system on the *micron-scale*. The design and implementation of the micron-scale system is advantageous due to the ability to visualize and image with optical microscopy, thus making single vesicle experiments feasible. While vesicles in this size regime are too large for most

biological applications, experimentation on this scale provides an insightful visual representation which is not possible on the nano-scale.

As mentioned in Chapter 1, dual-encapsulation within both the hydrophilic and hydrophobic regions of the polymersome can be achieved due to the hyperthick bilayer membrane. Figure 2-2 contains fluorescent images of micron-scale polymersomes. Figure 2-2A shows a representative image of polymersomes with Nile red fluorophore singly-encapsulated in the hydrophobic region of the membrane. Figure 2-2B shows the fluorescent overlay images of polymersomes dual-encapsulated with Nile red in the membrane and Fluorescein Isothiocyanate-dextran (FITC-dextran) in the aqueous core. This image allows for visualization of the two

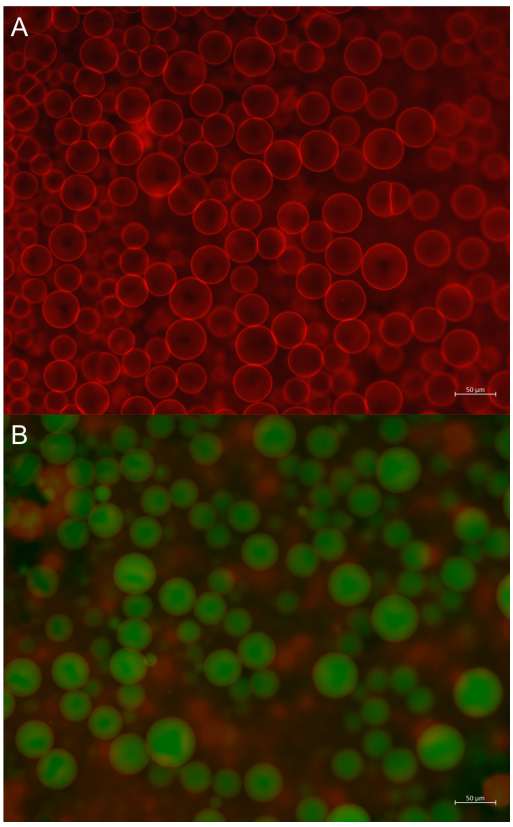

Figure 2-2: Fluorescence microscopy images of micron-scale polymersomes [52]

Polymersomes are prepared via gel rehydration and remain attached to the surface of an agarose coated coverslip. Scale bar represents 50μm.

A) Representative image of polymersomes with Nile Red fluorophore in the hydrophobic membrane.

B) Polymersomes with Nile red fluorophore in the hydrophobic membrane and FITC-dextran fluorophore in the hydrophilic core. Overlay of fluorescent images allows for visualization of the two distinct vesicle compartments.

distinct compartments and confirms the ability to dual-encapsulate within the vesicles.

Initial experiments sought to confirm the ability of AuNPs to photosensitize the polymersome and to determine the laser pulse energy required to initiate complete rupture of a single polymersome. The unique experimental designs requiring laser pulse delivery and subsequent imaging of polymersomes is made feasible through a custom *fs*-microscope system where the laser is steered directly into the upright microscope and focused through the objective, aligning the irradiation and imaging paths. Figure 2-3 displays an initial result where complete rupture of a polymersome is observed following a single *fs* pulse. Polymersomes were prepared with AuNPs in the hydrophobic region of the membrane and upon a single *fs* (532 nm, 83 nJ) pulse, complete vesicle rupture is observed. As a control, polymersomes without AuNPs in the hydrophobic membrane were subjected to identical *fs* irradiation and it was shown that ~5x the energy was required to initiate

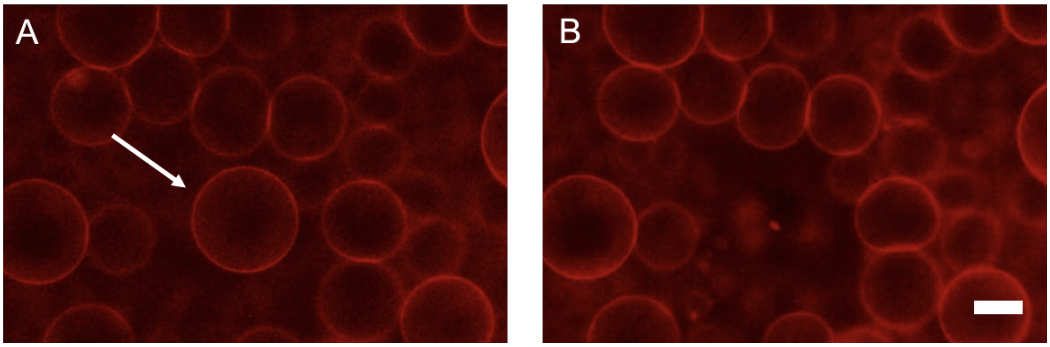

Figure 2-3: Complete rupture of an AuNP loaded polymersome [52]

A) Polymersome with 0.066% (w/v) AuNPs encapsulated in the hydrophobic region of the membrane prior to laser irradiation.
B) Image of irradiated polymersome immediately following an 83 nJ, 532 nm *fs* pulse. Complete rupture of the irradiated polymersome is observed, while the surrounding, non-irradiated vesicles remain intact. Scale bar represents 20 μm.

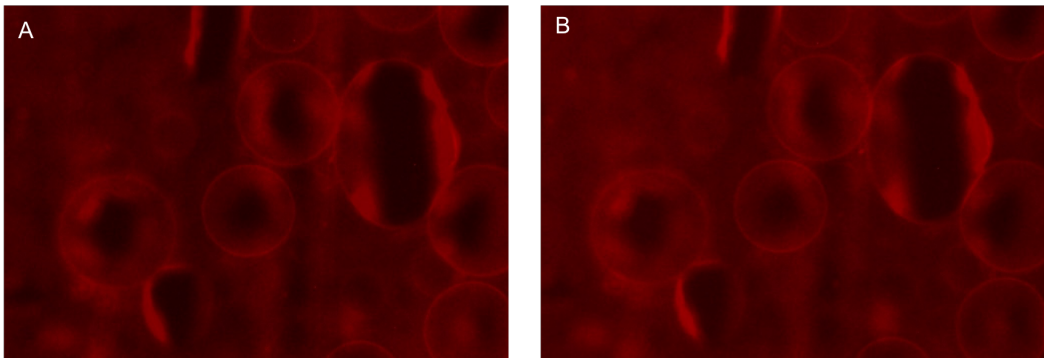

Figure 2-4: Polymersomes without AuNPs as a control [52]

Polymersomes prepared without AuNPs in the membrane were subjected to identical irradiation which did not result in rupture.

rupture [Figure 2-4]. It follows that complete vesicle rupture would immediately release core encapsulants into the surrounding environment.

FITC-dextran can be encapsulated within the aqueous lumen of the polymersome, as representative hydrophilic cargo, to track release after irradiation. Interestingly, irradiation with a reduced pulse energy results in poration of the vesicle, as opposed to complete rupture and a temporal diffusion of encapsulated

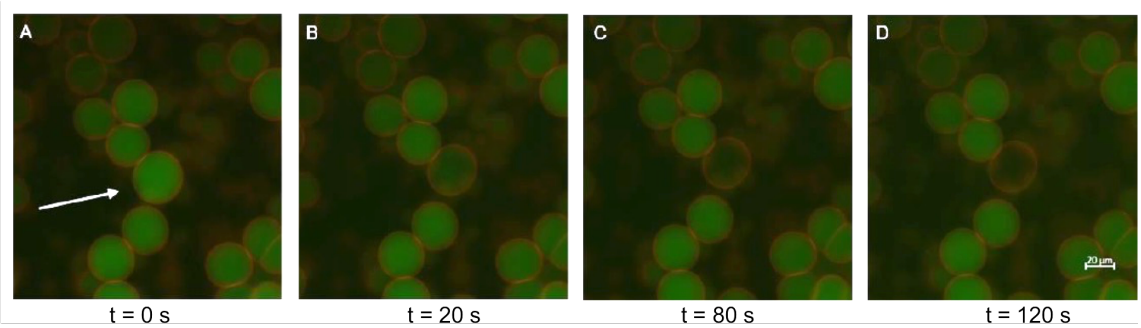

Figure 2-5: Time series of cargo release from a polymersome containing AuNPs in the membrane [52]

Time series of overlay images of polymersomes with 0.066% (w/v) AuNPs, Nile red (membrane), and FITC-dextran (core). A single vesicle, indicated by the white arrow, was imaged before (A) and post irradiation (B-D) with a single fs pulse (59 nJ, 532nm).

cargo is observed as shown in Figure 2-5. These polymersomes also contain Nile red as a membrane fluorophore and AuNPs for photosensitization. Figure 2-5A shows an image of the polymersome before irradiation and the white arrow points towards the individual vesicle subjected to a *fs* pulse. Following delivery, the vesicle is imaged every 10 seconds over the course of 2 minutes. In panels B-D, a decrease in the fluorescence intensity in the core can be observed, while the membrane remains visually intact. It is important to note that the other vesicles in the frame which were not irradiated, remain unaffected. The decrease in fluorescence intensity can be attributed to the formation of pore(s) within the polymersome membrane facilitating FITC-dextran release. Using ImageJ, the fluorescence intensity inside of the vesicle can be quantified and plotted as a function of time.

Pulse energy plays a role in the cargo release rate as shown with the trend in Figure 2-6, where decreasing the pulse energy changes the release kinetics as well as the overall amount of cargo delivered. Irradiation with a ~200 nJ pulse results in approximately 100% cargo release (blue), while a 32 nJ pulse results in only 10% release (purple). Mid-range cargo release (30-50%) can be obtained upon irradiation with energies ranging from 40-100 nJ, respectively. A control experiment was conducted where polymersomes lacking AuNPs were subjected to irradiation at the upper energy threshold for poration. Irradiation of this control sample with a 200 nJ pulse, resulted in negligible release from the polymersomes (green), which corresponds to the lower energy threshold for vesicles containing AuNPs. The ability to tune the amount of cargo released from an individual polymersome greatly

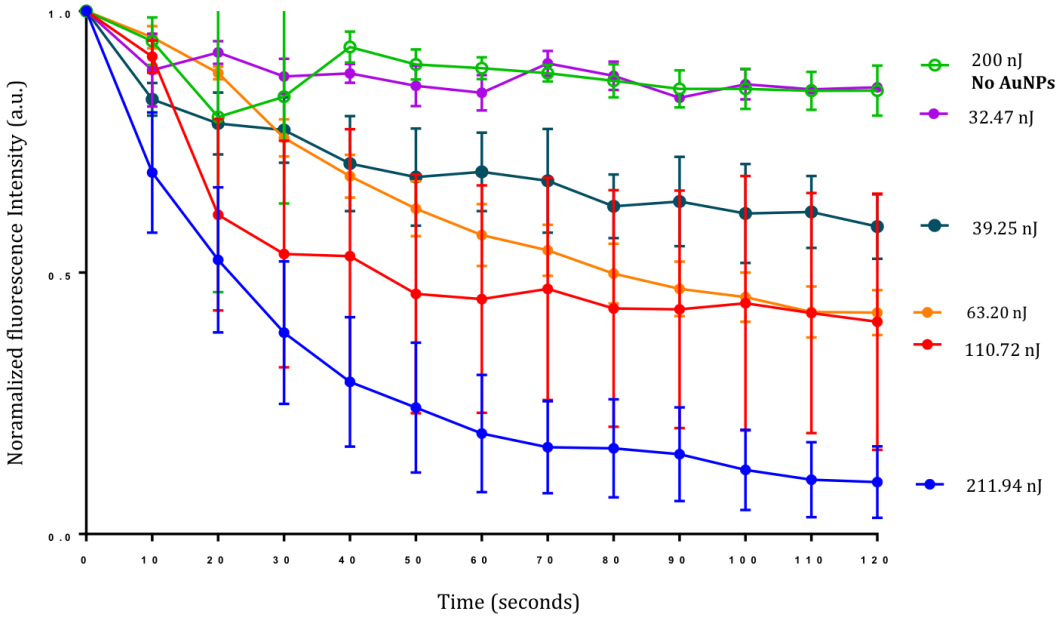

Figure 2-6: Cargo release from plasmonic polymersomes as a function of pulse energy [52]

increases the temporal control of this system, which is very promising for drug delivery applications.

The aforementioned experiments demonstrate the ability of AuNPs to photosensitize the polymersome system and mediate cargo release from the vesicles upon single pulse irradiation. Depending on pulse energy, polymersomes will either undergo complete vesicle rupture or membrane poration following single pulse irradiation with a wavelength on resonance with the LSPR of encapsulated AuNPs.

Methods and Materials

Micron-scale polymersome preparation

Polymersomes are prepared from the diblock copolymer, polyethylene oxide-b-polybutadiene (PEO_{20}-*b*-PBD_{35}) (Polymer Source, Quebec, Canada) by gel-assisted rehydration.[53] The diblock copolymer was dissolved in chloroform at a concentration of 5 mg/mL. To yield fluorescent vesicles, Nile red (Santa Crus Biotechnology, CA) was added to this organic copolymer solution to yield a final concentration of 0.5 mol%. Any other hydrophobic encapsulants, which are to be encapsulated in the polymersome membrane were included in this step. Therefore, 2-5 nm dodecanethiol functionalized spherical AuNPs (Alpha Aesar, Haverhill, MA) were added to the organic solution, in concentrations varying from 0.013-0.066% (w/v). The organic solution was spread atop an agarose coated coverslip. Agarose coated coverslips were prepared by spreading a 1% (w/v) agarose solution (Sigma Aldrich, MO) atop a 25x50x0.13-0.17 mm glass coverslip (Electron Microscopy Sciences) using a 1000 μL pipette tip. The agarose coated coverslips were then dried at 37° C to fully remove solvent from the agarose solution, resulting in a thin agarose film. Organic solution (55 μL) containing copolymer, nanoparticle, & Nile red fluorophore was spread on the agarose coated coverslip with the edge of a 12-gauge needle until organic solvent was visibly evaporated. The polymer coated coverslip was then dried under vacuum for at least 1 hour to aid in full removal of organic solvent. A custom-made polydimethylsiloxane (PDMS) well, prepared from Dow SYLGARD™ 170 Silicone Encapsulant Kit (Ellsworth Adhesives, WI), was adhered to the top of the polymer and

agarose coated coverslip. This allows for the rehydration buffer to be added and contained on top of the polymer coated agarose coverslip. The rehydration buffer (600 µL) was added to the well. At this step, any hydrophilic components to be encapsulated within the polymersome core were added to the rehydration buffer. The hydrophilic fluorophore, 3-5k molecular weight FITC-dextran (Sigma Aldrich, MO) was added to the 280 mM sucrose (Sigma Aldrich, MO) rehydration buffer to a final concentration of 0.5 mg/mL. Upon addition of the rehydration buffer and subjection to heat at temperatures ranging from 45-65° C for 45 minutes, polymersomes form and remain attached to the agarose gel. Figure 2-7 shows a schematic representation of the gel rehydration procedure.

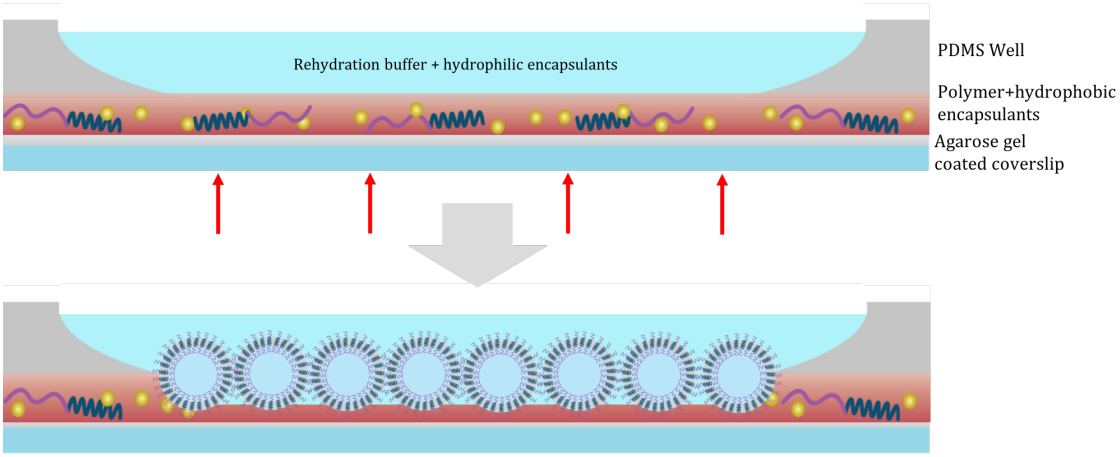

Figure 2-7: Gel-assisted rehydration method for polymersome preparation

Schematic representation of the polymersome preparation via gel-assisted rehydration. Upon addition of rehydration buffer and sample heating, vesicles form atop the agarose gel and remain attached to the surface.

Upon polymersome formation, the sample was imaged using a ZEISS Axio Examiner, fixed stage upright microscope. Figure 2-2 represents fluorescent images of polymersomes with (A) only Nile red fluorophore encapsulated within the polymersomes and (B) Nile Red and FITC-dextran encapsulated within the polymersomes to display dual encapsulation via overlaid images. A 20x (0.5 NA) dipping objective was used to image polymersomes within the aqueous solution.

For polymersomes prepared with encapsulants in the vesicle core, a buffer exchange was necessary to rid the sample of non-encapsulated components. Therefore, for polymersomes prepared with FITC-dextran, buffer exchange was required to minimize the sample of background fluorescence and facilitate imaging of the vesicle core [Figure 2-8]. Two pieces of tubing (0.012" IDx0.030"OD, Cole Parmer, IL) was inserted into the buffer solution through the sides of the PDMS well. Fresh buffer was slowly pumped into the well from one syringe pump, while the sample buffer containing free FITC-dextran was simultaneously pulled from the well using a second syringe pump. A gentle flow prevents vesicles from lifting off of the agarose gel and being removed from the sample well. As free FITC-dextran is removed from the sample well, encapsulated FITC-dextran fluorescence becomes distinguishable from the background and can be imaged within the vesicle core.

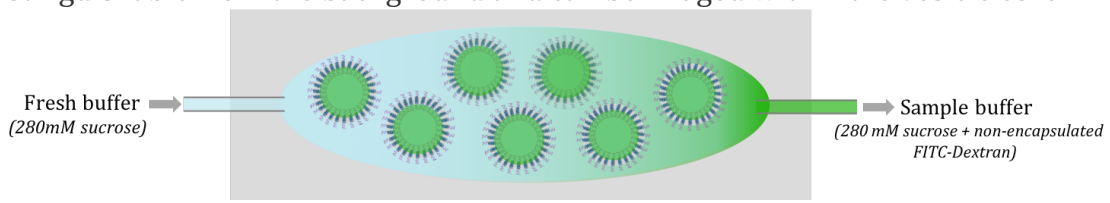

Figure 2-8: Top-down schematic for removal of non-encapsulated FITC-dextran

Buffer exchange is required for removal of non-encapsulated aqueous molecules. FITC-dextran is included in the hydration buffer for encapsulation within the polymersome core. Excess FITC-dextran which remains in the buffer must be removed in order to facilitate imaging of the polymersome core.

Polymersome Irradiation

Irradiation experiments were made feasible through a unique ultrafast laser system integrated with a multi-functional optical microscope. The laser is a femtosecond Ti:sapphire system pumping a fundamental wavelength of 800 nm. An automated optical parametric amplifier (OPA) allows for a broad selection of wavelengths between 240-2400 nm. The selected output (532 nm), is steered into the ZEISS Axio Examiner via a series of dichroic mirrors. The laser beam is focused through the microscope objective which allows for irradiation and subsequent imaging, as shown in Figure 2-9.

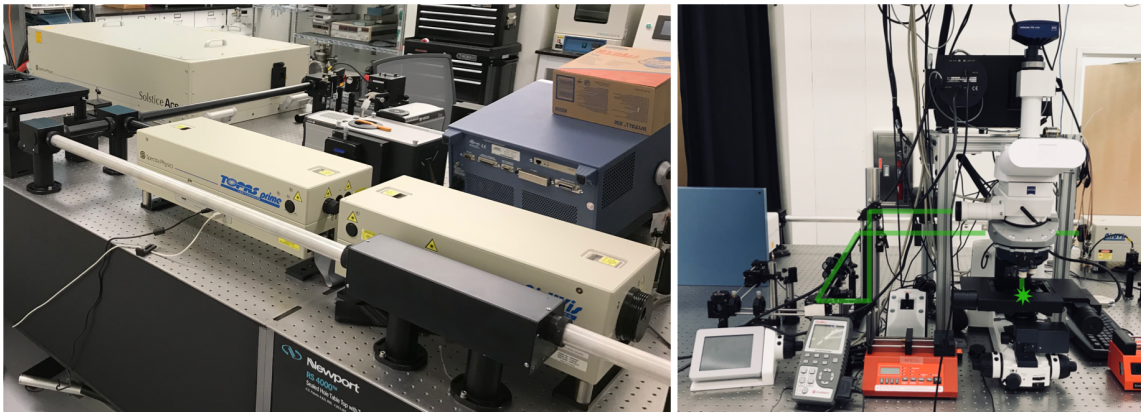

Figure 2-9: Ultrafast (*fs*) laser-microscope setup

Ti:Sapphire laser steered and focused into the Zeiss Axio Examiner upright microscope for irradiation and imaging studies. The beam path is represented by the green line.

The laser spot size was measured and adjusted through the 20x dipping objective to ensure the laser beam is focused directly on the polymersome to be irradiated. This spot size was measured through the use of a glass bottom petri dish where applied ink spots were submerged in water and irradiated. This allows for the identification of the precise beam location and spot size [Figure 2-10]. The pulse

energy was adjusted through the use of a laser beam attenuator and a series of neutral density filters. The pulse energy was measured using an energy meter placed on the microscope stage at the location of sample irradiation. No objective was used for this measurement, however, the 8% reduction in energy was taken into account when reporting pulse energy.

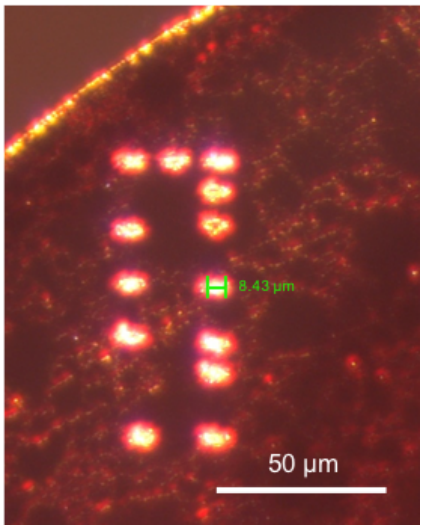

Figure 2-10: Pulse spot size determination

Spot size is measured using a glass bottom petri dish with a series of ink blots. Water is added to the dish to mimic experimental conditions. The ink is irradiated with a single pulse and the resulting damage spot is measured using the ZenPro software.

After laser beam alignment, spot size determination, and pulse energy optimization, the setup was ready for polymersome irradiation. To ensure consistency, a vesicle of optimal size was identified within the polymersome sample. This specific vesicle was focused and aligned to the precise position of pulse delivery and imaged prior to irradiation. A single pulse was delivered and the vesicle was immediately imaged. Imaging parameters were selected depending on the type of experiment (i.e. complete rupture or poration). For complete rupture, imaging following irradiation was manually captured and the vesicle membrane was imaged. However, in the case of polymersome poration, a time series was set up using the ZenPro software to image the polymersome every 10 seconds for 2 minutes following irradiation. In this case, either both the membrane and core, or solely the vesicle core was imaged. Imaging

the vesicle core, through the inclusion of FITC-dextran is necessary to quantify cargo release.

The ZenPro software was utilized for analysis of the polymersome time series following irradiation. A region of interest (ROI) was selected inside of the polymersome as well as a background region. The fluorescence intensity was measured for the chosen ROI and the background intensity was subtracted from this measurement. This was completed for both the images prior to and post irradiation. Note that the color histogram settings were matched across all images prior to measurements. Each measurement was normalized to the fluorescence intensity of the vesicle prior to irradiation and a percent decrease was calculated for each time series.

Results and Discussion

To study the effect of AuNP concentration on polymersome photo-response, vesicles with varying amounts of AuNPs encapsulated in the membrane were prepared. Polymersome samples with no AuNPs, 0.013%, 0.026%, 0.040%, 0.053%, and 0.066% (w/v) AuNPs were subjected to a single, 144 nJ *fs* pulse. The cargo diffusion rate and total release was quantified for each of the samples. There is a visible difference in the amount of fluorophore released from a minimally loaded sample with 0.013% AuNPs compared to a maximally loaded sample with 0.066% AuNPs, as displayed in Figure 2-11. For the minimally loaded sample there is negligible change in the fluorescence intensity in the vesicle core. However, for the maximally loaded sample, it is visually apparent that a significant amount of the

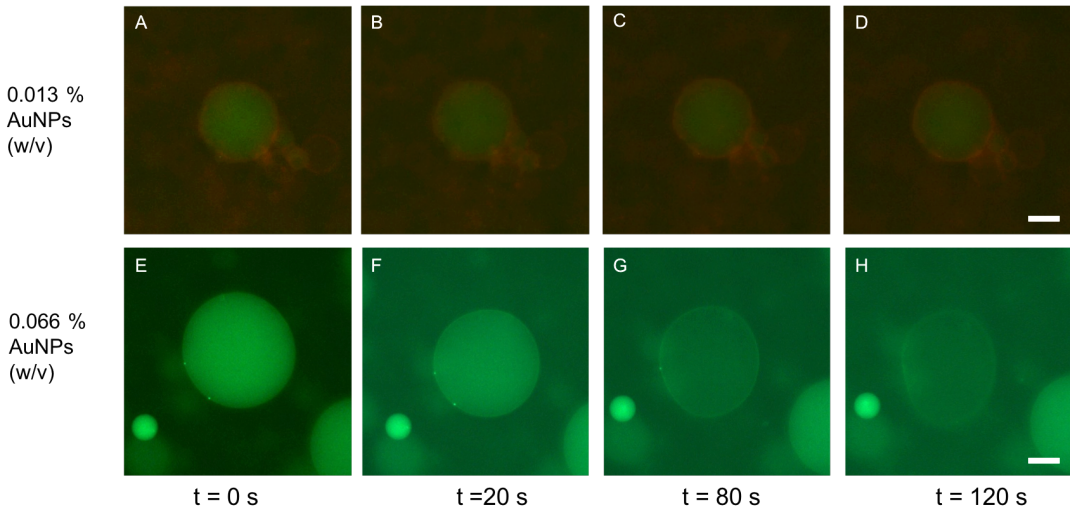

Figure 2-11: FITC-dextran diffusion from polymersomes with two different AuNP concentrations

Time series of polymersome poration and cargo diffusions for 0.013% (w/v) AuNPs (A-D) and 0.066% (w/v) AuNPs (E-H). Images A and E are taken before the polymersome is subjected to irradiation. After a single, 532 nm fs pulse (144 nJ), the polymersome is imaged every 10 seconds and select images are shown. The scale bar represents 10 μm.

fluorophore has diffused from the vesicle after 2 minutes, while changes in vesicle structure were noted to occur for a small population of vesicles. This structure change can be attributed to either a large membrane pore, or a large pore area to membrane surface area ratio; at some critical disturbance the vesicle is unable to self-heal and maintain structural stability. This occurrence was observed for a small population of vesicles at the upper boundary of AuNP encapsulation (0.066% (w/v)) where the initial poration leads to complete rupture [Figure 2-12].

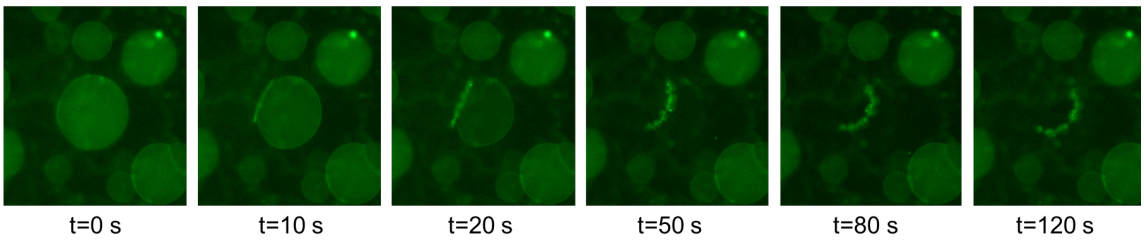

Figure 2-12: Polymersome poration leading to structural instability

A polymersome loaded with 0.066% (w/v) AuNPs is subjected to a single *fs* pulse (144 nJ). Upon irradiation, a large pore can be visually detected. Vesicle remains intact 10-20 seconds following the pulse, the vesicle structure is compromised after ~50 seconds.

A minimum of three vesicles from each different AuNP concentration were analyzed and the resulting average change in fluorescence intensity is plotted as a function of time, as shown in Figure 2-13. A pulse energy of 144 nJ was chosen as it falls between the two upper energy bounds shown in Figure 2-6; this was kept constant across each sample. As shown in Figure 2-13, irradiation of polymersomes with 0.066% (w/v) AuNPs results in 90-100% cargo release. As a control, polymersomes with no AuNPs were subjected to single pulse irradiation, and no cargo release is observed. As AuNP concentration is increased, there is a steady increase in the percent of cargo released from the vesicle following irradiation. In

summary, upon single pulse *fs* irradiation, polymersomes with 0.013%, 0.026%, 0.040%, and 0.053% AuNPs results in approximately 20%, 40%, 50%, and 75% cargo release, respectively. The importance of these results is two-fold. It is important to be able to effectively control the total amount of cargo released from an individual polymersome for future biological applications. However, in these systems it may be of equal importance to minimize the amount of incorporated AuNPs depending on future toxicity study results.

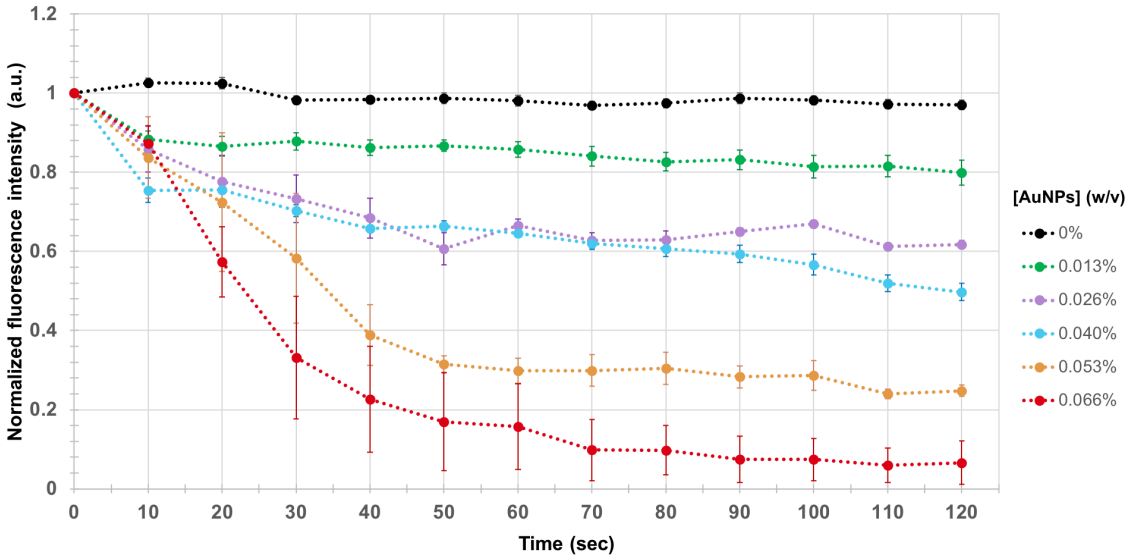

Figure 2-13: Polymersome cargo diffusion as a function of time with varying AuNP concentration

The fluorescence intensity inside of an individual vesicle is measured as a function of time following a single 532 nm, *fs* pulse (144 nJ). Each line represents the fluorescence decay in a ROI (3-4 replicates +/- SEM) with varying concentrations of AuNPs encapsulated within the polymersome membrane.

Conclusion

The inclusion of AuNPs within the polymersome membrane has been shown to successfully increase photo-responsiveness as compared to empty vesicles on the micron-scale. This was determined through a series of single vesicle experiments where parameters including pulse energy and AuNP concentration were varied. Complete vesicle rupture can be achieved with higher pulse energies, resulting in immediate release of hydrophilic cargo. However, upon a reduction in pulse energy, membrane poration and temporal cargo release results. Initial studies on maximally loaded polymersomes displayed a positive correlation between the pulse energy and the total amount of cargo released from the vesicle. A positive correlation was also observed between AuNP concentration and cargo release.

The timescale of these experiments is significant because control can be attained ranging from immediate and complete release to diffusion over the course of 2 minutes. This release timeframe is much shorter than those shown in prior examples utilizing CW irradiation.

Chapter 3 : Nano-scale system

Introduction

The work presented thus far has discussed results pertaining to the plasmonic polymersome system on the micron-scale. However, for in-vivo applications, carriers of the nanometer size regime are optimal in terms of distribution, biological fate, toxicity, and targeting ability.[5] Like micron-scale polymersomes, nanocarriers have large loading capacities, the ability to protect payload, the capability of achieving controlled release, and large surfaces which allow for ligand conjugation with the added benefit of sizes which are suitable for biological applications. Unless otherwise functionalized for cell uptake specificity, many nanocarrier systems will rely on the enhanced permeability and retention (EPR) effect to passively target tumor tissue. The EPR effect is a unique phenomenon of solid tumors where nanocarriers will distribute preferentially into tumor tissue through permeable tumor vessels and are then retained within the tumor bed due to reduced lymphatic drainage.[54] Once retained within the tumor tissue, drug release can be localized. As discussed in Chapter 1, there have been a variety of polymersome systems developed within the size range to utilize the EPR effect. Once localized within the tumor tissue, release from the polymersomes becomes a challenge. Therefore, it is of interest to scale our plasmonic polymersome system down to the nanometer size regime, specifically 80-200 nm in diameter, which has been deemed optimal for prolonged blood circulation and cell uptake. The use of ultrafast irradiation has the potential to trigger cargo release within the body with high spatiotemporal control while producing minimal unwanted effects.

This chapter will discuss the scale-down of the plasmonic polymersome system presented in Chapter 2, from the micron-scale to the nanometer size regime. One particular challenge associated with the scale down process is that nano-scale vesicles are unable to be directly visualized via optical and/or fluorescent microscopy, as is possible with micron-scale system. Thus, methodologies to determine polymersome disruption in colloidal solutions were developed. As shown in Figure 3-1, irradiation occurs for multiple nano-scale vesicles which intersect the laser beam. Additionally, the photoinduced mechanism by which AuNPs mediate polymersome rupture has been investigated by studying the fate of the excited nanoparticles upon vesicle disruption.

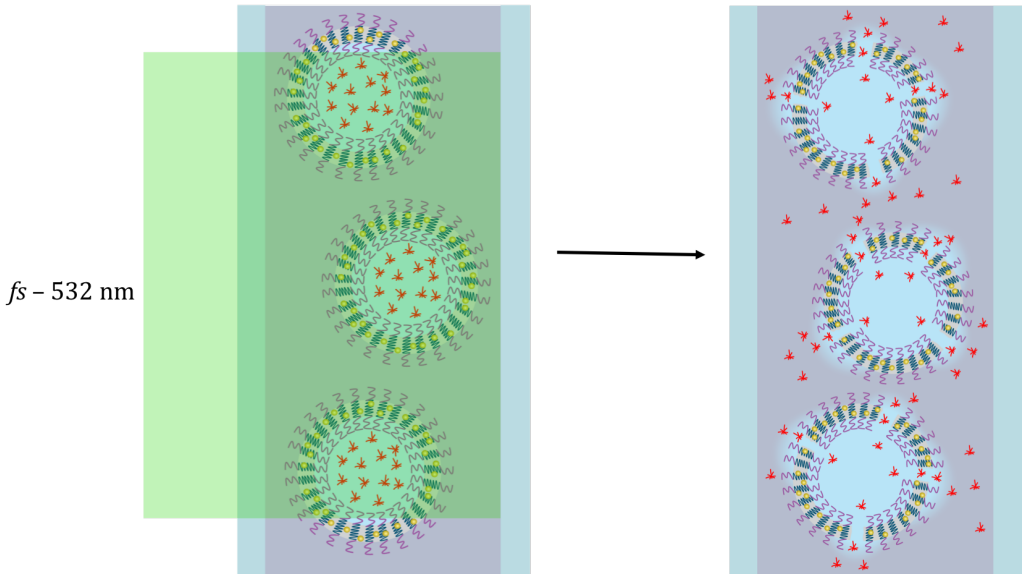

Figure 3-1: Graphical representation of the nano-scale plasmonic polymersomes

Materials and Methods

Nano-scale polymersome preparation

Nano-scale vesicles were prepared via the direct solvent injection method. The diblock copolymer, PEO_{20}-*b*-PBD_{35} (Polymer Source, Quebec, Canada), was dissolved in tetrahydrofuran (THF) (Sigma Aldrich, MO) to yield a concentration of 4 mg/mL, unless otherwise stated. Incorporation of various concentrations of AuNPs to the polymer-THF solution takes place by a resuspension process where 2-5 nm dodecanethiol functionalized, spherical AuNPs (Alpha Aesar, Haverhill, MA) suspended in toluene (2% v/v), were transferred to an open Eppendorf tube and gently heated to aid in solvent evaporation. The dry AuNPs were then re-suspended by adding 300 µL of the polymer-THF solution. To prepare for solvent injection, a stir bar was added to a glass vial containing 700 µL double deionized (DDI) (Milli-Q) water, and parafilm is used to seal the vial. The vial containing the aqueous solution was subjected to magnetic stirring. The copolymer-AuNP-THF solution was drawn into a 3 mL syringe and a 23 gauge 1" blunt tip needle with tubing (0.012" IDx0.030"OD) (Cole Parmer, IL) was attached. The organic solution was added dropwise (10 µL/second) to the aqueous solution under

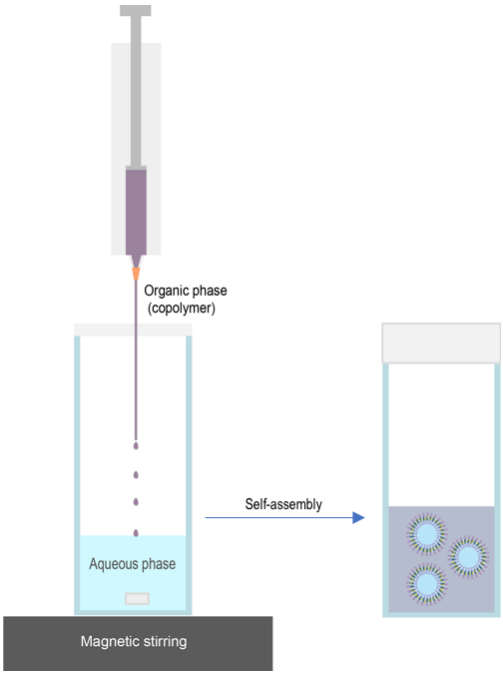

Figure 3-2: Direct solvent injection for nano-scale polymersome preparation

continuous stirring, which created an emulsion resulting in nano-polymersome self-assembly [Figure 3-2]. The polymersome sample was then filtered using a 0.45 μm PTFE syringe filter (GS-TEK, USA) to remove any large aggregates which possibly formed from copolymer and/or AuNPs which did not assemble into vesicular structures.

Size confirmation

Polymersome hydrodynamic diameter was determined via dynamic light scattering (DLS) using a Malvern Zetasizer. The polymersome sample was diluted (~33 fold), using DDI H_20, in a polystyrene cuvette to a final volume of 1 mL. The vesicle diameter was reported from the number distribution and the PDI was used to determine mono-dispersity for each sample.

Visualization with cryo-TEM

To visualize the nano-scale polymersomes, samples were prepared for cryogenic–transmission electron microscopy (cryo-TEM). To rid the sample of organic solvent (THF), polymersome samples were either subjected to size exclusion centrifugal filtration or dialysis. The polymersome sample was added to a 50K Amicon Ultra – 4 Centrifugation Filter (Millipore Sigma) and diluted to 5 mL. The sample was spun at 33K rpm for 10 minutes and repeated 3 times. For a gentler buffer exchange, Slide-A-Lyzer Dialysis Cassette G2 (20K, 3 mL) (Thermo Fischer Scientific, MA) were utilized. The sample was added to the cassette and spun in a 1L beaker against H_2O under refrigeration. Buffer was changed every 8 hours for 48 hours.

To prepare for cryo-TEM, the sample was vitrified using the FEI Vitrobot system. Samples were imaged using both the FEI Talos TEM (Rutgers-University Institute for Quantitative Biomedicine) and the FEI Titan Krios TEM (Arizona State University, Eyring Materials Center). Images were analyzed using ImageJ for polymersome diameter, membrane thickness, and nanoparticle measurements.

Studying the fate of the incorporated AuNPs upon polymersome irradiation

Polymersome samples were prepared with 0.05% (w/v) AuNPs. Preparation for electron microscopy was performed by drop casting samples onto a copper TEM grid containing a lacey carbon support structure and a thin carbon film. The nanoparticles were imaged by high resolution TEM (HR-TEM) using a 300kV FEI Titan system equipped with a Gatan 794 camera, achieving a maximum resolution of 0.205 nm (University of Virginia). Sample irradiation occurred by pipetting a colloidal polymersome solution into a custom-made PDMS well atop a glass slide, to which a small magnetic stir bar was added. The *fs* laser was aligned into the optical microscope as described in Chapter 2. The sample was then placed under the upright microscope and the dipping objective was lowered into the colloidal solution. While stirring, the polymersome sample was continuously irradiated with 532 nm *fs* pulses (80 nJ, 500 Hz) for 20 minutes. Following irradiation, the sample was drop-casted on a TEM grid, dried under vacuum, and imaged. Additionally, another sample was irradiated using the nanosecond laser (10.3 μJ, 500 Hz). The AuNP size distribution for both irradiated samples, as well as a non-irradiated sample, was determined using ImageJ.

Irradiation studies for nano-polymersomes

Polymersomes were prepared with 0.07% (w/v) AuNPs. The sample was diluted and transferred into a small volume quartz cuvette, with a 10 mm path length. Vesicle diameter was measured prior to any irradiation. The cuvette was then set on a vertical translation stage. The *fs* laser beam was directed through an attenuator and then focused using 100 cm plano-convex lens. The cuvette was placed 68.9 cm from the lens, resulting in a quasi-unfocused beam passing through the sample. Spot size was measured using a Newport beam profiler. The beam profiler was placed at the central position of the cuvette and a spot size, of 59.8 μm, was measured using ImageJ [Figure 3-3].

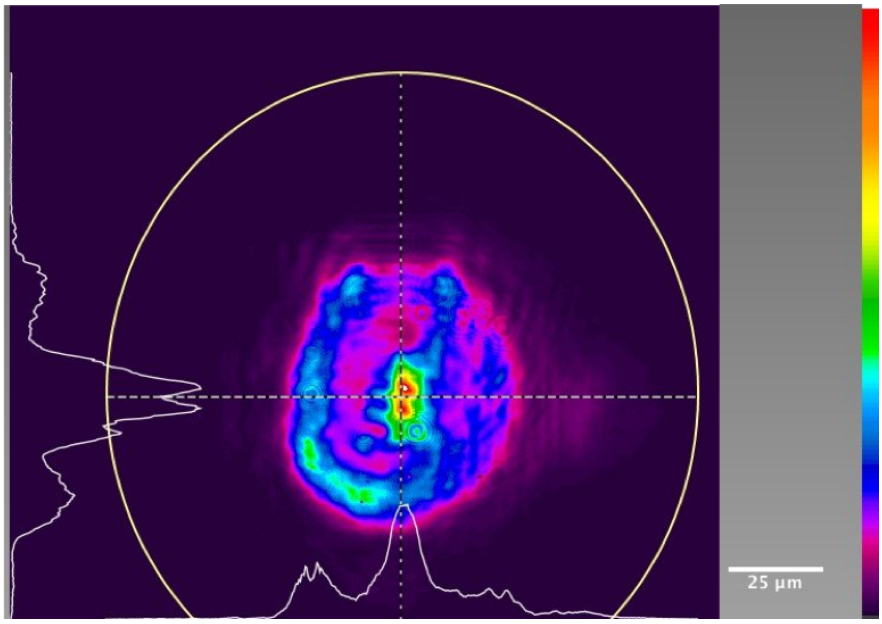

Figure 3-3: Beam profile for nano-scale polymersome irradiation

The sample was irradiated at 100 Hz with energies ranging from 35-188 μJ, for 20-180 seconds [Figure 3-4]. The stage was slowly translated during irradiation to ensure that uniform exposure to the entire sample. After irradiation, the sample was immediately measured using DLS. To study AuNP concentration dependence on

rupture time, polymersomes were prepared with 0-0.07% (w/v) AuNPs and subjected to irradiation at 180 μJ (100 Hz). The rupture point is determined via DLS measurements.

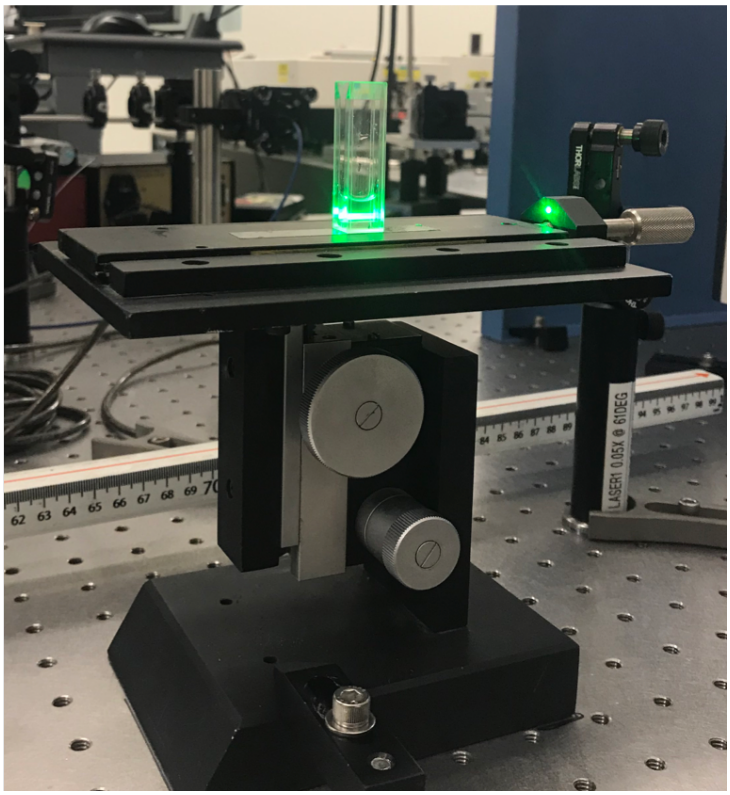

Figure 3-4: Irradiation setup for nano-scale polymersome irradiation

Image of polymersome sample under continuous, pulsed fs irradiation. The stage that the cuvette is mounted on is translated vertically to ensure uniform sample irradiation.

Surfactant experiments

Polymersomes were prepared with AuNP concentrations varying from 0-0.07% (w/v). Each polymersome sample was measured using DLS. Triton X-100 (Sigma Aldrich, MO) was added in small increasing increments, to a fresh polymersome sample, until rupture is observed. Due to viscosity of the surfactant, the sample was thoroughly mixed to ensure dissolution. Rupture is observed for Triton X-100 at final concentrations ranging from 2.5 mM-23 mM. This experiment was repeated with Tween 20 (Sigma Aldrich, MO), where polymersome rupture was

observed between final concentrations 1.3 mM - 42 mM. Three samples were each measured per concentration value using DLS for each addition of surfactant.

Results and Discussion

Nano-scale polymersome characterization

To study the effect of AuNP encapsulation on nano-vesicle self-assembly, various samples were prepared and the size was measured using DLS. Varying AuNP concentrations, ranging from 0-0.07% (w/v) were prepared and the size was measured. As shown in Figure 3-5, the encapsulation of AuNPs, at all prepared concentrations, does not significantly affect polymersome size. Polymersomes self-assembled with 0.01% AuNPs result in sizes ranging from ~80-120nm. Polymersomes with 0.07% AuNPs result in diameters ranging from ~90-130nm, which is consistent with the size range of polymersomes self-assembled with no AuNPs, which ranges from ~85-120 nm.

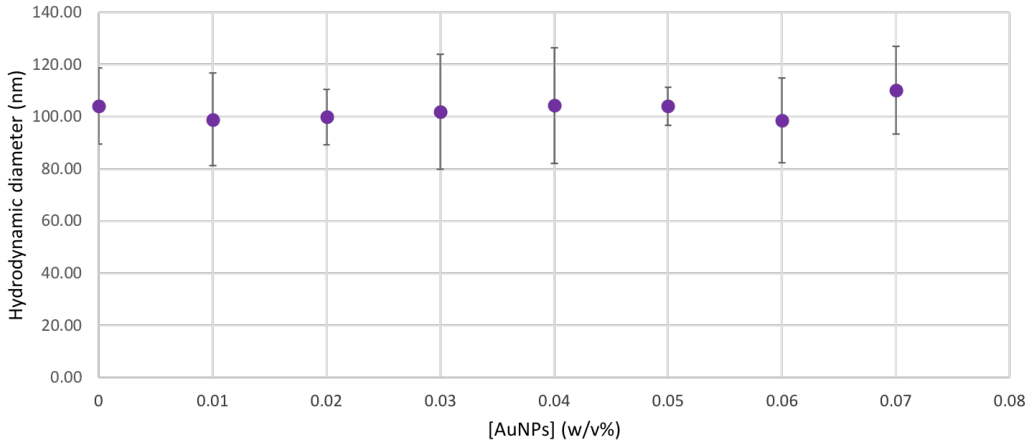

Figure 3-5: Nano-scale polymersome size as a function of AuNP concentration

Hydrodynamic diameter of nano-scale polymersome samples prepared with varying concentrations of AuNPs. Each point represents 6-10 polymersome samples +/- standard deviation.

To confirm nanoparticle loading within the hydrophobic region of the polymersome membrane, samples were prepared both with and without AuNPs and imaged by cryo-TEM. The vitrification process allows for retention of the native

structure in an aqueous environment. Figure 3-6 show a cryo-TEM image of polymersomes that do not contain AuNPs in the membrane. In the case of empty polymersomes, it is possible to visualize the hydrophobic region of the membrane. ImageJ was used to measure ~100 polymersome membranes and the average thickness was found to be 10.97 nm +/- 1.54 nm, which is consistent with literature values for PEO_{20}-*b*-PBD_{35}.

In addition to the vesicular structures seen in Figure 3-6, there is a population of smaller circular structures which is believed to represent micelles that can form during the self-assembly process.

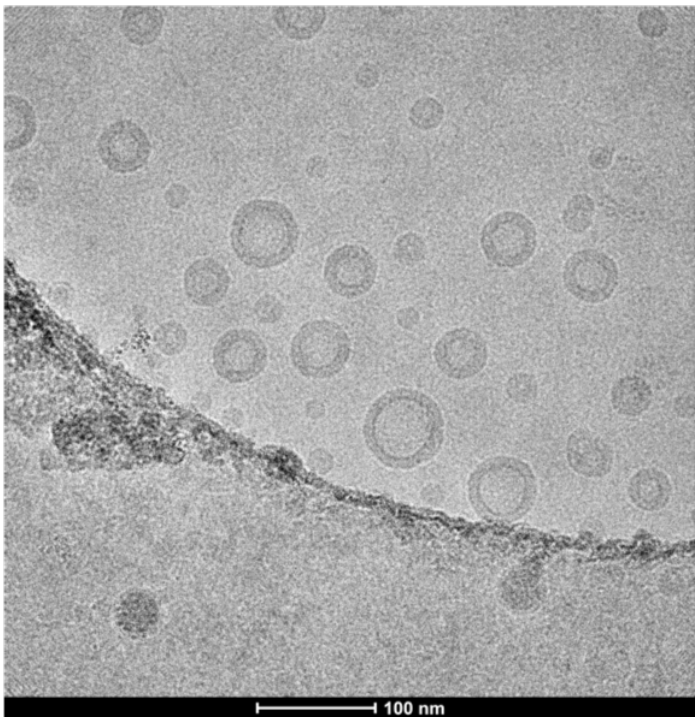

Figure 3-6: Representative cryo-TEM image of polymersomes prepared without AuNPs

Figure 3-7 shows two cryo-TEM images of a polymersome sample prepared with 0.05% (w/v) AuNPs. The high contrast associated with the AuNPs in the vesicle hinders visualization of the membrane, as in Figure 3-6, and thus membrane measurements were not acquired. However, it is possible to measure the overall polymersome diameter and thus approximately 200 polymersomes, both with and without AuNPs, were analyzed using ImageJ as shown in Figure 3-8. As compared to DLS results [Figure 3-5], polymersomes measured from cryo-TEM are slightly smaller

in diameter, as expected. For both cases, there is no significant change in polymersome size upon AuNP encapsulation.

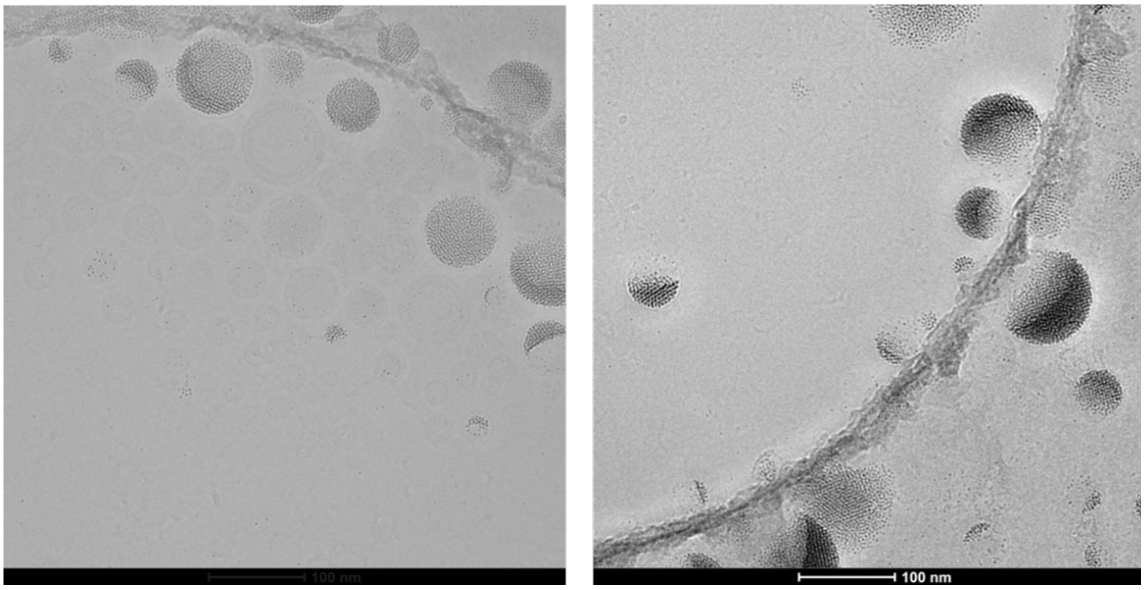

Figure 3-7: Representative cryo-TEM images of AuNP (0.05% (w/v)) loaded polymersomes

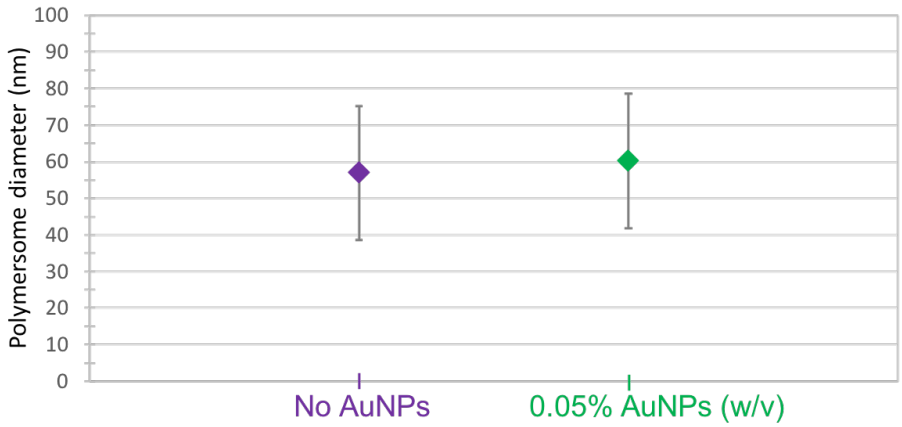

Figure 3-8: Cryo-TEM polymersome size analysis

Cryo-TEM size analysis, showing agreement between the polymersome diameters measured for samples without and with (0.05% (w/v)) AuNPs. Approximately 200 vesicles were measured.

A significant finding from the image shown in Figure 3-7 is that it appears as though AuNPs are primarily encapsulated within the polymersome membrane. Interestingly, it can also be observed that within the hydrophobic membrane there is a segregation of the AuNPs to one side. It was initially believed that the centrifugal filtration used to rid the organic solvent was responsible for NP segregation, however, when the preparation was changed to use dialysis, which is a much gentler technique, the findings were identical. Thus, the NP packing and segregation is attributed to stronger NP-NP interactions due to the hydrophobic dodecanethiol functionalization. The hydrophobic interactions between the nanoparticles supersede the hydrophobic interaction between the AuNP and the PBD blocks within the membrane. Additionally, to confirm membrane-only NP loading, a 3D tomogram was constructed using a series of tilt images acquired on a single vesicle [Figure 3-9]. The tomogram confirms that nanoparticles partition into the hydrophobic region during the self-assembly process.

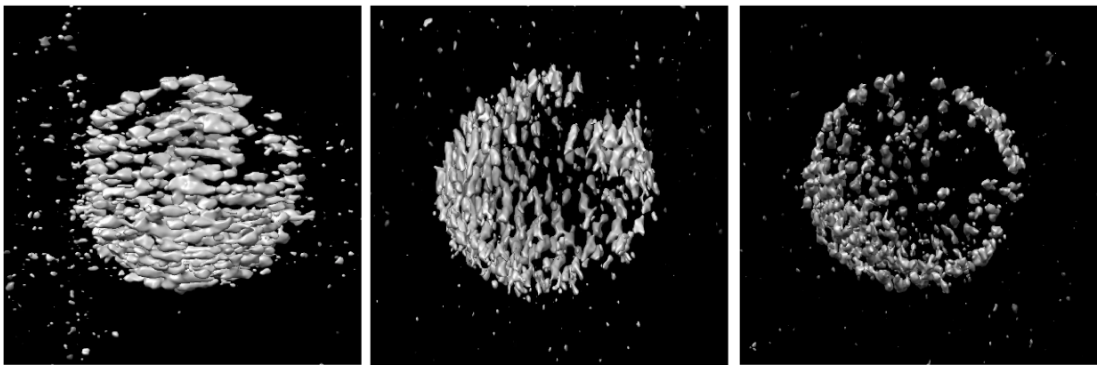

Figure 3-9: Representative views of a cryo-TEM tomogram of one AuNP loaded polymersome

Upon analysis of Figure 3-10, which is another cryo-TEM image of polymersomes prepared with 0.05% (w/v) AuNPs, it was observed that the AuNPs in the membrane conformed to a 2D hexagonal array. It has been shown that dodecanethiol stabilized AuNPs of a similar size will organization into super lattice structures.[55] This 2D hexagonal array is also observed in the external AuNP aggregates that did not partition into the membrane during self-assembly. As shown in Figure 3-11, both packing structures were

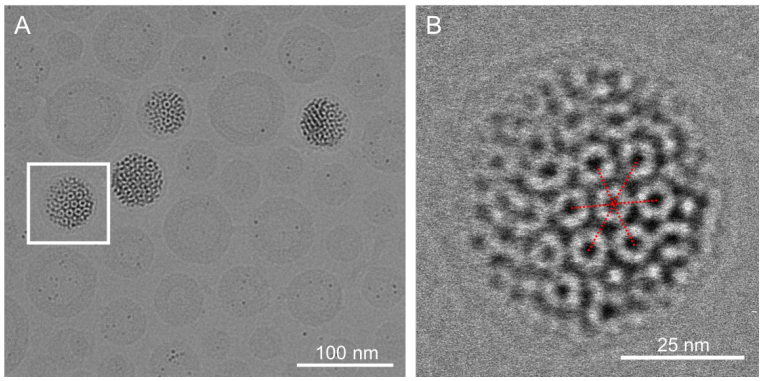

Figure 3-10: 2D Hexagonal array of AuNPs within polymersomes

Panel A shows a cryo-TEM image with AuNP loaded polymersomes. 2D hexagonal array of the AuNPs is observed. Zooming in on the indicated vesicle (B) allows for measurement.

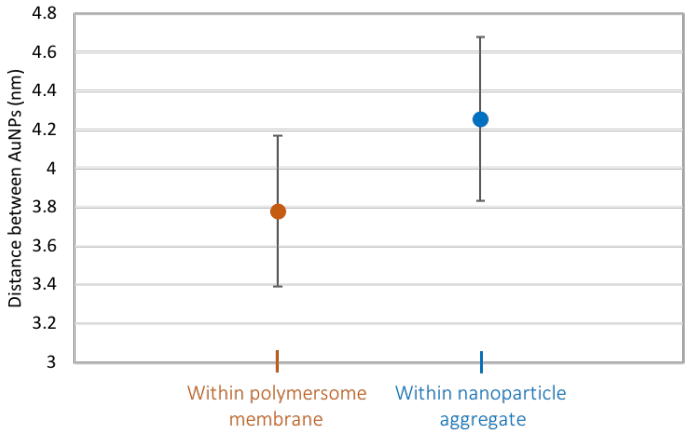

Figure 3-11: Spacing of AuNPs in 2D hexagonal array

The distance between the AuNPs in 2D hexagonal array structures were measured for AuNPs within the polymersome membrane and within an external aggregate. Each point represents ~50 distances +/- standard deviation.

compared and it was found that the average distance for AuNPs within the polymersome membrane is smaller than those within the external AuNP aggregates (~3.8 nm vs. 4.3 nm, respectively). This can be attributed to the additive hydrophobic effect between NP membrane interaction.

Probing the photoinduced mechanism of membrane disruption

In order to gain maximum tunability over the light responsive polymersome system, it is important to gain an understanding of the mechanism(s) by which AuNPs induce rupture or poration of the vesicle membrane. While the micron scale vesicles provide an excellent size regime that facilitates single vesicle imaging, the nano-scale regime gives the ability to examine the fate of the nanoparticles in response to excitation using HR-TEM. The size and shape of the particles after excitation will provide clues as to which processes are leading to membrane disruption. In general, after excitation, heat will diffuse away from the AuNPs into the surrounding environment, which can disrupt the self-assembly of the copolymer. Alternatively, more energetic effects which result in mechanical disruption can take place, such as the formation of a rapidly expanding vapor bubble around the particle, or fragmentation of the AuNP by coulombic explosion. To probe these mechanistic contributions, three polymersome samples containing AuNPs were subjected to different irradiation conditions and subsequently imaged with HR-TEM. Samples included a non-irradiated sample as control, a sample that was irradiated with *fs* pulse durations, and a sample that was irradiated with *ns* pulse durations. The pulse

durations of the femtosecond laser (100 fs) and the nanosecond laser (7 ns) are of particular interest as they lie on either side of the electron phonon coupling time, which is on the order of picoseconds.[56] Thus, it is expected that nanoparticle energy dissipation will be attributed to different primary processes within the two regimes.

The AuNP size distribution along with the mode for each sample is shown in Figure 3-12. In summary, the mode peak size for the non-irradiated, *ns* irradiated, and *fs* irradiated samples are 2.51 nm, 2.44 nm 2.22 nm, respectively. While the AuNPs are trending towards smaller diameters with decreasing pulse duration the

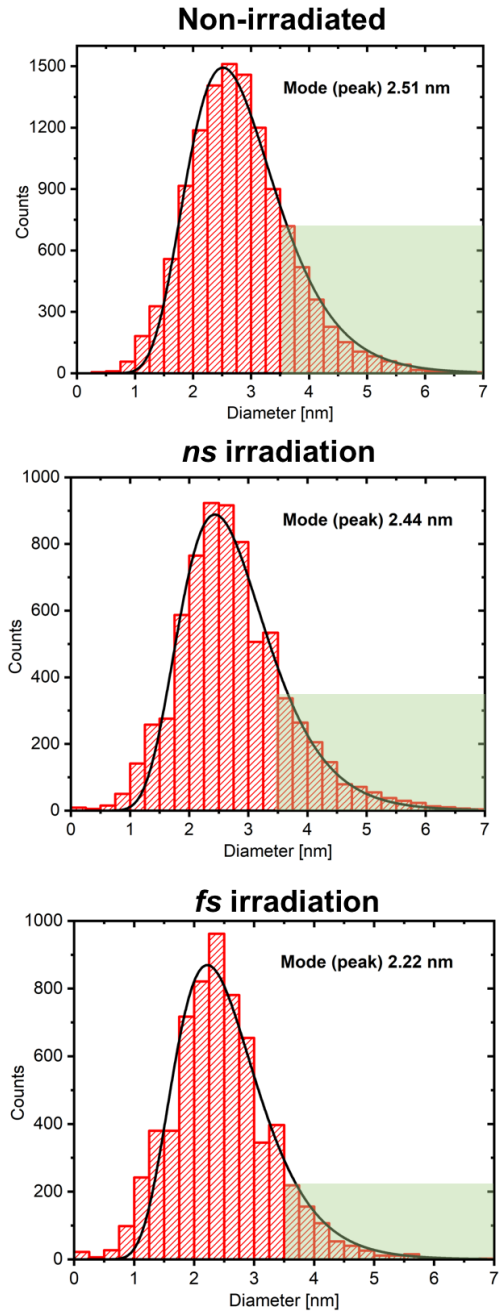

Figure 3-12: Fate of AuNPs following vesicle irradiation

The diameter of numerous AuNPs were measured for AuNP loaded polymersomes without irradiation and after ns irradiation and fs irradiation.

difference becomes more apparent upon the analysis of the population of AuNPs greater than 3.5 nm. For each sample, this region is represented by the green shaded area in Figure 3-12. For the non-irradiated polymersome sample and the *ns* irradiated polymersome sample, the percentage of AuNPs greater than 3.5 nm is approximately 13% whereas this region only represents 7% of the total population for the *fs* irradiated polymersome sample. This suggests that a larger population of nanoparticles undergo size reduction in response to *fs* irradiation. This is consistent with literature findings in that larger particles will preferentially undergo fragmentation under *fs* irradiation. [57] Figure 3-13 shows the data overlay of the irradiated and non-irradiated samples for both *ns* (3-13A) and *fs* (3-13B) pulse durations. The green triangle highlights the size region of interest where particle fragmentation is apparent. Concurrently, the opposite trend is seen for

AuNPs within a smaller size range. The amount of AuNPs which fall below 2.5 nm trend towards larger counts for the *fs* irradiated sample in comparison to the control

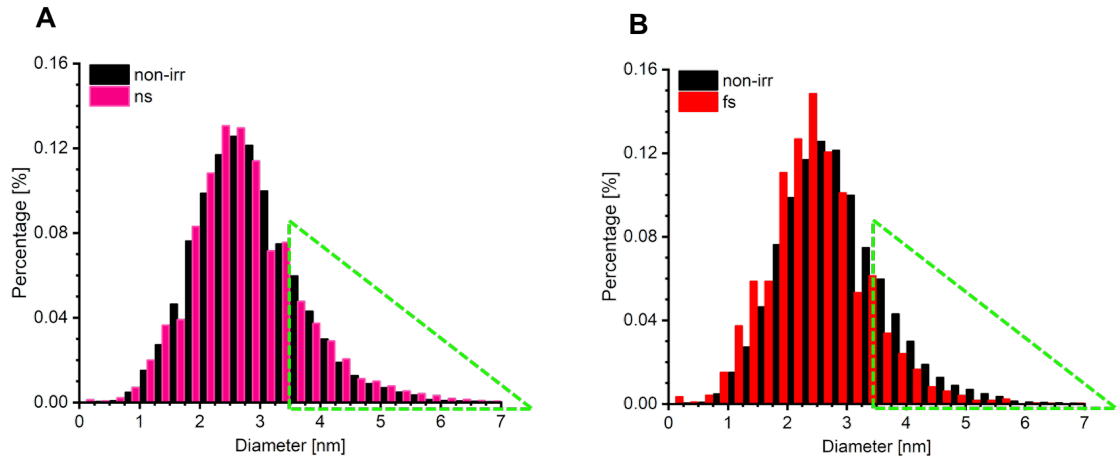

Figure 3-13: Comparative population overlays for irradiated vs non-irradiated samples

sample. Whereas this trend is not visible for ns irradiation.

The data shown in Figures 3-12 and 3-13 suggest that pulse duration plays a significant role in vesicle rupture mechanism. In the case of *ns* irradiation, thermal relaxation through electron-phonon coupling begins to occur before the pulse delivery has been completed (*ps*<*ns* timescale). Thus, thermal energy dissipation predominates and minimal fragmentation will occur. However, in the case of *fs* irradiation, the entirety of the pulse is delivered before energy can be dissipated through thermal pathways (*fs*<*ps*). Thus, this high energy density results in nanoparticle fragmentation.

Nano-scale polymersome irradiation studies

To study nano-scale polymersome rupture thresholds, colloidal samples of polymersomes were subjected to quasi-unfocused *fs* 532 nm irradiation. Polymersomes were prepared with 0.07% (w/v) AuNPs and subjected to irradiation at various pulse energies. As nano-scale polymersomes are unable to be visualized by optical microscopy, DLS is used as a characterization technique to quantify size changes associated with vesicle rupture. As shown in Figure 3-14, vesicle size vs. irradiation time is used to determine the dosage thresholds required for rupture with various pulse energies. Rupture is characterized by the observation of a large spike in hydrodynamic diameter, which is due to the formation of copolymer aggregates upon vesicle disassembly. Prior to this spike, polymersome size remains steady at ~100 nm, suggesting minimal disturbance to the structure. While this size range for the spike is broad, ranging from 200-600 nm in size, this is consistent with what

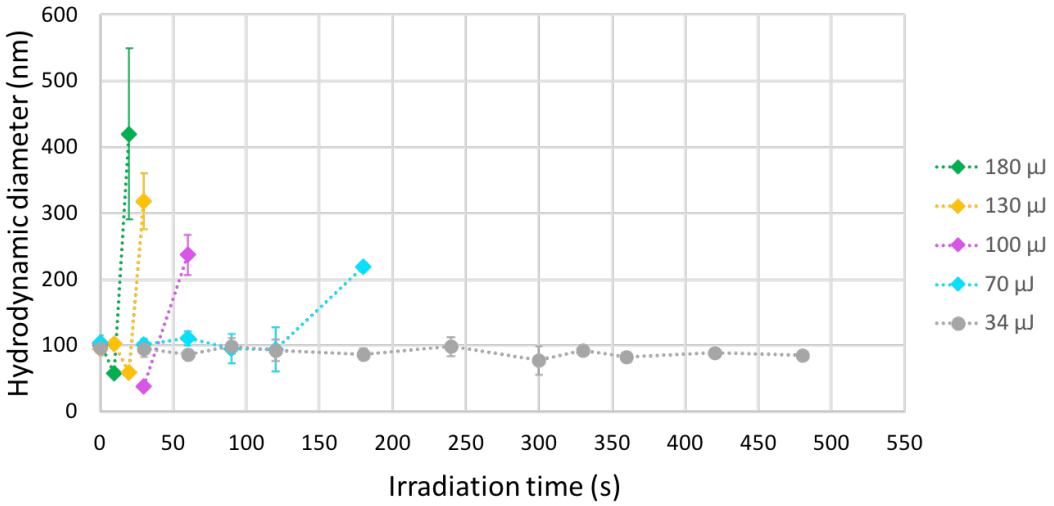

Figure 3-14: Nano-scale polymersome size as a function of time at various pulse energies

DLS measurements are acquired immediately following irradiation. Each data point represents 3-4 polymersome samples +/- SEM.

would be expected for a non-specific copolymer aggregate. Overall, increasing pulse energy results in shorter irradiation times required to induce rupture. While the spike associated with rupture is observed for the higher pulse energies (70 µJ, 100 µJ, 130 µJ, and 180 µJ). It is not observed upon irradiation with 34 µJ, suggesting that this is below the energy threshold for rupture. This is further represented in Figure 3-15, which displays the irradiation time required as a function of pulse energy. As pulse energy decreases, longer irradiation times are required to rupture polymersomes until the lower threshold is reached, where no rupture occurs.

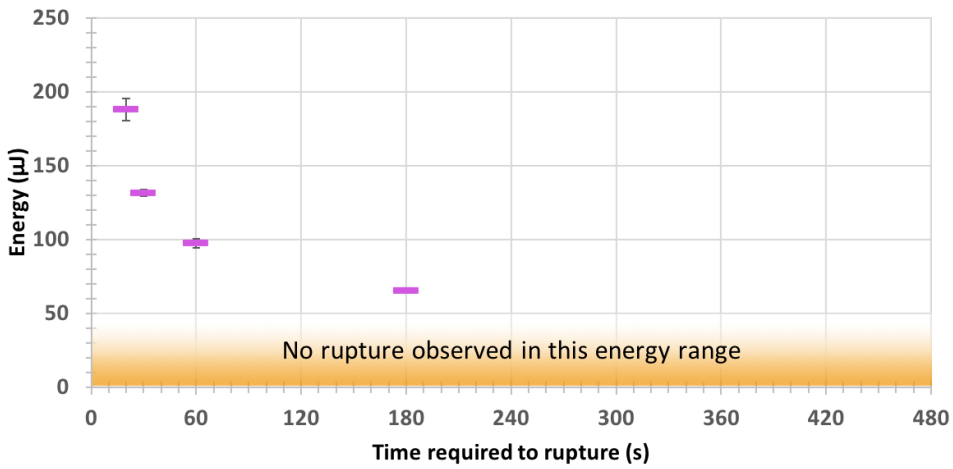

Figure 3-15: Time required to rupture polymersomes at varying pulse energies

For future applications in vivo, AuNPs will be of central importance, thus, it is necessary to understand the effect of AuNP concentration on rupture thresholds. While keeping the pulse energy constant at 180 µJ, polymersomes samples with 0-0.07% (w/v) AuNPs were irradiated and the time required to rupture is reported in Figure 3-16. Similarly, rupture is defined by the large spike in hydrodynamic diameter measured by DLS. It is observed that for higher concentrations of AuNPs, the irradiation time required to rupture is shorter than that of polymersomes with lower concentrations of AuNPs. Figure 3-17 represents the overall trend in the time required to rupture polymersomes as AuNP concentration is decreased. No rupture is observed for polymersomes without encapsulated AuNPs at this pulse energy.

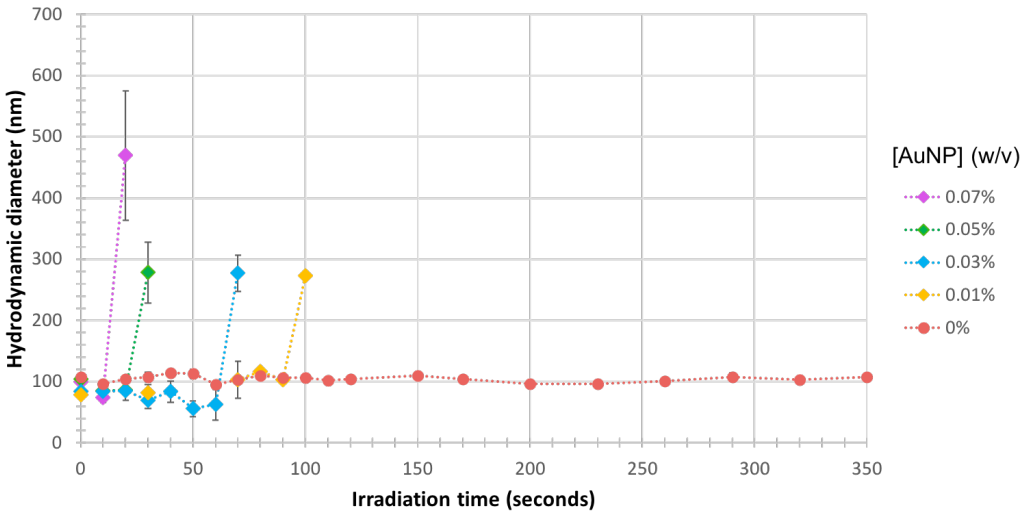

Figure 3-17: Rupture threshold detection for nano-scale polymersomes with varying AuNP concentrations

DLS measurements are acquired immediately following irradiation. Each data point represents 3-4 polymersome samples +/- SEM.

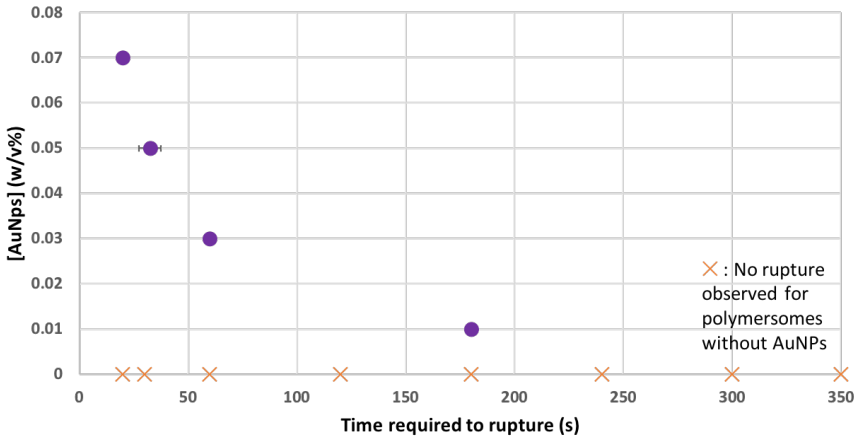

Figure 3-16: Time required for polymersome rupture with varying AuNP concentrations

To gain more insight into the vesicle structural disturbances upon rupture, cryo-TEM would be an ideal method to characterize the resulting aggregates. However, practical limitations, due to aggregate stability, prohibit vitrification immediately following irradiation. Figure 3-18 displays the fate of the polymer aggregate over time. As initially shown in Figures 3-14 and 3-16, rupture is characterized by a large size spike detected by DLS, which is attributed to a non-specific aggregate. The size of these aggregates was tracked over the course of 8 hours. By the 60-minute measurement, the aggregate size significantly decreases, suggesting a rearrangement of the initially formed structure. Due to the instability of the aggregate, there is only a short window in which the sample could be vitrified for an accurate structural representation. While these experiments are not excluded from future plans, it will first be necessary to make arrangements for irradiation and vitrification to take place within the same location.

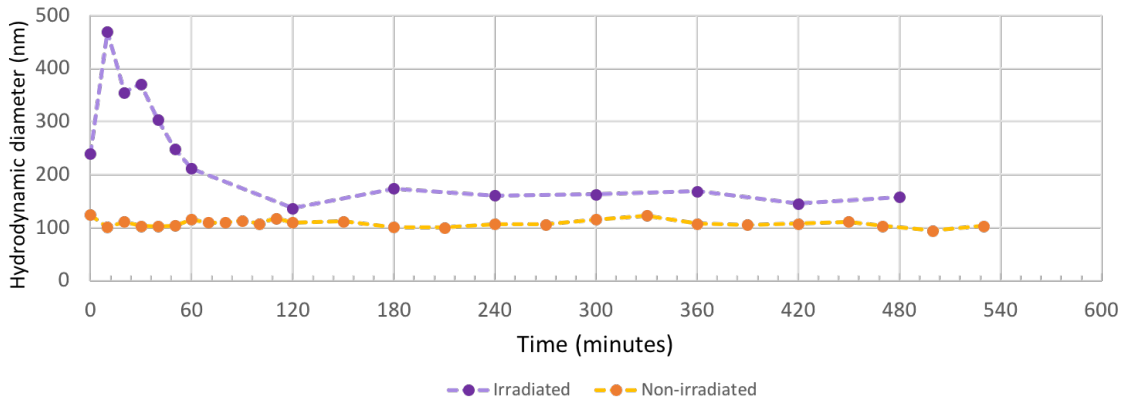

Figure 3-18: Size time series following rupture

A polymersome sample, with 0.07% AuNPs, is irradiated at the respective energy and duration to initiate vesicle rupture and formation of large aggregates. Upon detection of a large aggregate, the same sample was measured over the course of 8 hours.

Surfactant resistance

An alternate method to induce vesicle rupture is through the addition of a surfactant. Surfactants are known to disrupt polymersome self-assembly, initiating vesicle rupture.[58] To investigate the appearance of the non-specific aggregates via surfactant disruption, two non-ionic surfactants, Triton X-100 and Tween 20, were added to the colloidal solution at various concentrations. Interestingly, it was found that the expected surfactant concentration did not induce rupture for AuNP loaded polymersomes. In fact, as the amount of AuNP loading within the membrane was increased, the vesicle structure was stabilized over significantly increased concentrations of surfactant, as compared to the control sample, without AuNPs.

As shown Figure 3-19, the concentration of Triton X-100 was titrated upwards. The polymersomes size remained stable (~100 nm) until a threshold concentration of Triton X was reached. In contrast to the size spike seen during irradiation, a significant size decrease was observed (~7 nm). Given that the threshold concentrations, in all cases, lies significantly above the critical micelle concentration (CMC) for Triton X-100 (0.22-0.24 mM), the 7 nm entity can be attributed to the dominating population of surfactant micelles in solution once polymersomes are no longer present. An identical experiment was performed with a second non-ionic surfactant, Tween 20 (CMC = 0.06 mM), which resulted in the same trend, as shown in Figure 3-20.

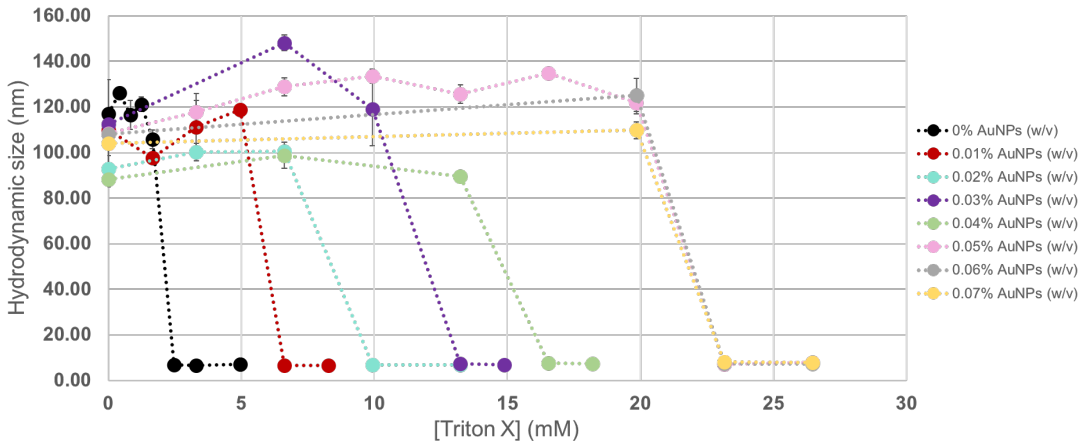

Figure 3-19: DLS results for Triton X resistant polymersomes

Hydrodynamic size of polymersome samples plotted as a function of Triton X concentration. Each point represents 3-4 trials +/- SEM.

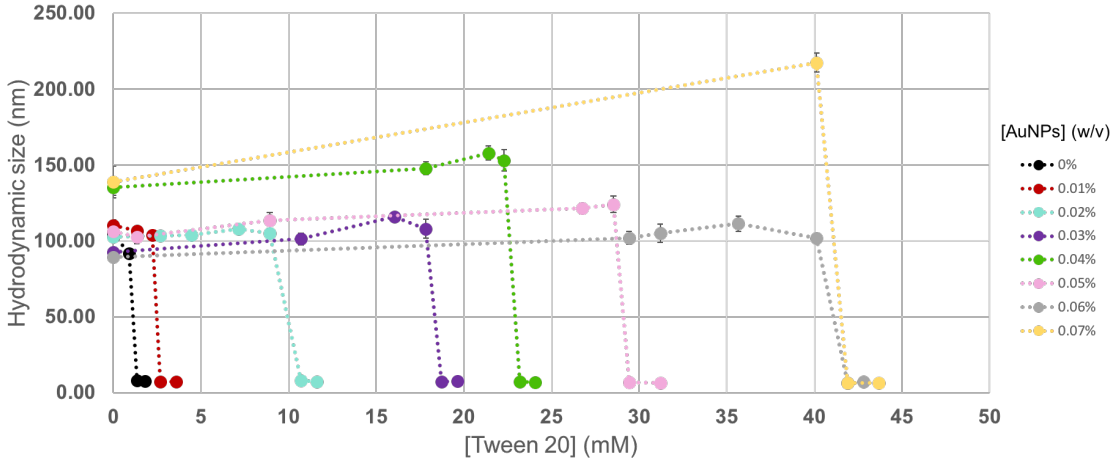

Figure 3-20: DLS results for Tween 20 resistant polymersomes

Hydrodynamic size of polymersome samples plotted as a function of Tween 20 concentration. Each point represents 3-4 trials +/- SEM.

The increased stability against Triton X-100 and Tween 20 is better represented in Figure 3-21 where it is shown that maximally loaded polymersomes display a 10x higher resistance to Triton X-100, and a 32 x higher resistance to Tween 20. The higher resistance to Tween 20 as compared to that of Triton X is understood as Triton X-100 is considered a relatively strong and harsh surfactant. [59] This is a significant finding as it shows that AuNP loading within the polymersome membrane has the ability to stabilize the vesicle structure, while increasing specificity for photo triggered response.

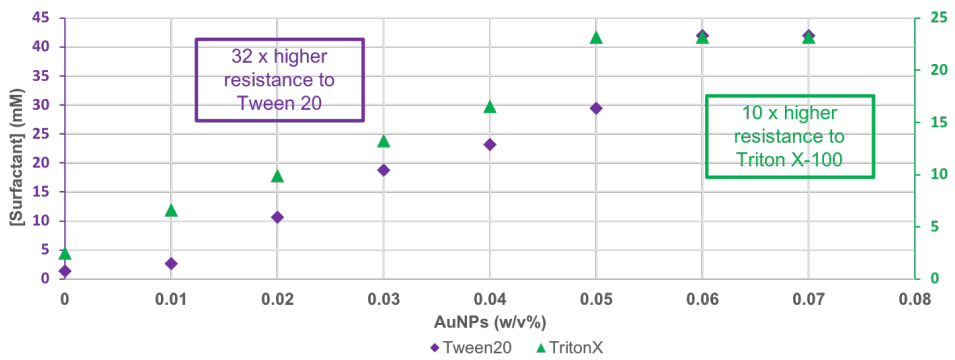

Figure 3-21: Surfactant resistant polymersomes

Prior studies where hydrophobic molecules are loaded into polymersome membranes have not shown such an effect[35], and as expected a control experiment where hydrophobic Nile red is encapsulated within the membrane concurred [Figure 3-22]. Nile red fluorophore was encapsulated within the vesicle membrane at two different concentrations and DLS measurements were taken as a function of Triton X concentration. Vesicles with both concentrations of Nile red ruptured at the same

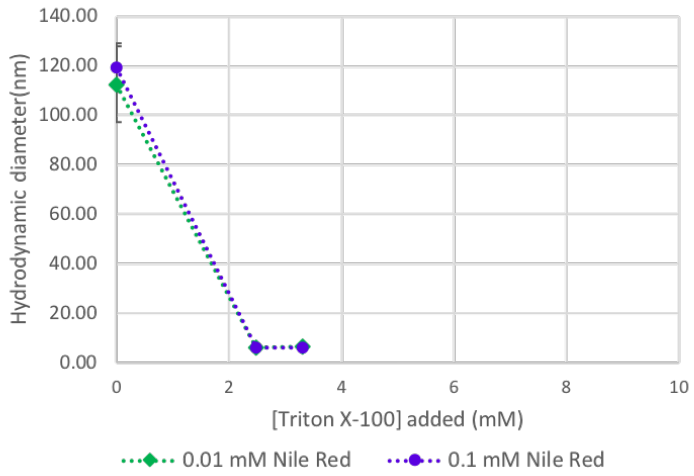

Figure 3-22: Nile red control experiment

Polymersomes are prepared with 0.01 mM and 0.1 mM Nile red. DLS measurements are taken before and immediately following the addition of Triton X.

concentration of Triton X-100, which aligns with the concentration required to rupture empty polymersomes. These data suggest that there is an interaction between the AuNPs and the polymersome membrane, resulting in stabilization. As the AuNPs are functionalized with dodecane chains to render them hydrophobic for membrane incorporation, it is likely that the dodecane chain is able to entangle with the inner PBD blocks, resulting in a more rigid structure that resists surfactant penetration.

Conclusion

The plasmonic polymersome system has been designed and proven effective for light mediated rupture on the nano-scale. Nano-scale polymersomes are prepared through direct solvent injection resulting in polymersomes with a nominal size of approximately 100 nm, which is optimal for in-vivo drug delivery applications, and it has been confirmed that AuNP encapsulation does not affect polymersome size. Cryo-TEM confirms AuNP loading within the polymersome membrane, and additionally reveals preferential segregation of the AuNPs to one side of the vesicle.

The mechanism through which AuNPs mediate polymersome rupture was explored through the use of irradiation with two different pulse durations. Analysis of AuNP sizes after vesicle irradiation suggest that *fs* pulse durations result in membrane disruption primarily via a mechanical event induced by nanoparticle fragmentation, whereas membrane disruptions upon *ns* pulse durations are initiated through thermal relaxation. This is consistent with electron phonon coupling times.

AuNP mediated photosensitivity was confirmed for polymersomes on the nano-scale and rupture thresholds were studied as a function of pulse energy for a given AuNP concentration, and as a function of AuNP concentration for a given pulse energy. While it was found that increased AuNP concentration renders the vesicles more photoresponsive, it also renders the vesicles less susceptible to surfactant mediated rupture. This combination renders this system extremely promising for drug delivery applications, as increased stability decreases the likelihood of non-specific release in vivo.

Chapter 4 : System optimization

Introduction

Optimizing polymersome formation for both the micron-scale and nano-scale systems is important for the future development of this system. Ultimately, it is of interest to develop a library of polymersomes which are photosensitive to a range of visible and NIR wavelengths. This is feasible through the encapsulation of NPs of various sizes, compositions (i.e. silver), and structural conformations (i.e nanorods). Therefore, the encapsulation of a variety of noble metal nanoparticles must be optimized. It has been shown that polymersome size, prepared via gel rehydration, is affected upon changes in temperature.[53] This chapter seeks to optimize polymersome formation, for both the micron-scale and nano-scale system. Changes in polymer concentration, temperature, and AuNP incorporation are studied, which are important for the future development in the incorporation of various types of metal nanoparticles.

Materials and Methods

Micron-scale polymersome optimization

Micron-scale polymersomes are prepared via gel-assisted rehydration as described in Chapter 2. The polymer rehydration step was relocated to the microscope to facilitate imaging during vesicle formation, as shown in Figure 4-1. Rehydration was performed at 35°C, 45°C, and 55°C. The upper temperature range is limited to 55°C as to remain within the safe operating temperature range of the objective. Polymersomes were visualized via fluorescent microscopy, and upon initial formation, imaged every five minutes for one hour. Multiple individual vesicles were tracked and measured using ImageJ.

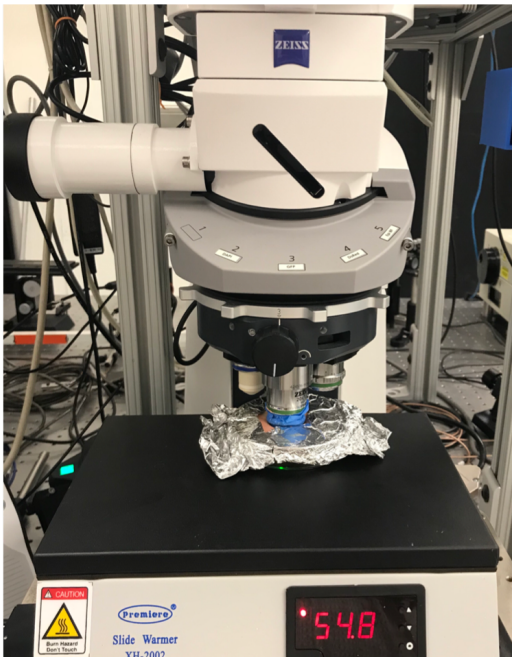

Figure 4-1: Setup for visualizing real-time gel-assisted rehydration

Nanoscale polymersome optimization

Nano-scale polymersomes are prepared via direct solvent injection as described in detail in Chapter 3. The diblock copolymer is prepared in concentrations of 2 mg/mL, 4 mg/mL, and 8 mg/mL. Polymersome samples are prepared for each polymer concentration, both with and without 0.05% (w/v) AuNPs. The polymersome sizes are measured using DLS number distribution. The stability of polymersome samples is determined by tracking PDI and size for 10 days.

Results and Discussion

Polymersome size is tracked by imaging vesicles throughout the duration of the rehydration and heating phase of micron-scale vesicle preparation. Measurements begin upon initial vesicle formation, which occurs approximately 5-15 minutes into the rehydration process. Figure 4-2 displays a time series of vesicle formation images for a sample prepared with no AuNPs, rehydrated at 45°C.

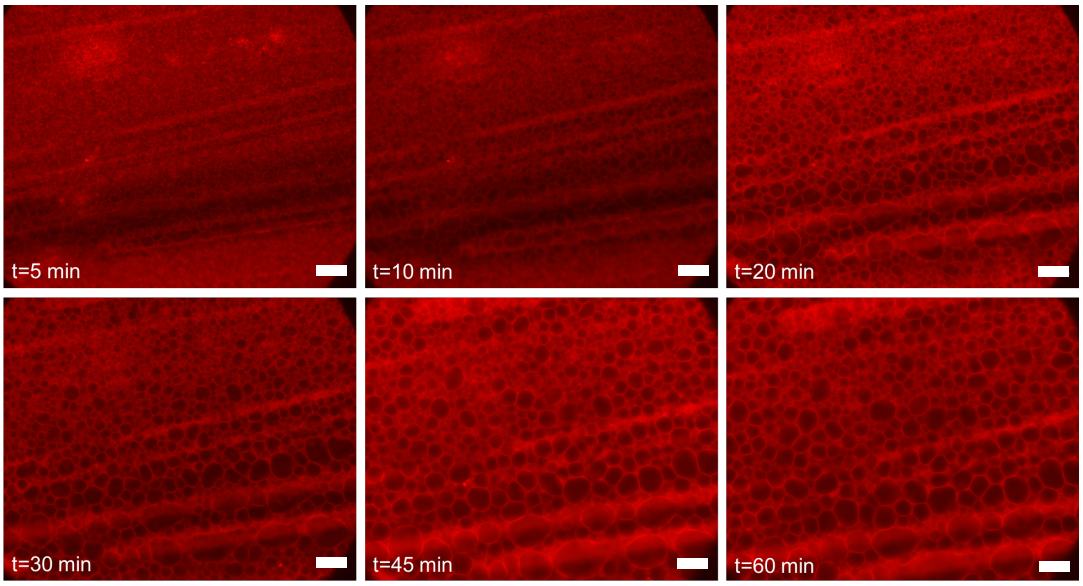

Figure 4-2: Polymersome formation time series

Polymersomes prepared without AuNPs, rehydrated at 45°C, are imaged as a function of time during the formation process. The scale bar represents 50 μm.

Two trials were conducted for polymersome formation without AuNPs at 35°C, 45°C, and 55°C. Measurements of approximately 50 polymersomes per trial are reported in Figure 4-3. For polymersomes rehydrated at 35°C, measurable vesicle formation occurs at approximately 10 minutes post rehydration with an average diameter of ~3 μm. Following one hour of heated rehydration, polymersome diameter increases to an average of ~10μm. For polymersomes rehydrated at 45°C, measurable vesicle

formation occurs at approximately 20 minutes post rehydration. Vesicle diameter initially measures an average of 10μm and following one hour of heated rehydration, the diameter increases to an average of ~18μm. For a polymersome sample rehydrated at 55°C, measurable vesicle formation occurs at approximately 10 minutes post rehydration and is ~10 μm. Following one hour of heated rehydration, polymersome diameter increases to an average of ~22 μm. It is therefore confirmed, for this polymersome system, that larger vesicles form as a result of higher rehydration temperatures.

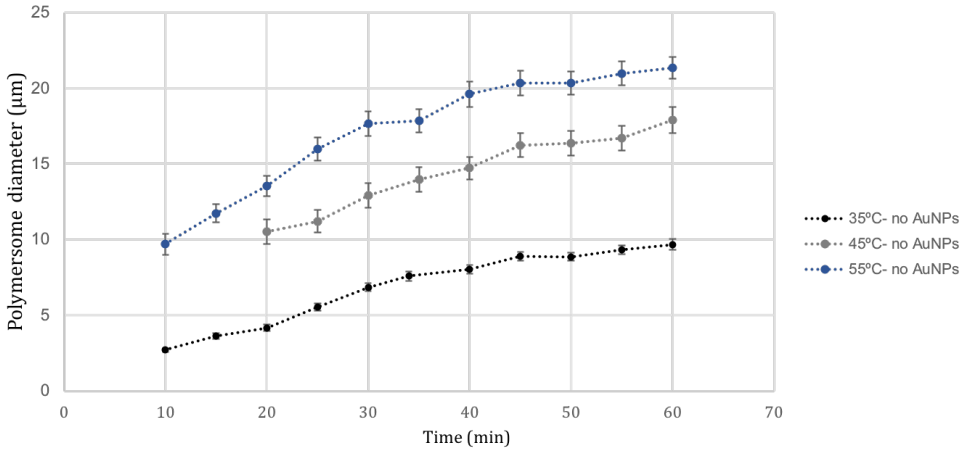

Figure 4-3: Polymersome size optimization – without AuNPs

Polymersome diameter is measured as a function of time during the rehydration process. Each point represents an average of two trials of at least 50 polymersomes +/- SEM.

During the experiments preformed in Chapter 2, it is visually observed that there is a change in polymersome formation for vesicles containing AuNPs as compared to samples without. A polymersome sample, containing 0.066% (w/v) AuNPs is subjected to rehydration at 55°C. Time series imaging and measurements is

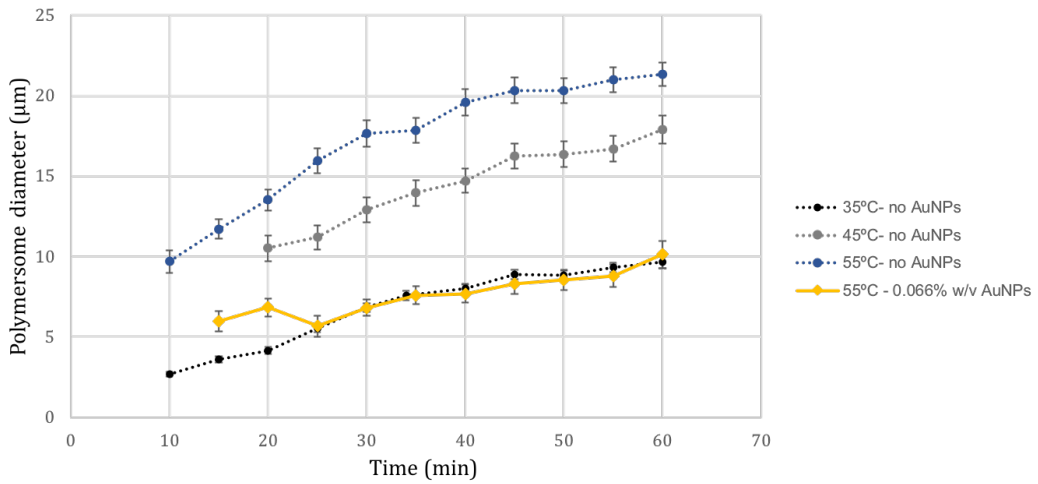

Figure 4-4: Polymersome size optimization – w/ AuNPs

Polymersomes prepared with 0.066% (w/v) AuNPs is rehydrated at 55°C and measured. Polymersome diameters are measured as a function of time during the rehydration process. The gold line shows how the formation with AuNPs compared to the formation without AuNPs. Each point represents two trials of at least 50 polymersomes +/- SEM.

completed for two trials at this condition, as shown in Figure 4-4 and as compared to results shown in Figure 4-3. It is observed that the average size of AuNP loaded polymersomes, after 1 hour of rehydration at 55°C is only ~10µm. This aligns in size with the polymersome sample prepared with no AuNPs and rehydrated at only 35°C (black line) as opposed to the blue line which matches in rehydration temperature. There is a significant difference in the size of polymersomes formed at the same rehydration temperature for those with and without AuNPs, therefore, it is confirmed that AuNP encapsulation affects polymersome formation.

As it is shown that AuNP encapsulation affects micron-scale polymersome formation, size specific optimization is of interest for nano-scale polymersomes as well. Nano-scale polymersomes are prepared with varying concentrations of copolymer to study its effect and resulting sizes of samples prepared with 2 mg/mL,

4 mg/mL, and 8 mg/mL are measured using DLS and hydrodynamic diameter and PDI are reported in Figure 4-5. It is observed that for lower concentrations of copolymer, the average vesicle diameter is ~120 nm, however, for higher copolymer concentrations, the average vesicle size was measures respectively lower at ~70nm. and there is no trend in PDI (blue diamonds) with concentration.

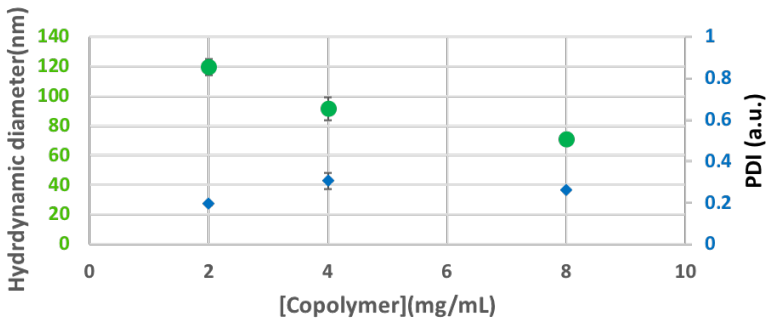

Figure 4-5: Vesicle size and PDI as a function of diblock copolymer concentration

Polymersome size and PDI is reported as a function of diblock copolymer concentration. Each point represents two samples +/- standard deviation.

To study the size effects upon introduction of AuNPs, polymersomes were prepared at each of the three concentrations as above, with and without AuNPs. The vesicle size is measured for each sample using DLS. The results are displayed in Figure 4-6. In general, upon the encapsulation of 0.05% AuNPs, it does not appear that there is a significant change in polymersome size, in contrast to what was found for micron-scale polymersomes. However, as diblock copolymer concentration decreases (2 mg/mL), the encapsulation of AuNPs begin to affect the vesicle size. Overall, in contrast to micron-scale polymersomes, it does not appear as though the formation effect upon the encapsulation of AuNPs within nano-scale polymersomes is as significant.

Figure 4-6: Size effects upon AuNP encapsulation

Polymersome diameter is measured as a funciton of polymer and AuNP concentration.

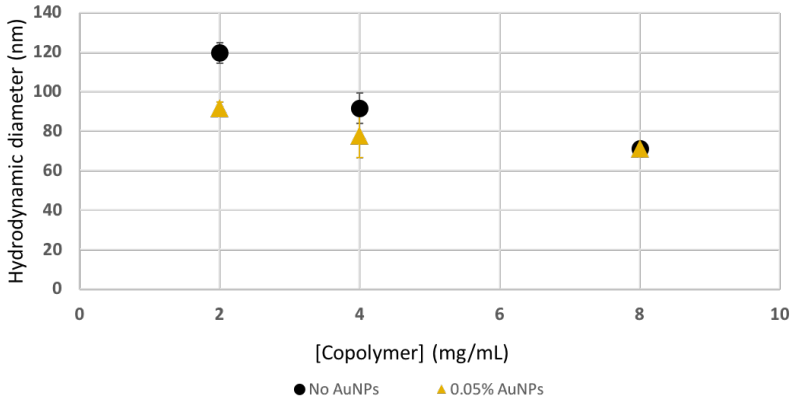

As this nano-scale polymersome system will ultimately be implemented into biological systems, it is important to study the stability of the vesicles. It has been found that there is a resistance to surfactants upon the encapsulation of AuNPs, therefore it is of interest to determine and optimize overall stability of the system as a function of time. Polymersome samples are prepared with three different concentrations of diblock copolymer, each with and without AuNPs. Vesicle stability is determined through size changes, via DLS measurements, and the percent change in vesicle size after 10 days is reported in Figure 4-7. Over the course of 10 days, all prepared samples show less than 16% change in size and each polymersome size remains within the optimal size range for nano-scale vesicles.

Sample	Change in vesicle size 10 days after preparation
2 mg/mL – No AuNPs	2.80%
2 mg/mL – w/AuNPs	2.85%
4 mg/mL – No AuNPs	3.44%
4 mg/mL – w/ AuNPs	15.64%
8 mg/mL – No AuNPs	2.29%
8 mg/mL – w/ AuNPs	5.77%

Figure 4-7: Table displaying the percent change in polymersome size after 10 days

It is concluded that the encapsulation of AuNPs does not significantly affect the overall formation of nano-scale polymersomes. However, polymersomes prepared with 4 mg/mL copolymer result in the optimal size, with minimal change upon AuNP encapsulation, and maintain stability in terms of size, as compared to vesicles prepared with varying copolymer concentrations.

Conclusion

Optimization of polymersome formation for both micron-scale and nano-scale vesicles is important for the future direction of the plasmonic polymersome system. It has been shown that micron-scale polymersome formation is affected by rehydration temperature, yet more interestingly by encapsulation of AuNPs. As the plasmonic polymersome system will eventually aim to encapsulate nanoparticles of a variety of shapes, sizes, and compositions, it is important to elucidate formation trends due to temperature and encapsulation concentrations.

It is promising that AuNP encapsulation does not significantly affect nano-scale polymersome formation. As temperature is not a factor in the direct solvent injection method, polymer concentration is the most significant variable, and was thus varied to determine optimal conditions for nano-scale vesicle preparation. It is shown that 4 mg/mL yields polymersomes of optimal size for future in-vivo applications; additionally, they are relatively stable over time and minimally affected by the encapsulation of AuNPs.

Chapter 5 : Concluding remarks

Conclusion

The work presented in this thesis has discussed the design and study of the plasmonic polymersome system on both the micron-scale and nano-scale. Polymersomes are fully synthetic, tunable vesicles composed of a hydrophobic membrane and a hydrophilic core, which allows for stable dual-encapsulation of a wide variety of molecules. While there are prior examples of polymersome systems designed to respond to various stimuli, this thesis presents the first example of triggered release from polymersomes upon ultrafast single pulse, visible irradiation, which has high potential for achieving precise, spatiotemporal control in future applications. Plasmonic polymersome are responsive to visible light upon the encapsulation of AuNPs within the hydrophobic membrane. AuNPs act as photosensitizer due to their strong interaction with light on resonance with the LSPR of the nanoparticle, resulting in membrane disruptions and cargo release.

The preparation of anchored micron-scale polymersomes facilitates vesicle imaging with optical microscopy as well as single vesicle experimentation. Cargo release dynamics from AuNP loaded polymersomes can be controlled with dependence on *fs* pulse energy, resulting in either complete rupture or poration. In the case of vesicle poration, cargo diffusion occurs. Additionally, the concentration of AuNPs within the vesicle membrane can also dictate the percent of cargo release.

While micron-scale experiments provide a means to visualize and quantify polymersome release at the single vesicle level, the system must be scaled down to the nano-size regime to be used in future biological applications. Nano-scale

polymersomes are prepared via direct solvent injection, yielding polymersomes of sizes ranging from 80-120 nm. Polymersome formation and size was confirmed via DLS and cryo-TEM, and further, nanoparticle loading within the vesicle membrane was confirmed via cryo-TEM. Interestingly, there exists an internal ordering of AuNPs within the hydrophobic polymersome membrane consistent with 2D hexagonal arrays. AuNPs were loaded into nano-scale polymersomes at different concentrations, and vesicle size was not significantly affected.

Mechanistic studies, to determine how AuNP excitation results in membrane disruption were performed and provided insight into the relative thermal and mechanical mechanistic contributions. By altering the pulse duration from the *fs* timescale, which is shorter than electron photon coupling time, to the *ns* timescale, which is longer than the electron phonon coupling time, a reduction in resulting NP fragmentation occurred. This suggests that while *fs* irradiation results in primarily mechanical disruptions, *ns* relaxation pathways can occur primarily through thermal diffusion.

Nano-scale irradiation studies have aligned with micron-scale studies which demonstrate that both *fs* pulse energy and AuNP concentration affect polymersome release dynamics. By increasing either the pulse energy or concentration of AuNP encapsulation, the critical irradiation times for rupture can be decreased. In addition to increased photosensitivity, the incorporation of AuNPs were also shown to increase the polymersome resistance to two non-ionic surfactants, as a function of AuNP concentration. Thus, increasing AuNP concentration is beneficial for both stability and specificity to light-response.

Overall, this system represents the first example of polymersomes responsive to ultrafast, single pulse visible light on both the micron-scale and nano-scale. While the micron-scale offers an excellent platform for visualization, the nano-scale system is extremely promising for future applications in drug delivery. By controlling the time and concentration of cargo delivery at a specific location, the harsh side effects may be mitigated by limiting off target drug interactions. Additionally, the surfactant resistance shown with increasing concentrations of AuNPs holds promise for avoiding non-specific rupture due to increased vesicle stability.

Future directions

The overall goal of precision drug delivery is to control where, when, and how much of a therapeutic is delivered. There are often times when a cocktail of drugs must be delivered in a particular time sequence. By creating a library of polymersomes which are responsive to a range of irradiation wavelengths, we can gain the control to deliver an individual therapeutic from some subset of polymersomes within a cocktail at a specified time, while another population remain unaffected until acted upon with a different wavelength. Therefore, the encapsulation of various types of nanoparticles, including silver nanoparticles, gold/silver alloy nanoparticles, as well as gold nanorods, will shift polymersome response wavelength spanning the visible and NIR regions of the spectra, as shown below in Figure 5-1. This broad selection of trigger wavelengths will be beneficial for a variety of applications including microreactors and nanoreactors.

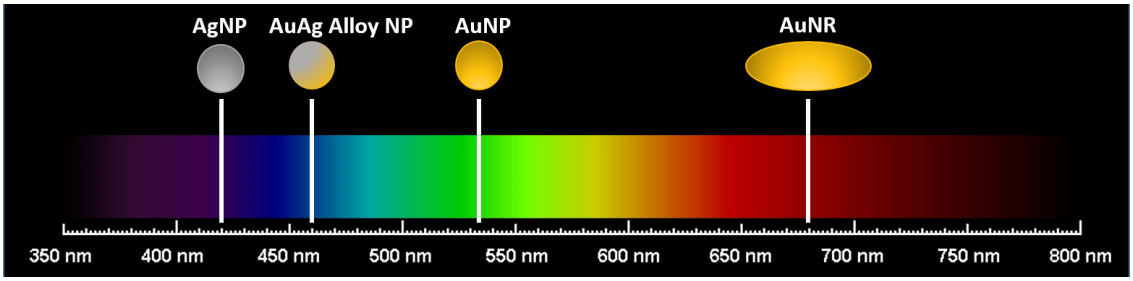

Figure 5-1: Plasmonic polymersomes spanning the visible and NIR wavelengths

Appendix

Table of Abbreviations

AuNPs	*Gold nanoparticles*
DDT	*Dodecanethiol*
AuNRs	*Gold nanorods*
PEO	*Polyethylene oxide*
PBD	*Polybutadiene*
DLS	*Dynamic Light Scattering*
PDI	*Poly dispersity index*
FITC-dextran	*Fluorescein isothiocyanate*
EPR	*Enhanced permeation and retention*
CMC	*Critical micelle concentration*
fs	*Femtosecond*
ps	*Picosecond*
ns	*Nanosecond*
HR-TEM	*High resolution – Transmission Electron Microscopy*
Cryo-TEM	*Cryogenic-Transmission Electron Microscopy*
IR	*Infrared*
NIR	*Near-Infrared*
LSPR	*Localized surface plasmon resonance*
ROI	*Region of interest*
UV	*Ultraviolet*
PDMS	*Polydimethylsiloxane*
TEM	*Transmission Electron Microscopy*
DDI	*Double deionized*
AFM	*Atomic force microscopy*
Rpm	*Revolutions per minute*

Data tables

Figure 2-13 data

[AuNPs]	Vesicle #	diameter(nm)	time (sec)	Vesicle intensity	Background intensity	Difference	Ratio
0	1	31.023	0	2155.369	722.229	1433.14	1
			10	2151.232	726.111	1425.121	0.99440459
			20	2112.425	729.499	1382.926	0.96496225
			30	2078.219	731.395	1346.824	0.93977141
			40	2084.612	733.163	1351.449	0.94299859
			50	2058.79	733.38	1325.41	0.9248294
			60	2052.183	732.252	1319.931	0.92100632
			70	2034.068	733.034	1301.034	0.90782059
			80	2004.464	728.448	1276.016	0.89036382
			90	2012.562	724.363	1288.199	0.89886473
			100	2008.214	724.918	1283.296	0.89544357
			110	1997.962	727.369	1270.593	0.88657982
			120	1983.887	726.145	1257.742	0.87761279
	2	25.126	0	1771.524	771.353	1000.171	1
			10	1751.193	781.14	970.053	0.96988715
			20	1736.556	764.727	971.829	0.97166285
			30	1712.856	769.785	943.071	0.94290976
			40	1717.24	769.197	948.043	0.94788091
			50	1731.014	786.857	944.157	0.94399558
			60	1747.427	806.39	941.037	0.94087611
			70	1769.346	806.39	962.956	0.96279136
			80	1800.868	808.568	992.3	0.99213035
			90	1791.006	806.638	984.368	0.9841997
			100	1818.803	787.713	1031.09	1.03091371

			110	1787.003	789.476	997.527	0.99735645
			120	1791.441	790.713	1000.728	1.0005569
	3	29.876	0	354.175	185.067	169.108	1
			10	342.805	154.183	188.622	1.11539371
			20	340.03	147.511	192.519	1.13843816
			30	325.383	145.183	180.2	1.06559122
			40	318.504	139.367	179.137	1.0593053
			50	321.316	136.639	184.677	1.09206543
			60	321.421	138.478	182.943	1.08181162
			70	310.977	135.644	175.333	1.0368108
			80	309.308	133.361	175.947	1.04044161
			90	310.18	127.633	182.547	1.07946992
			100	306.323	133.694	172.629	1.02082101
			110	306.519	131.789	174.73	1.03324503
			120	306.519	131.789	174.73	1.03324503
	4	34.151	0	1771.524	771.353	1000.171	1
			10	1751.193	781.14	970.053	0.96988715
			20	1736.556	764.727	971.829	0.97166285
			30	1712.856	769.785	943.071	0.94290976
			40	1717.24	769.197	948.043	0.94788091
			50	1731.014	786.857	944.157	0.94399558
			60	1747.427	806.39	941.037	0.94087611
			70	1769.346	806.39	962.956	0.96279136
			80	1800.868	808.568	992.3	0.99213035
			90	1791.006	806.638	984.368	0.9841997
			100	1818.803	787.713	1031.09	1.03091371
			110	1787.003	789.476	997.527	0.99735645
			120	1791.441	790.713	1000.728	1.0005569

	AVERAGE			Average	Standard deviation	SEM	
			0	1	0	0	
			10	1.012393151	0.069632905	0.034816452	
			20	1.011681525	0.084563436	0.042281718	
			30	0.972795539	0.061881475	0.030940737	
			40	0.974516428	0.056572748	0.028286374	
			50	0.976221494	0.077755994	0.038877997	
			60	0.971142541	0.074371589	0.037185795	
			70	0.967553528	0.052946355	0.026473177	
			80	0.97876653	0.063182378	0.031591189	
			90	0.986683515	0.073787522	0.036893761	
			100	0.994523003	0.066224081	0.033112041	
			110	0.978634437	0.06365898	0.03182949	
			120	0.977992908	0.068671274	0.034335637	
[AuNPs] (w/v)	Vesicle #	diameter(nm)	time (sec)	Vesicle intensity	Background intensity	Difference	Ratio
0.013%	1	22.16	0	1193	673.111	519.889	1
			10	1438.538	1002.04	436.498	0.83959845
			20	1430.979	1007.467	423.512	0.81462004
			30	1443.559	1013.551	430.008	0.82711502
			40	1436.846	1006.993	429.853	0.82681688
			50	1409.371	971.425	437.946	0.84238366
			60	1381.343	959.503	421.84	0.81140397
			70	1342.378	934.243	408.135	0.78504258
			80	1316.608	913.64	402.968	0.77510392
			90	1307.79	904.744	403.046	0.77525395
			100	1281.986	891.951	390.035	0.75022745
			110	1278.874	888.391	390.483	0.75108917
			120	1281.713	904.4	377.313	0.72575684
	2	18.44	0	3233.706	1057.93	2175.776	1

			10	3089.912	1077.51	2012.402	0.92491231
			20	3084.949	1086.514	1998.435	0.91849299
			30	3077.316	1083.359	1993.957	0.91643487
			40	3065.855	1090.816	1975.039	0.90774004
			50	3048.229	1090.633	1957.596	0.89972313
			60	3039.778	1092.992	1946.786	0.89475479
			70	3031.111	1097.172	1933.939	0.88885023
			80	3010.498	1104.104	1906.394	0.87619038
			90	3016.933	1101.264	1915.669	0.88045323
			100	2999.074	1106.281	1892.793	0.86993928
			110	2981.185	1106.58	1874.605	0.86157996
			120	2966.296	1108.236	1858.06	0.85397578
	3	21.64	0	2340.759	1059.714	1281.045	1
			10	2217.535	1080.981	1136.554	0.88720849
			20	2210.93	1103.336	1107.594	0.86460195
			30	2225.803	1082.57	1143.233	0.8924222
			40	2205.859	1113.028	1092.831	0.85307776
			50	2202.803	1101.215	1101.588	0.85991359
			60	2211.958	1101.738	1110.22	0.86665184
			70	2211.296	1124.748	1086.548	0.84817317
			80	2177.662	1115.607	1062.055	0.82905362
			90	2169.718	1095.234	1074.484	0.83875586
			100	2164.197	1109.514	1054.683	0.82329895
			110	2177.662	1106.897	1070.765	0.83585276
			120	2158.901	1112.318	1046.583	0.81697598
	4	18.81	0	2470.608	1026.385	1444.223	1
			10	1977.728	1086.389	891.339	0.61717546
			20	2120.801	1125.631	995.17	0.68906949

			30	2158.409	1119.217	1039.192	0.71955093
			40	2167.616	1138.744	1028.872	0.71240522
			50	2165.359	1120.645	1044.714	0.72337444
			60	1122.919	2162.823	-1039.904	-0.7200439
			70	2144.411	1104.091	1040.32	0.72033197
			80	2156.111	1110.089	1046.022	0.72428011
			90	2153.061	1119.323	1033.738	0.7157745
			100	2142.969	1107.707	1035.262	0.71682974
			110	2135.341	1106.589	1028.752	0.71232213
			120	2134.267	1117.865	1016.402	0.70377082
	AVERAGE			Average	Standard deviation	SEM	
			0	1	0	0	
			10	0.817223678	0.13785818	0.06892909	
			20	0.821696116	0.09806535	0.049032675	
			30	0.838880755	0.088051818	0.044025909	
			40	0.825009975	0.082290463	0.041145232	
			50	0.831348705	0.075875397	0.037937699	
			60	0.463191668	0.789583248	0.394791624	
			70	0.810599487	0.073793272	0.036896636	
			80	0.801157009	0.065820585	0.032910293	
			90	0.802559384	0.072237659	0.036118829	
			100	0.790073855	0.069365766	0.034682883	
			110	0.790211006	0.070175714	0.035087857	
			120	0.775119856	0.071873927	0.035936963	
[AuNPs] (w/v)	Vesicle #	diameter(nm)	time (sec)	Vesicle intensity	Background intensity	Difference	Ratio
0.026%	1	38.84	0	568.322	395.512	172.81	1
			10	549.15	391.104	158.046	0.91456513

			20	534.886	389.42	145.466	0.84176842
			30	528.887	387.774	141.113	0.8165789
			40	529.523	395.299	134.224	0.77671431
			50	531.928	410.773	121.155	0.7010879
			60	520.836	401.893	118.943	0.68828771
			70	512.971	399.389	113.582	0.6572652
			80	501.462	388.313	113.149	0.65475956
			90	494.012	383.603	110.409	0.638904
			100	496.277	383.118	113.159	0.65481743
			110	498.237	389.819	108.418	0.62738267
			120	493.415	389.975	103.44	0.59857647
	2	27.267	0	130.101	75.827	54.274	1
			10	117.468	78.465	39.003	0.71863139
			20	114.026	80.449	33.577	0.61865718
			30	108.795	76.919	31.876	0.58731621
			40	108.077	77.203	30.874	0.56885433
			50	109.327	77.325	32.002	0.58963776
			60	108.359	74.598	33.761	0.62204739
			70	105.436	73.919	31.517	0.58070163
			80	105.622	74.678	30.944	0.57014408
			90	110.058	75.473	34.585	0.63722961
			100	113.093	75.682	37.411	0.68929874
			110	106	73.229	32.771	0.60380661
			120	116.224	82.861	33.363	0.61471423
	3	22.26	0	219.11	133.704	85.406	1
			10	219.27	138.832	80.438	0.94183078
			20	210.181	135.808	74.373	0.87081704
			30	204.848	136.942	67.906	0.79509636

			40	197.004	136.63	60.374	0.70690584
			50	199.307	154.091	45.216	0.52942416
			60	194.652	136.197	58.455	0.68443669
			70	193.415	138.269	55.146	0.64569234
			80	189.8	133.37	56.43	0.66072641
			90	190.633	133.086	57.547	0.67380512
			100	191.511	134.641	56.87	0.66587828
			110	190.4	138.598	51.802	0.60653818
			120	190.715	136.136	54.579	0.63905346
	AVERAGE			Average	Standard deviation	SEM	
			0	1	0	0	
			10	0.858342434	0.121758926	0.070297549	
			20	0.77708088	0.137965598	0.079654475	
			30	0.732997158	0.12661982	0.073103987	
			40	0.68415816	0.1057806	0.061072458	
			50	0.606716609	0.087096928	0.050285435	
			60	0.664923932	0.037182066	0.021467076	
			70	0.62788639	0.041270865	0.023827745	
			80	0.628543353	0.05066317	0.029250395	
			90	0.649979577	0.020650502	0.011922573	
			100	0.669998149	0.017605973	0.010164813	
			110	0.612575823	0.01289564	0.007445301	
			120	0.617448054	0.020376507	0.011764382	
[AuNPs] (w/v)	Vesicle #	diameter(nm)	time (sec)	Vesicle intensity	Background intensity	Difference	Ratio
0.04	1	32.264	0	696.755	449.2	247.555	1
			10	658.157	455.485	202.672	0.81869484
			20	624.688	439.958	184.73	0.74621801
			30	604.482	428.268	176.214	0.71181758

			40	592.984	427.042	165.942	0.67032377
			50	583.8	424.386	159.414	0.64395387
			60	580.653	425.202	155.451	0.62794531
			70	572.417	427.472	144.945	0.58550625
			80	567.34	426.44	140.9	0.56916645
			90	558.116	424.205	133.911	0.54093434
			100	555.943	430.886	125.057	0.50516855
			110	557.283	436.232	121.051	0.48898629
			120	552.803	437.539	115.264	0.46560966
	2	42.309	0	758.277	347.596	410.681	1
			10	631.221	347.746	283.475	0.69025594
			20	655.667	344.898	310.769	0.75671628
			30	622.884	349.017	273.867	0.66686065
			40	616.768	347.559	269.209	0.65551852
			50	618.174	350.203	267.971	0.65250401
			60	615.246	349.932	265.314	0.64603427
			70	615.61	355.61	260	0.63309479
			80	593.797	346.797	247	0.60144005
			90	607.681	353.661	254.02	0.61853361
			100	607.13	354.559	252.571	0.61500532
			110	565.411	361.271	204.14	0.49707681
			120	555.356	360.305	195.051	0.47494527
	3	32.486	0	697.42	350.039	347.381	1
			10	571.603	309.425	262.178	0.75472752
			20	576.103	310.938	265.165	0.76332615
			30	562.236	308.475	253.761	0.73049764
			40	537	312.325	224.675	0.64676825
			50	548.014	306.038	241.976	0.69657235

			60	532.024	301.675	230.349	0.6631019
			70	537.759	314.65	223.109	0.64226023
			80	528.831	302.938	225.893	0.65027448
			90	523.325	307.2	216.125	0.6221555
			100	507.193	306.15	201.043	0.57873919
			110	508.073	309.85	198.223	0.57062131
			120	498.841	306.95	191.891	0.55239348
	AVERAGE			Average	Standard deviation	SEM	
			0	1	0	0	
			10	0.754559431	0.064219612	0.03707721	
			20	0.755420147	0.008627401	0.004981032	
			30	0.703058622	0.03271018	0.018885231	
			40	0.657536843	0.011906757	0.00687437	
			50	0.664343411	0.028236584	0.0163024	
			60	0.645693824	0.017580768	0.010150261	
			70	0.620287088	0.030467709	0.01759054	
			80	0.606960326	0.040834831	0.023576001	
			90	0.593874482	0.045883261	0.026490713	
			100	0.566304354	0.055964257	0.032310979	
			110	0.5188948	0.044978748	0.025968492	
			120	0.497649473	0.047638937	0.027504353	
[AuNPs] (w/v)	Vesicle #	diameter(nm)	time (sec)	Vesicle intensity	Background intensity	Difference	Ratio
0.053%	1	38.17	0	221.07	129.526	91.544	1
			10	220.256	127.345	92.911	1.01493271
			20	217.246	123.123	94.123	1.02817225
			30	205.123	125.827	79.296	0.86620641
			40	178.18	130.469	47.711	0.52118107
			50	172.451	140.173	32.278	0.35259547

			60	165.393	133.025	32.368	0.35357861
			70	165.916	132.234	33.682	0.36793236
			80	158.773	124.506	34.267	0.37432273
			90	158.557	128.222	30.335	0.33137071
			100	157.139	124.864	32.275	0.3525627
			110	151.844	127.988	23.856	0.260596
			120	156.198	131.198	25	0.27309272
	2	24.263	0	303.2	135.6	167.6	1
			10	248.542	138.039	110.503	0.65932578
			20	203.583	133	70.583	0.42113962
			30	176.262	126.319	49.943	0.29798926
			40	174.432	131.432	43	0.25656325
			50	173.454	126.976	46.478	0.27731504
			60	177.247	136.268	40.979	0.24450477
			70	175.989	137.383	38.606	0.23034606
			80	174.457	135.135	39.322	0.23461814
			90	173.861	134.554	39.307	0.23452864
			100	175.99	138.949	37.041	0.22100835
			110	175.587	138.897	36.69	0.21891408
			120	176.692	139.348	37.344	0.22281623
	AVERAGE			Average	Standard deviation	SEM	
			0	1	0	0	
			10	0.837129243	0.251452075	0.177803467	
			20	0.724655932	0.429236887	0.303516313	
			30	0.582097837	0.401790203	0.284108577	
			40	0.388872159	0.187113059	0.132308913	
			50	0.314955255	0.053231308	0.037640219	
			60	0.29904169	0.077126847	0.054536917	

			70	0.299139211	0.097288205	0.068793149	
			80	0.304470434	0.098786064	0.069852296	
			90	0.282949673	0.068477683	0.048421034	
			100	0.286785528	0.093022972	0.065777174	
			110	0.239755039	0.029473566	0.020840958	
			120	0.247954475	0.035550848	0.025138246	
[AuNPs] (w/v)	Vesicle #	diameter(nm)	time (sec)	Vesicle intensity	Background intensity	Difference	Ratio
0.066%	1	38.964	0	661.408	472.19	189.218	1
			10	595.567	414.736	180.831	0.95567546
			20	534.811	404.993	129.818	0.68607638
			30	476.348	402.237	74.111	0.39166993
			40	437.559	401.702	35.857	0.189501
			50	413.444	397.004	16.44	0.08688391
			60	408.822	391.234	17.588	0.09295099
			70	396.447	387.968	8.479	0.04481075
			80	397.442	384.357	13.085	0.06915304
			90	398.396	386.604	11.792	0.06231965
			100	401.305	387.419	13.886	0.07338625
			110	401.798	393.047	8.751	0.04624824
			120	408.994	397.224	11.77	0.06220338
	2	35.489	0	594.987	425.219	169.768	1
			10	537.964	402.32	135.644	0.79899628
			20	507.313	399.418	107.895	0.6355438
			30	491.528	395.682	95.846	0.56457047
			40	476.257	395.723	80.534	0.4743768
			50	464.933	394.708	70.225	0.41365275
			60	457.793	395.454	62.339	0.36720112
			70	448.869	406.448	42.421	0.2498763

			80	441.113	404.365	36.748	0.21646011
			90	435.767	404.854	30.913	0.18208968
			100	431.013	402.868	28.145	0.16578507
			110	427.405	403.599	23.806	0.14022666
			120	428.568	400.798	27.77	0.16357617
	3	52.066	0	737.654	530.876	206.778	1
			10	706.114	527.35	178.764	0.86452137
			20	628.812	546.241	82.571	0.39932198
			30	564.823	556.841	7.982	0.03860179
			40	518.951	515.578	3.373	0.01631218
			50	483.969	482.198	1.771	0.00856474
			60	475.798	473.542	2.256	0.01091025
			70	479.788	479.892	-0.104	-0.000503
			80	490.144	488.786	1.358	0.00656743
			90	483.068	487.071	-4.003	-0.0193589
			100	475.686	479.367	-3.681	-0.0178017
			110	461.814	463.398	-1.584	-0.0076604
			120	458.2	463.929	-5.729	-0.027706
	AVERAGE			Average	Standard deviation	SEM	
			0	1	0	0	
			10	0.873064371	0.078688176	0.04543064	
			20	0.573647386	0.153069906	0.088374951	
			30	0.331614061	0.268077965	0.154774885	
			40	0.226729992	0.231290503	0.133535634	
			50	0.169700467	0.214867425	0.124053765	
			60	0.157020787	0.186586442	0.107725733	

			70	0.098061365	0.133413508	0.077026325	
			80	0.097393527	0.107758425	0.062214356	
			90	0.075016801	0.101322741	0.058498712	
			100	0.073789875	0.091794051	0.05299732	
			110	0.059604839	0.074842795	0.043210508	
			120	0.066024506	0.09569834	0.055251463	

Figure 3-5 data

AuNPs														
Volume (µL)	Concentration (w/v%)	Hydrodynamic diameter (nm)											Average	St. Deviation
0	0	117.07	104.45	113.10	121.00	98.46	78.32	114.1	103.6	110.5	80.59		104.12	14.63
5	0.01	109.7	100.70	115.70	113.80	85.08	74.11	77.7	119	113.70	80.58		99.01	17.76
10	0.02	99.93	105.00	103.30	94.76	79.11	104.30	112.9					99.90	10.68
15	0.03	142.10	130.30	92.62	89.74	94.95	88.65	79.89	83.93	115.2			101.93	21.98
20	0.04	95.66	82.03	86.66	123.40	138.50	99.54						104.30	22.09
25	0.05	112.30	99.97	112.40	108.60	101.40	108.50	89.82	99.94	103.2			104.01	7.26
30	0.06	87.03	89.15	91.92	117.90	121.00	84.94						98.66	16.30
35	0.07	145.80	114.00	98.20	105.30	108.70	101.8	97.67					110.21	16.73

Figure 3-6 data

Diameter (nm)	
No AuNPs	0.05% w/v AuNPs
65.694	81.858
69.492	92.052
68.55	67.258
30.036	50.887
69.283	88.606
62.726	86.301
48.809	86.573
37.724	113.412

44.008	86.221
46.831	87.809
41.222	30.09
51.046	26.26
58.616	57.534
53.882	51.925
41.76	36.288
39.397	49.852
41.597	38.647
36.678	44.543
56.971	33.935
71.387	41.315
51.26	89.411
46.725	46.917
41.576	44.248
58.025	48.083
44.785	37.776
50.474	43.068
36.697	42.777
49.29	28.613
49.103	29.203
47.767	45.148
42.92	89.706
73.956	69.331
69.13	52.842
67.363	59.298
81.657	46.026
119.858	62.244
102.636	84.555
51.43	78.318
48.911	85.049
62.162	60.203
51.419	78.319
92.235	42.045
44.78	75.233
61.472	46.902
51.512	43.363
43.664	39.38
36.941	57.98

101.256	61.068
59.52	75.669
55.94	57.966
83.3	70.376
39.575	70.376
109.333	53.547
46.51	50.017
46.963	45.577
59.251	58.407
43.539	36.728
47.855	43.807
58.624	37.171
41.088	43.399
41.945	50.892
40.437	62.833
39.129	66.827
94.252	57.095
43.686	73.042
75.926	56.639
48.397	55.752
64.308	49.575
37.76	46.911
36.19	67.269
36.825	75.222
59.292	88.505
51.838	52.229
41.602	57.107
68.732	47.345
66.855	39.38
96.467	50
57.218	44.749
75.091	47.071
86.888	45.652
52.871	52.662
42.187	54.883
70.234	62.838
62.337	54.426
64.073	50.45
38.549	49.123

70.77	46.905
42.307	52.229
56.536	50.049
	89.385
	61.518
	59.292
	102.246
	23.077
	61.222
	52.212
	51.862
	76.106
	58.407
	73.748
	55.47
	53.1
	33.649
	43.068
	40.226
	44.853
	36.654
	57.865
	94.992
	102.08
	70.522
	60.542
	52.085
	73.271
	67.583
	65.382
	56.639
	76.554
	57.164
	88.744
	64.699
	81.033
	38.802
	76.118
	42.993

	46.192
	58.648
	97.427
	79.248
	62.048
	62.414
	74.78
	54.728
	50.769
	73.485
	76.107
	56.653
	63.33
	56.2
	52.332
	46.978
	68.607
	67.374
	49.607
	67.374
	49.607
	77.206
	56.223
	60.699
	61.102
	62.429
	66.816
	68.212
	113.07
	45.444
	42.561
	43.635
	64.173
	122.445
	101.18
	60.518
	60.19848447
No AuNPs	0.055 w/v% AuNPs

Average	
56.9540787	60.19848447
St. Deviation	
18.2982298	18.29920708

Figure 3-11 data

Spacing in 2D hexagonal array (nm)	
In polymersome	In aggregate
4.085	4.323
3.627	5.022
3.641	4.969
3.701	4.349
3.352	4.691
3.661	4.804
4.102	3.939
4.123	4.193
3.485	3.859
3.424	4.235
4.44	4.161
3.931	3.871
3.405	4.107
4.175	4.346
3.727	4.202
3.727	4.244
3.789	4.3
3.258	3.513
3.491	3.693
2.771	4.806
4.123	4.4
4.08	4.83
3.755	5.291
3.644	3.885
3.129	4.0002
3.564	3.831
3.886	4.258
3.266	4.509

4.132	4.818
3.92	4.04
2.811	4.358
3.473	4.462
3.409	4.227
3.402	4.123
3.048	4.634
3.312	4.114
4.107	3.606
3.394	3.232
4.334	3.806
4.99	3.532
4.193	4.419
5.155	3.904
5.523	4.532
4.648	3.87
4.132	3.562
4.222	4.244
4.536	4.544
4.338	4.874
4.735	4.773
4.419	4.224
4.266	4.591
4.342	4.1
4.785	4.311
4.134	4.461
	4.555
	4.57
	3.894
	3.829
AVERAGE	
3.909666667	4.25586552
ST. DEVIATION	
0.570924342	0.42222823

Figure 3-14 data

Irradiaiton time (sec)	0	10	20	30	60	90	120	180	240	300	330	360	420	480
Pulse energy (μJ)														
180μJ	112.7	52.9	666											
	97.67	60.4	370.5											
	101.8	62.92	224.5											
AVG	104.056667	58.74	420.333333											
ST. DEV	7.7649619	5.21217805	224.929063											
SEM	4.48310284	3.0092524	129.862855											
133μJ	89.82	96.23	60.62	352.1										
	99.5	109.6	56.4	235.1										
	96.23		60.62	367.7										
AVG	95.1833333	102.915	59.2133333	318.3										
ST. DEV	4.92414798	9.45401766	2.43641814	72.4742713										
SEM	2.84295816	5.45827964	1.40666667	41.8430 4										
95.5μJ	89.81			42.68	274.4									
	111.5			34.79	200.5									
AVG	100.655			38.735	237.45									
ST. DEV	15.3371461			5.5790725	52.2551911									
SEM	8.85490542			3.22107901	30.1695487									
67.4μJ	89.81			91.83	97.97	68.7	52.89	213.1						
	118			111.5	124.2	122.6	135.5	226.4						
AVG	103.905			101.665	111.085	95.65	94.195	219.75						
ST. DEV	19.9333402			13.9087904	18.5474109	38.1130555	58.4140912	9.40452019						

SEM	11.5085193			8.03024387	10.7083527	22.0045829	33.7253913	5.42970226						
34.0μJ	77.82			76.24	80.56	81.87	61.88	77.06	74.24	51.65	89.5	76.77	85.02	86.77
	116.7			121.4	95.71	122.2	116.9		123.3		97.46		93.81	
	96.67			89.85	83.49	94.67	100.5	97.51	99.02	103.3		89.8		83.5
	97.0633333			95.83	86.5866667	99.58	93.0933333	87.285	98.8533333	77.475	93.48	83.285	89.415	85.135
	19.429842			23.1662837	8.03570988	20.6084521	28.2479049	14.4603337	24.5304246	36.5220652	5.62856998	9.21360136	6.21546861	2.31223917
	11.2254121			13.3750601	4.63941926	11.8982954	16.3089355	8.34867754	14.1626473	21.0860242	3.24965639	5.31947522	3.58850247	1.33497191

Figure 3-16 data

[AuNP] (w/v%)												
0.07%	**Irradiation time (sec)**	**0**	**10**	**20**								
180μJ		101.8	88.65	219.6								
		97.67	60.4	370.5								
		89.1	86.39	666								
				622.7								
AVG		99.735	74.525	**469.7**								
ST.DEV		2.065	14.125	183.25756								
SEM		1.1922283 1	8.1550725 5	105.80380 4								
0.05%		**0**	**10**	**20**	**30**	**40**						
180μJ		125.8	126.1	101.1	127.9	162.6						
		99.94	101	66.59	382.1							
		99.94	70.07	132.2	252.5							
		89.82	44.77	44.35	352.1							
AVG		103.875	85.485	86.06	**278.65**							
ST.DEV		13.315565 1	30.763724 2	33.443632 4	99.380820 6							
SEM		6.6577825 7	15.381862 1	16.721816 2	49.690410 3							

0.03%		**0**	**10**	**20**	**30**	**40**	**50**	**60**	**70**			
180µJ		88.65	86.53	81.38	82.07	42.07	34.79	123.2	349.5			
		79.89	83.31	85.6	37.15	99.37	87.72	28.2	248.3			
		83.93	82.69	88.24	89.36	109.9	44.81	36.22	233.7			
AVG		84.156666 7	84.176666 7	85.073333 3	69.526666 7	83.78	55.773333 3	62.54	**277.166667**			
ST.DEV		3.5798448 1	1.6831980 1	2.8252354 9	23.086394 7	29.80507	22.957093 8	43.017878 5	51.4935163			
SEM		2.0668243 7	0.9717948 3	1.6311504 7	13.328936 2	17.207965 2	13.254284 3	24.836383 7	29.7297955			
0.01%		**0**	**10**	**20**	**30**	**40**	**50**	**60**	**70**	**80**	**90**	**100**
180µJ		85.08			79.56				115.7	120	85.89	248.5
		74.11			83.05				113.7	111.8	112.4	283
		77.7			82.32				80.15	119.2	113	286.5
AVG		78.963333 3			81.643333 3				103.183333	117	103.763333	**272.666667**
ST.DEV		4.5667080 3			1.5029822 2				16.3074795	3.6914315 2	12.6407287	17.1480482
SEM		2.6365901 1			0.8677471 9				9.4151277	2.1312489 8	7.2981281 2	9.90043022

0 % (NO AuNPs)		**0**	**10**	**20**	**30**	**40**	**50**	**60**	**70**	**80**	**90**	**100**	**110**	**120**	**150**	**170**	**200**	**230**	**260**	**290**	**320**	**350**
180 µJ		**100.7**	**94.19**	**100.7**	**96.19**	**121.1**	**123.1**	**96.25**	**107.5**	**116.6**	**103.3**	**111.1**	**95.92**	**99.76**	**105.5**	**102.6**	**91.9**	**95.72**	**95.21**	**97.74**	**106.3**	**114.5**
		103.6			125.2			86.49						112.8		108.1		94.31		122.9		
		120.2	92.63	107.9		118.7			**100.7**		112.8		108.1		122.9				108.6			
		108.5	**103.2**	**103**	**101.6**	**102.2**	**102.5**	**103.2**	**102.1**	**102.8**	**103.3**	**101.4**	**101.4**	**101.6**	**101.2**	**102.1**	**101.4**	**100.5**	**100.5**	**101.6**	**100.8**	**101.7**
AVG		108.25	96.67333333	103.866667	107.663333	114	112.8	95.31333333	103.433333	109.7	106.466667	106.25	101.806667	104.72	109.866667	104.266667	96.65	96.843333	101.436667	107.413333	103.55	108.1
ST.DEV		8.592438 54	5.7058245 1	3.6774085 1	15.4262125	10.2893148	14.5663997	8.3942857 5	3.5907288 8	9.7580358	5.4848275 6	6.8589578	6.1001748 6	7.0577501	11.4901407	3.3291640 6	6.7175144 2	3.2442924 2	6.7439627 3	13.550001 2	3.8898973	9.0509668
SEM		4.2962192 7	2.8529122 5	1.8387042 5	7.7131062 7	5.1446574 2	7.2831998 5	4.1971428 8	1.7953644	4.8790367 9	2.7424137 8	3.4294678 9	3.0508743	3.5288525	5.7450703 5	1.6645820 3	3.3587572 1	1.6221462 1	3.3719813 7	6.7750062	1.9445436 5	4.5254834

Figure 3-18 data

	0.07 % w/v AuNPs		
	Ruptured	Non-rradiated	
Time (minutes)	Hydrodynamic diameter (nm)		Time (minutes)
0	239.4	124.1	0
10	469.3	100.5	10
20	354.6	110.9	20
30	371	103.1	30
40	303.6	102.2	40
50	248.2	103.7	50
60	211.1	115.2	60
120	136.3	109.9	70
180	173.4	109.7	80
240	160.3	113.2	90
300	162.9	107.7	100
360	168.6	117.3	110
420	145.2	109.9	120
480	157.3	112	150
		101.1	180
		99.83	210
		106.4	240
		106	270
		115.6	300
		122.8	330
		107.6	360
		105.1	390
		107.2	420
		110.9	450
		102.9	470
		94.23	500
		103.3	530

Figure 3-19 data

No AuNP	Triton X (µL)	[TritonX] (mM)	PDI 1	PDI 2	PDI 3	PDI Avg	PDI SD	PDI % Change	SE	Number 1	Number 2	Number 3	Number AVG	Number SD	SEM
	0	0	0.264	0.251	0.269	0.261	0.00758654	0.00%		113.10	121.00	117.10	117.07	3.22524762	1.862097583
	0.25	0.41344667	0.223	0.230	0.243	0.232	0.00828654	-11.22%	0.00068044	127.40	125.80	124.80	126.00	1.07082523	0.618241233
	0.5	0.82689334	0.242	0.237	0.244	0.241	0.00294392	-7.78%	0.0003377	123.60	124.70	100.80	116.37	11.0164523	6.360351726
	0.75	1.24034001	0.266	0.283	0.256	0.268	0.0111455	2.68%	0.00090051	114.00	122.30	127.00	121.10	5.37463177	3.103045099
	1	1.65378670 8	0.232	0.272	0.255	0.253	0.01639105	-3.19%	0.00169005	102.20	115.70	99.27	105.72	7.15526069	4.131091686
	1.5	2.48068006 2	0.314	0.520	0.342	0.392	0.09122865	50.00%	0.02827578	6.59	6.73	7.24	6.85	0.2807304	0.1620779 7
	2	3.30757341 6	0.501	0.509	0.352	0.454	0.0721988	73.72%	0.01542454	7.323	6.394	5.856	6.52	0.60594958	0.349845151
	3	4.96136012 4	0.495	0.523	0.505	0.508	0.01158543	94.26%	0.0006388	7.39	6.69	6.883	6.99	0.295202	0.170434956
0.01 % AuNP	**Triton**		**PDI 1**	**PDI 2**	**PDI 3**	**PDI Avg**	**PDI SD**	**PDI % Change**	**SE**	**Number 1**	**Number 2**	**Number 3**	**Number avg**	**Number SD**	
	0	0	0.226	0.213	0.231	0.223	0.00758654	0.00%		113.70	112.70	102.70	109.70	4.96655481	2.867441756
	1	1.65378670 8	0.239	0.269	0.198	0.235	0.02910136	5.37%	0.0050832	93.55	96.96	102.6	97.70	3.73184792	2.154583 4
	2	3.30757341 6	0.223	0.220	0.292	0.245	0.03325658	9.70%	0.00629009	124.00	127.00	82.30	111.10	20.4014705	11.7879451
	3	4.96136012 4	0.273	0.280	0.308	0.287	0.01512173	28.51%	0.00138991	113.00	123.50	120.00	118.83	4.36526695	2.520288049
	4	6.61514683 2	0.354	0.397	0.320	0.357	0.03150661	59.85%	0.00400484	6.86	5.74	6.87	6.49	0.53226643	0.307304168
	5	8.26893353 9	0.3	0.5	0.5	0.477	0.11979241	113.73%	0.03996688	6.731	6.051	6.705	6.4956666 7	0.31460593	0.181637816

			12	92	28										
0.02 % AuNP	**Triton**		**PDI 1**	**PDI 2**	**PDI 3**	**PDI Avg**	**PDI SD**	**PDI % Change**	**SE**	**Number 1**	**Number 2**	**Number 3**	**Number avg**	**Number SD**	
	0	0	0.230	0.245	0.201	0.225	0.0182635	0.00%		94.76	79.11	104.30	92.72	10.3841236	5.995276536
	2	3.30757341 6	0.205	0.208	0.225	0.213	0.00880656	-5.62%	0.00101019	96.85	109.3	94.24	100.13	6.57113384	3.793845894
	4	6.61514683 2	0.270	0.264	0.318	0.284	0.02416609	26.04%	0.00193644	98.89	95.93	106.10	100.31	4.27102122	2.465875248
	6	9.92272024 7	0.459	0.269	0.453	0.394	0.08818667	74.70%	0.01162717	7.01	7.19	6.51	6.90	0.28680346	0.165586052
	8	13.2302936 6	0.567	1.000	0.598	0.722	0.19721787	220.27%	0.03032069	6.77	6.79	6.71	6.76	0.03487438	0.020134731
0.03 % AuNP	**Triton**		**PDI 1**	**PDI 2**	**PDI 3**	**PDI Avg**	**PDI SD**	**PDI % Change**	**SE**	**Number 1**	**Number 2**	**Number 3**	**Number avg**	**Number SD**	
	0	0	0.186	0.165	0.201	0.184	0.01476482	0.00%		142.10	64.91	130.30	112.44	33.9499439	19.60100923
	4	6.61514683 2	0.197	0.205	0.246	0.216	0.02146315	17.39%	0.00315088	139.7	152.6	151.8	148.03	5.90160054	3.407290658
	6	9.92272024 7	0.255	0.286	0.206	0.249	0.03293428	35.33%	0.00608157	80.33	132.80	143.50	118.88	27.6044276	15.937424 37
	8	13.2302936 6	0.476	0.500	0.477	0.484	0.01108553	163.22%	0.00067414	7.78	6.31	7.72	7.27	0.68102194	0.393188203
	9	14.8840803 7	0.466	0.521	0.478	0.488	0.02361261	165.40%	0.00184467	6.91	6.83	6.61	6.78	0.12670263	0.073151796
0.04 % AuNP	**Triton**		**PDI 1**	**PDI 2**	**PDI 3**	**PDI Avg**	**PDI SD**	**PDI % Change**	**SE**	**Number 1**	**Number 2**	**Number 3**	**Number avg**	**Number SD**	
	0	0	0.202	0.265	0.203	0.223	0.02946561	0.00%		95.66	82.03	86.66	88.12	5.65895357	3.267198369
	4	6.61514683 2	0.248	0.298	0.263	0.270	0.02094968	20.75%	0.00187 17	112.5	94.06	89.68	98.75	9.88809835	5.708896242

	8	13.2302936	0.287	0.305	0.310	0.301	0.00987702	34.63%	0.00142947	94.85	89.80	83.50	89.38	4.64297558	2.680623 2
	10	16.5378670 8	0.480	0.320	0.463	0.421	0.07175421	88.51%	0.00546983	7.74	7.39	7.48	7.54	0.14741401	0.085109516
	11	18.1916537 9	0.592	0.523	0.508	0.541	0.03657868	142.24%	0.00215871	7.209	7.823	6.947	7.33	0.36712335	0.211958766
0.05 % AuNP	**Triton**		**PDI 1**	**PDI 2**	**PDI 3**	**PDI Avg**	**PDI SD**	**PDI % Change**	**SE**	**Number 1**	**Number 2**	**Number 3**	**Number avg**	**Number SD**	
	0	0	0.139	0.162	0.149	0.150	0.0094163	0.00%		112.30	99.97	112.40	108.22	5.83613076	3.369491664
	2	3.30757341 6	0.149	0.172	0.207	0.176	0.02384673	17.33%	0.0040591	127.6	128.1	97.2	117.63	14.4499904	8.342705 84
	4	6.61514683 2	0.198	0.200	0.228	0.209	0.01369509	39.11%	0.0015823	119.50	131.60	135.50	128.87	6.81191766	3.932862495
	6	9.92272024 7	0.149	0.216	0.228	0.198	0.03475949	31.78%	0.0071190 8	139.90	133.20	127.20	133.43	5.18737784	2.994933994
	8	13.2302936 6	0.263	0.264	0.252	0.260	0.0054365	73.11%	0.0007486 3	126.90	133.50	116.40	125.60	7.0413067	4.065300317
	10	16.5378670 8	0.266	0.266	0.261	0.264	0.00235702	76.22%	0.0006500 7	130.4	138.2	135.4	134.67	3.22628097	1.862694186
	12	19.8454404 9	0.247	0.299	0.273	0.273	0.02122891	82.00%	0.0023808 8	109.9	128.7	126.6	121.73	8.41123587	4.856229295
	14	23.1530139 1	0.475	0.326	0.339	0.380	0.06738447	153.33%	0.0133175 8	6.48	7.00	7.62	7.03	0.46449423	0.268175868
	16	26.4605873 3	0.493	0.341	0.322	0.385	0.07652596	156.89%	0.0167676 5	6.52	8.474	8.092	7.70	0.84512813	0.487934953
0.06 % AuNP	**Triton**		**PDI 1**	**PDI 2**	**PDI 3**	**PDI Avg**	**PDI SD**	**PDI % Change**	**SE**	**Number 1**	**Number 2**	**Number 3**	**Number avg**	**Number SD**	
	0	0	0.212	0.170	0.175	0.186	0.01873203	0.00%		117.90	121.00	84.94	107.95	16.3173228	9.420810691
	12	19.8454404 9	0.411	0.292	0.455	0.386	0.0688525	107.90%	0.0075653 3	112.4	142.4	120.8	125.20	12.6364552	7.295660811

	14	23.153013 91	0.526	0.558	0.734	0.606	0.09144762	226.39%	0.00837585	7.35	7.47	7.28	7.37	0.08155707	0.047086996
	16	26.4605873 3	0.686	0.698	0.709	0.698	0.00939267	275.76%	0.00107641	7.80	7.04	7.19	7.34	0.329592	0.190290032
0.07% AuNP	**Triton**		**PDI 1**	**PDI 2**	**PDI 3**	**PDI Avg**	**PDI SD**	**PDI % Change**	**SE**	**Number 1**	**Number 2**	**Number 3**	**Number avg**	**Number SD**	
	0	0	0.132	0.143	0.121	0.132	0.00898146	0.00%		98.20	105.30	108.70	104.07	4.37442406	2.525572909
	12	19.8454404 9	0.276	0.284	0.219	0.260	0.02894055	96.72%	0.00427 17	106.7	103.8	118.7	109.73	6.44997847	3.723896804
	14	23.153013 91	0.320	0.556	0.467	0.448	0.09731164	239.14%	0.02423241	8.81	7.25	7.76	7.94	0.64884633	0.374611601
	16	26.4605873 3	0.442	0.555	0.559	0.519	0.05423611	292.93%	0.00699495	7.73	8.13	7.63	7.83	0.21680765	0.125173953

Figure 3-20 data

0% AuNP	**Tween 20 (µL)**	**[Tween 20] (mM)**	**PDI 1**	**PDI 2**	**PDI 3**	**PDI Avg**	**PDI SD**	**Number 1**	**Number 2**	**Number 3**	**Number avg**	**Number SD**	**SEM**
	0	0	0.223	0.219		0.221	0.002	104.3	104.60		104.45	0.15	0.08660254
	1	0.891693811	0.298	0.297		0.298	0.0005	89.86	93.52		91.69	1.83	1.056550993
	1.5	1.337540717	0.303	0.319		0.311	0.008	7.71	8.40		8.05	0.343	0.198031142
	2	1.783387622	0.329	0.335		0.332	0.003	6.87	8.39		7.63	0.758	0.437631504
0.01% AuNP	**Tween 20 (µL)**		**PDI 1**	**PDI 2**	**PDI 3**	**PDI Avg**	**PDI SD**	**Number 1**	**Number 2**	**Number 3**	**Number avg**	**Number SD**	
	0	0	0.292	0.291	0.253	0.279	0.0181536 7	100.70	115.70	113.80	110.07	6.6684997 5	3.850060125
	1.5	1.337540717	0.285	0.275	0.266	0.275	0.0077603	111.70	103.40	104.30	106.47	3.7187214 1	2.147004804
	2.5	2.229234528	0.372	0.244	0.302	0.306	0.0523322 7	108.90	106.90	95.90	103.90	5.7154760 7	3.299831646
	3	2.675081433	0.306	0.379	0.313	0.333	0.0328870 1	7.14	7.86	6.38	7.13	0.6055423 6	0.349610047

	4	3.566775244	0.419	0.510	0.505	0.478	0.0417692 1	8.07	5.44	7.91	7.14	1.2064660 1	0.696553473
0.02% AuNP	**Tween 20 (µL)**		**PDI 1**	**PDI 2**	**PDI 3**	**PDI Avg**	**PDI SD**	**Number 1**	**Number 2**	**Number 3**	**Number avg**	**Number SD**	**SEM**
	0	0	0.186	0.176	0.183	0.182	0.0041899 4	99.93	105.00	103.30	102.74	2.1069145 4	1.216427678
	3	2.675081433	0.249	0.213	0.327	0.263	0.0475815 1	103.50	109.50	96.60	103.20	5.2706735 8	3.043024811
	5	4.458469055	0.253	0.246	0.235	0.245	0.0074087	99.55	106.80	105.30	103.88	3.1247222 1	1.804059209
	8	7.133550489	0.294	0.275	0.286	0.285	0.0077888 8	101.60	108.90	113.20	107.90	4.7881798 9	2.764456949
	10	8.916938111	0.322	0.292	0.293	0.302	0.0139124 2	99.15	109.10	106.70	104.98	4.2395623 5	2.447712462
	12	10.70032573	0.358	0.436	0.327	0.374	0.0458572 7	8.62	6.37	8.42	7.80	1.0166674 3	0.586973215
	13	11.59201954	0.340	0.352	0.492	0.395	0.0689991 9	7.274	7.155	6.344	6.92	0.4132233 7	0.238574625
0.03% AuNP	**Tween 20 (µL)**		**PDI 1**	**PDI 2**	**PDI 3**	**PDI Avg**	**PDI SD**	**Number 1**	**Number 2**	**Number 3**	**Number avg**	**Number SD**	**SEM**
	0	0	0.120	0.167	0.160	0.149	0.0207042 7	92.62	89.74	94.95	92.44	2.1309205 1	1.23028753
	12	10.70032573	0.287	0.264	0.258	0.270	0.0124988 9	107.00	92.25	104.50	101.25	6.4452825 1	3.721185594
	18	16.0504886	0.285	0.301	0.289	0.292	0.0067986 9	109.00	118.80	120.20	116.00	4.9826365 2	2.876726535
	20	17.83387622	0.288	0.314		0.301	0.013	118.90	96.96		107.93	10.97	6.333532453
	21	18.72557003	0.327	0.497	0.549	0.458	0.0948027 2	7.44	6.73	6.54	6.91	0.3879716 5	0.223995536
	22	19.61726384	0.359	0.547	0.327	0.411	0.0970498 2	7.392	7.705	7.182	7.43	0.2148896 4	0.124066589
0.03% AuNP	**Tween 20 (µL)**		**PDI 1**	**PDI 2**	**PDI 3**	**PDI Avg**	**PDI SD**	**Number 1**	**Number 2**	**Number 3**	**Number avg**	**Number SD**	**SEM**
	0	0	0.160	0.141	0.155	0.152	0.0080415 6	143.30	123.40	138.50	135.07	8.4791246 9	4.895424924
	20	17.83387622	0.280	0.286	0.300	0.289	0.0083798 7	153.80	152.10	137.40	147.77	7.3631213 2	4.251100075
	24	21.40065147	0.299	0.29	0.299	0.296	0.0042426 4	156.7	149.2	168	157.97	7.7271527	4.461273693

	25	22.29234528	0.321	0.278	0.321	0.300	0.0202703 9	135.70	161.50	162.10	153.10	12.306096 1	7.104927867
	26	23.18403909	0.339	0.326	0.313	0.326	0.0106144 6	6.68	7.30	7.50	7.16	0.3499066 5	0.202018701
	27	24.0757329	0.324	0.474	0.33	0.376	0.0693397 4	7.127	6.949	5.751	6.61	0.6110341	0.3527807
0.04% AuNP	**Tween 20 (µL)**		**PDI 1**	**PDI 2**	**PDI 3**	**PDI Avg**	**PDI SD**	**Number 1**	**Number 2**	**Number 3**	**Number avg**	**Number SD**	**SEM**
	0	0	0.139	0.134	0.114	0.129	0.0108012 3	108.60	101.40	108.50	106.17	3.3707895 5	1.946126257
	1.5	1.337540717	0.173	0.169	0.149	0.164	0.0104986 8	98.24	114.00	95.90	102.71	8.0378493 5	4.640654488
	10	8.916938111	0.223	0.226	0.217	0.222	0.0037416 6	112.00	102.90	125.40	113.43	9.2413322 8	5.335485677
	30	26.75081433	0.284	0.286	0.272	0.281	0.0061824 1	112.90	123.5	127.6	121.33	6.1937244 2	3.575948463
	32	28.53420195	0.309	0.281			0.014	114.5	133.6		124.05	9.55	5.513695071
	33	29.42589577	0.32	0.299	0.299	0.310	0.0098994 9	6.788	7.275	5.906	6.66	0.5665935 2	0.327122924
	35	31.20928339	0.319	0.297	0.383	0.340	0.0364783	7.011	5.241	7.123	6.46	0.8619982	0.49767489
0.05% AuNPs	**Tween 20 (µL)**		**PDI 1**	**PDI 2**	**PDI 3**	**PDI Avg**	**PDI SD**	**Number 1**	**Number 2**	**Number 3**	**Number avg**	**Number SD**	**SEM**
	0	0	0.147	0.148	0.127	0.141	0.0096724 1	87.03	89.15	91.92	89.37	2.0022043 4	1.155973215
	33	29.42589577	0.291	0.263	0.288	0.281	0.0125521 1	105.10	108.90	91.92	101.97	7.2760856 4	4.200850002
	35	31.20928339	0.272	0.274	0.31	0.285	0.0174610 7	106.3	116.9	91.82	105.01	10.279628 2	5.934946098
	40	35.66775244	0.256	0.289	0.305	0.283	0.0204015 2	117.1	99.06	118.1	111.42	8.7493695	5.051450837
	45	40.1262215	0.311	0.302	0.299	0.304	0.0050990 2	97.5	104.8	102.7	101.67	3.0684777 3	1.771586441
	47	41.90960912	0.312	0.323	0.461	0.365	0.0677954 4	5.8	6.758	6.364	6.31	0.3931491 1	0.226984744
	48	42.80130293	0.522	0.63	0.353	0.502	0.1139951 3	6.69	7.472	7.156	7.11	0.3212019 1	0.185446009
0.07% AuNPs	**Tween 20 (µL)**		**PDI 1**	**PDI 2**	**PDI 3**	**PDI Avg**	**PDI SD**	**Number 1**	**Number 2**	**Number 3**	**Number avg**	**Number SD**	**SEM**

	0	0	0.185	0.145	0.209	0.180	0.0263986 5	156.40	145.80	114.00	138.73	18.016535 6	10.40185169
	45	40.1262215	0.274	0.277	0.294	0.282	0.0088065 6	224.8	225.6	202.4	217.60	10.752984 1	6.208238254
	47	41.90960912	0.473	0.428	0.521	0.474	0.0379736 8	5.63	6.60	6.64	6.29	0.4679781 6	0.270187315
	49	43.69299674	0.522	0.461	0.336	0.440	0.0774180 6	6.641	6.035	6.7	6.46	0.3005443 2	0.173519345

Figure 3-22

CONTROLS	**Triton X (µL)**	**[Triton X] (mM)**										
NILE RED			**PDI 1**	**PDI 2**	**PDI 3**	**AVG**	**Number 1**	**Number 2**	**Number 3**	**AVG**	**st. dev**	**st. error**
1 µL (1 mg/mL) Nile Red	0	0	0.234	0.226	0.243	0.23	92.46	142.7	102.6	**112.59**	26.5671702	15.3385629
	1.5	2.48	0.327	0.462	0.46	0.42	6.639	5.976	6.197	**6.27**	0.33758308	0.19490368
	2	3.31					6.715	6.573		**6.64**	0.10040916	0.05797126
10 µL (1 mg/mL) Nile Red	0	0	0.314	0.396	0.224	**0.311**	119	136.3	102.5	**119.27**	16.9015778	9.75813051
0.1mM	1.5	2.48	0.523	0.463	0.448	**0.478**	5.885	6.173	6.002	**6.02**	0.14484129	0.08362416
	2	3.31					6.712	5.898	6.013	**6.21**	0.44053415	0.25434251

Figure 4-3

Rehydration temp (ºC)	**Rehydration time**	**Avg diameter (nm)**	**St. dev**	**SEM**
35ºC	60	9.666919305	0.11316094	0.36391802
	55	9.327569798	0.49265124	0.29938
	50	8.861812301	0.08532522	0.2707973
	45	8.876419141	0.01285952	0.28450925
	40	8.034554083	0.09424466	0.29193917
	34	7.579507158	0.56819629	0.30299504
	30	6.852898727	0.10516395	0.26201559
	25	5.537481301	1.19310415	0.2471378
	20	4.166460976	1.58439864	0.20877862
	15	3.614038211	1.92252216	0.18345808
	10	2.699361973	1.33984114	0.12886627
Rehydration temp (ºC)	Rehydration time	Avg diameter (nm)	St. dev	SEM
45ºC	20	10.52033647	4.09443126	0.7966059
	25	11.21091048	4.20558382	0.74707399
	30	12.91291547	4.4009452	0.79264413

	35	13.96948503	5.74888553	0.79586153
	40	14.72092489	5.85701995	0.73449231
	45	16.23314052	5.73602395	0.77812843
	50	16.36970288	6.07581266	0.80043921
	55	16.7041153	5.34139055	0.8102637
	60	17.8862694	5.14297577	0.85762736
Rehydration temp (ºC)	Rehydration time	Avg diameter (nm)	St. dev	SEM
55ºC	10	9.697771429	0	0.70003343
	15	11.72339874	2.58505363	0.59188219
	20	13.53385034	2.18988565	0.64906775
	25	15.97044532	2.17240002	0.77880824
	30	17.65460663	2.52499822	0.80349242
	35	17.84235153	1.43500034	0.77530934
	40	19.59876701	2.58938415	0.82188883
	45	20.33877876	2.04648706	0.79517201
	50	20.32839773	1.1551957	0.76584854
	55	20.9807254	1.08936422	0.78472463
	60	21.32563651	1.2971279	0.72388541
*****Each average vesicle diameter is the average of ~50 vesicles**				

Figure 4-4 data (same as table above + data below)

25µL AuNPs				
	Rehydration time (min)	Avg. diameter (µm)	St. Dev	SEM
	60	10.365	2.80347937	0.88653802
	55	9.0011	2.14709969	0.67897254
	50	8.4264	2.02312047	0.63976687
	45	8.0612	1.91776656	0.60645103
	40	7.7607	1.66071256	0.52516342
	35	7.4867	1.64962038	0.52165577
	30	6.1529	1.22109733	0.38614488
	25	3.8193	1.99238455	0.63004732
	Rehydration time (min)	Avg. diameter (µm)	St. Dev	SEM
	60	9.9105	2.56454352	0.81097987
	55	8.6388	2.35128938	0.74354299
	50	8.698	1.99246084	0.63007144
	45	8.546	2.00027303	0.63254187
	40	7.638	1.90958849	0.6038649
	35	7.7299	1.78871258	0.56564058

	30	7.5163	1.95923485	0.61956446
	25	7.5461	2.0881573	0.66033332
	20	6.849	1.77907403	0.56259261
	15	6.0017	1.99967578	0.632353
AVERAGE	Rehydration time (min)	Diameter (nm)	St. Dev	SEM
	60	10.13775	2.68401145	0.84875894
	55	8.81995	2.24919454	0.71125776
	50	8.5622	2.00779066	0.63491915
	45	8.3036	1.95901979	0.61949645
	40	7.69935	1.78515053	0.56451416
	35	7.6083	1.71916648	0.54364818
	30	6.8346	1.59016609	0.50285467
	25	5.6827	2.04027092	0.64519032
	20	6.849	1.77907403	0.56259261
	15	6.0017	1.99967578	0.632353

Figure 4-5 data

Concentration of polymer/THF	**AuNPs(µL)**	**DLS results**											
Day 1		Z- average (nm) / Number (nm) / PDI			Z- average (nm) / Number (nm) / PDI			Average Z-avg (nm)	St. Dev.	Average number size (nm)	St. Dev.	Average PDI	St. Dev.
2 mg/mL	0	170.6	114.4	0.201	167.5	124.9	0.19	169.05	1.55	119.65	5.25	0.1955	0.0055
4 mg/mL	0	146.6	83.93	0.267	175	99.26	0.344	160.8	14.2	91.595	7.665	0.3055	0.0385
8 mg/mL	0	123.8	72.58	0.263	120.8	69.82	0.259	122.3	1.5	71.2	1.38	0.261	0.002

Figure 4-6 data

	No AUNPs	0.05% AuNPs	No AuNPs	0.05% AuNPs	No AuNPs	0.05% AuNPs
[Diblock copolymer] mg/mL	2	2	4	4	8	8
Size (nm)	119.65	91.62	91.595	87.6	71.2	71.165

Figures 4-7 data

	Day	No AuNPs	0.05 % AuNPs	No AuNPs	0.05% AuNPs	No AuNPs	0.05% AuNPs
		2	2	4	4	8	8
Hydrodynamic diameter (nm)	1	119.65	91.62	91.595	87.6	71.2	71.165
	10	123	89.01	94.75	101.3	69.57	67.06
% change	1	0	0	0	0	0	0
	10	2.79983285	2.84872299	3.44451116	15.6392694	2.28932584	5.76828497

References

1. Hoffman, A. S. The origins and evolution of "controlled" drug delivery systems. *J Control Release* **2008***, 132*, 153-163.

2. Wang, Y.; Liu, L.; Xue, X.; Liang, X. Nanoparticle-based drug delivery systems: What can they really do. *F1000Research* **2017***, 6*, 681.

3. Pavlopoulou, A.; Spandidos, D. A.; Michalopoulos, I. Human cancer databases (Review). *Oncology Reports* **2015***, 33*, 3-18.

4. Manuel Arruebo; Nuria Vilaboa; Berta Saez-Gutierrez; Julio Lambea; Alejandro Tres; Mónica Valladares; africa Gonzalez-Fernandez Assessment of the Evolution of Cancer Treatment Therapies. *Cancers* **2011***, 3*, 3279-3330.

5. Khodabandehloo, H.; Zahednasab, H.; Ashrafi Hafez, A. Nanocarriers usage for drug delivery in cancer therapy. *Iranian journal of cancer prevention* **2016***, 9*, e3966.

6. Din, F. U.; Aman, W.; Ullah, I.; Qureshi, O. S.; Mustapha, O.; Shafique, S.; Zeb, A. Effective use of nanocarriers as drug delivery systems for the treatment of selected tumors. *International journal of nanomedicine* **2017***, 12*, 7291-7309.

7. Cho, K.; Wang, X.; Nie, S.; Chen, Z. G.; Shin, D. M. Therapeutic nanoparticles for drug delivery in cancer. *Clin. Cancer Res.* **2008***, 14*, 1310-1316.

8. Kauscher, U.; Holme, M. N.; Björnmalm, M.; Stevens, M. M. Physical stimuli-responsive vesicles in drug delivery: Beyond liposomes and polymersomes. *Advanced Drug Delivery Reviews* **2018**.

9. Rideau, E.; Dimova, R.; Schwille, P.; Wurm, F. R.; Landfester, K. Liposomes and polymersomes: a comparative review towards cell mimicking. *Chem Soc Rev* **2018***, 47*, 8572-8610.

10. Allen, T. M.; Cullis, P. R. Liposomal drug delivery systems: From concept to clinical applications. *Advanced Drug Delivery Reviews* **2013***, 65*, 36-48.

11. Barenholz, Y. Doxil®--the first FDA-approved nano-drug: lessons learned. *J Control Release* **2012***, 160*, 117-134.

12. Manzoor, A.; Lindner, L.; Landon, C.; Park, J.; Simnick, A.; her, M.; Shiva Das; Hanna, G.; Park, W.; Chilkoti, A.; Koning, G.; Hagen, T.; Needham, D.; Dewhirst, M. Overcoming limitations in nanoparticle drug delivery: Triggered, intravascular

release to improve drug penetration into tumors. *Cancer Research* **2012***, 72*, 5566-5575.

13. Sercombe, L.; Veerati, T.; Moheimani, F.; Wu, S. Y.; Sood, A. K.; Hua, S. Advances and challenges of liposome assisted drug delivery. *Frontiers in pharmacology* **2015***, 6*, 286.

14. Karayianni, M.; Pispas, S. Self-Assembly of Amphiphilic Block Copolymers in Selective Solvents. In *Fluorescence Studies of Polymer Containing Systems*; Procházka, K., Ed.; Springer International Publishing: 2016; pp 27-63.

15. Salim, M.; Minamikawa, H.; Sugimura, A.; Hashim, R. Amphiphilic designer nano-carriers for controlled release: from drug delivery to diagnostics. **2014***, 5*, 162-1618.

16. Hu, X.; Zhang, Y.; Xie, Z.; Jing, X.; Bellotti, A.; Gu, Z. Stimuli-Responsive Polymersomes for Biomedical Applications. *Biomacromolecules* **2017***, 18*, 649-673.

17. Gerweck, L. E.; Seetharaman, K. Cellular pH Gradient in Tumor versus Normal Tissue: Potential Exploitation for the Treatment of Cancer. *Cancer Res* **1996***, 56*, 1194-1198.

18. Ahmed, F.; Pakunlu, R. I.; Srinivas, G.; Brannan, A.; Bates, F.; Klein, M. L.; Minko, T.; Discher, D. E. Shrinkage of a rapidly growing tumor by drug-loaded polymersomes: pH-triggered release through copolymer degradation. *Molecular pharmaceutics* **2006***, 3*, 340-350.

19. Trail, P. A.; Willner, D.; Bianchi, A. B.; Henderson, A. J.; TrailSmith, M. D.; Girit, E.; Lasch, S.; Hellström, I.; Hellström, K. E. Enhanced Antitumor Activity of Paclitaxel in Combination with the Anticarcinoma Immunoconjugate BR96-Doxorubicin. *Clin Cancer Res* **1999***, 5*, 3632-3638.

20. Nahire, Rahul|Haldar, Manas K.|Paul, Shirshendu|Ambre, Avinash H.|Meghnani, Varsha|Layek, Buddhadev|Katti, Kalpana S.|Gange, Kara N.|Singh, Jagdish|Sarkar, Kausik|Mallik, Sanku Multifunctional polymersomes for cytosolic delivery of gemcitabine and doxorubicin to cancer cells. *Biomaterials* **2014***, 35*, 6482-6497.

21. Anajafi, T.; Mallik, S. Polymersome-based drug-delivery strategies for cancer therapeutics. *Therapeutic Delivery* **2015***, 6*, 521-534.

22. Gamcsik, M. P.; Kasibhatla, M. S.; Teeter, S. D.; Colvin, O. M. Glutathione levels in human tumors. *Biomarkers* **2012***, 17*, 671-691.

23. Liu, F.; Kozlovskaya, V.; Medipelli, S.; Xue, B.; Ahmad, F.; Saeed, M.; Cropek, D.; Kharlampieva, E. Temperature-sensitive polymersomes for controlled delivery of anticancer drugs. *Chemistry of Materials* **2015***, 27*, 7945-7956.

24. Mazzotta, E.; Tavano, L.; Muzzalupo, R. Thermo-Sensitive Vesicles in Controlled Drug Delivery for Chemotherapy. *Pharmaceutics* **2018***, 10*.

25. Pitt, W. G.; Husseini, G. A.; Staples, B. J. Ultrasonic drug delivery - a general review. *Expert Opinion on Drug Delivery* **2004***, 1*, 37-56.

26. Chen, W.; Du, J. Ultrasound and pH Dually Responsive Polymer Vesicles for Anticancer Drug Delivery. *Scientific reports* **2013***, 3*, 2162.

27. Zhao, Y.; Du, L.; Lu, C.; Jin, Y.; Ge, S. Potential and problems in ultrasound-responsive drug delivery systems. *International journal of nanomedicine* **2013***, 8*, 1621-1633.

28. MacDonell-Yilmaz, R. Delivery. *Journal of clinical oncology : official journal of the American Society of Clinical Oncology* **2016***, 34*, 3705.

29. Smith, A. M.; Mancini, M. C.; Nie, S. Second window for in vivo imaging. *Nat Nanotechnol* **2009***, 4*, 710-711.

30. Mabrouk, E.; Cuvelier, D.; Brochard-Wyart, F.; Nassoy, P.; Li, M. Bursting of sensitive polymersomes induced by curling. *PNAS* **2009***, 106*, 7294-7298.

31. Barhoumi, A.; Liu, Q.; Kohane, D. S. Journal of controlled release. *Journal of controlled release* **1984***, 219*, 31-42.

32. Jayakumar, M. K. G.; Idris, N. M.; Zhang, Y. Remote activation of biomolecules in deep tissues using near-infrared-to-UV upconversion nanotransducers. *Proc Natl Acad Sci U S A* **2012***, 109*, 8483-8488.

33. Mabrouk, E.; Cuvelier, D.; Brochard-Wyart, F.; Nassoy, P.; Li, M. Bursting of sensitive polymersomes induced by curling. *ResearchGate* **2009***, 17*.

34. Robbins, G. P.; Jimbo, M.; Swift, J.; Therien, M. J.; Hammer, D. A.; Dmochowski, I. J. Photoinitiated destruction of composite porphyrin-protein polymersomes. *J. Am. Chem. Soc.* **2009***, 131*, 3872-3874.

35. Griepenburg, J. C.; Sood, N.; Vargo, K. B.; Williams, D.; Rawson, J.; Therien, M. J.; Hammer, D. A.; Dmochowski, I. J. Caging Metal Ions with Visible Light-Responsive Nanopolymersomes. *Langmuir : the ACS journal of surfaces and colloids* **2015***, 31*, 799-807.

36. Skoog, D. A.; Holler, F. J.; Crouch, S. R. *Principles of Instrumental Analysis;* Thomson Brooks/Cole: 2007; .

37. Yadav, R. K. Definitions in Laser Technology. *J Cutan Aesthet Surg* **2009***, 2*, 45-46.

38. Eugene Hecht *Optics;* Addison Wesley: 2002; , pp 581-607.

39. Hao, J.; Ghosh, P.; Li, S. K.; Newman, B.; Kasting, G. B.; Raney, S. G. Heat effects on drug delivery across human skin. *Expert opinion on drug delivery* **2016***, 13*, 755-768.

40. University of Cairo Journal of Advanced Research University of Cairo Journal of Advanced Research. **2010***, 1*, 13-28.

41. Sibbett, W.; Lagatsky, A. A.; Brown, C. T. A. The development and application of femtosecond laser systems. *Optics express* **2012***, 20*, 6989.

42. Helmchen, F.; Denk, W. Deep tissue two-photon microscopy. *Nature Methods* **2005***, 2*, 932-940.

43. Shen, Y. R. The principles of nonlinear optics. *New York, Wiley-Interscience, 1984, 575 p.* **1984**.

44. Holzer, M. P.; Rabsilber, T. M.; Auffarth, G. U. Femtosecond laser-assisted corneal flap cuts: morphology, accuracy, and histopathology. *Invest. Ophthalmol. Vis. Sci.* **2006***, 47*, 2828-2831.

45. Aghlara, H.; Rostami, R.; Maghoul, A.; SalmanOgli, A. Noble metal nanoparticle surface plasmon resonance in absorbing medium. *Optik* **2015***, 126*, 417-420.

46. AnonymousGold Nanoparticles: Optical Properties. https://nanocomposix.com/pages/gold-nanoparticles-optical-properties (accessed Mar 28, 2019).

47. Hinman, J. G.; Stork, A. J.; Varnell, J. A.; Gewirth, A. A.; Murphy, C. J. *APER;* The Royal Society of Chemistry: 2009; Vol. 1, pp 9-33.

48. Jain, P. K.; Lee, K. S.; El-Sayed, I. H.; El-Sayed, M. A. Calculated absorption and scattering properties of gold nanoparticles of different size, shape, and composition: applications in biological imaging and biomedicine. *J Phys Chem B* **2006***, 110*, 7238-7248.

49. Meng Zhou; Chenjie Zeng; Yuxiang Chen; Shuo Zhao; Matthew Y Sfeir; Manzhou Zhu; Rongchao Jin Evolution from the plasmon to exciton state in ligand-protected atomically precise gold nanoparticles. *Nature Communications* **2016***, 7*, 13240.

50. Xia, Y. Younan Xia. *Angewandte Chemie (International ed. in English)* **2011**, *50*, 6958-6959.

51. Amstad, E.; Kim, S.; Weitz, D. A. Photo- and thermoresponsive polymersomes for triggered release. *Angew. Chem. Int. Ed. Engl.* **2012**, *51*, 12499-12503.

52. DiSalvo, G. Temporal control of encapsulant release from nanoparticle loaded polymersomes via single pulse irradiation. **2018**.

53. Greene, A. C.; Sasaki, D. Y.; Bachand, G. D. Forming Giant-sized Polymersomes Using Gel-assisted Rehydration. *Journal of Visualized Experiments* **2016**.

54. Nakamura, Y.; Mochida, A.; Choyke, P. L.; Kobayashi, H. Nanodrug Delivery: Is the Enhanced Permeability and Retention Effect Sufficient for Curing Cancer? *Bioconjug. Chem.* **2016**, *27*, 2225-2238.

55. Stoeva, S. I.; Prasad, B. L. V.; Uma, S.; Stoimenov, P. K.; Zaikovski, V.; Sorensen, C. M.; Klabunde, K. J. Face-Centered Cubic and Hexagonal Closed-Packed Nanocrystal Superlattices of Gold Nanoparticles Prepared by Different Methods. *The Journal of Physical Chemistry B* **2003**, *107*, 7441-7448.

56. Klein-Wiele, J. -.; Simon, P.; Rubahn, H. -. Size-Dependent Plasmon Lifetimes and Electron-Phonon Coupling Time Constants for Surface Bound Na Clusters. *Phys. Rev. Lett.* **1998**, *80*, 45-48.

57. Delfour, L.; Itina, T. E. Mechanisms of Ultrashort Laser-Induced Fragmentation of Metal Nanoparticles in Liquids: Numerical Insights. *J. Phys. Chem. C* **2015**, *119*, 13893-13900.

58. Song, Z.; Huang, Y.; Prasad, V.; Baumgartner, R.; Zhang, S.; Harris, K.; Katz, J. S.; Cheng, J. Preparation of Surfactant-Resistant Polymersomes with Ultrathick Membranes through RAFT Dispersion Polymerization. *ACS Appl Mater Interfaces* **2016**, *8*, 17033-17037.

59. Koley, D.; Bard, A. J. Triton X-100 concentration effects on membrane permeability of a single HeLa cell by scanning electrochemical microscopy. (SECM). *PNAS* **2010**, *107*, 16783-16787.